Title
Spatial memory precision and learning in medial temporal and prefrontal networks

Author
Stevenson, Rebecca

Publication Date
2019

Peer reviewed|Thesis/dissertation

UNIVERSITY OF CALIFORNIA,
IRVINE

Spatial memory precision and learning in medial temporal and prefrontal networks

DISSERTATION

submitted in partial satisfaction of the requirements
for the degree of

DOCTOR OF PHILOSOPHY

in Biological Sciences

by

Rebecca Farwell Stevenson

Dissertation Committee:
Professor Michael A. Yassa, Chair
Professor Craig E. L. Stark
Professor Jack J. Lin

2019

DEDICATION

To the patient volunteers at the UC Irvine Medical Center, whose strength and resilience is an inspiration and without whom this research would not be possible.

TABLE OF CONTENTS

Acknowledgements

I would like to thank my advisor, Mike Yassa, and my co-mentor, Jack Lin, for their outstanding mentorship, fearless enthusiasm, and for making it seem as if the possibilities of neuroscience research are limitless. I thank Craig Stark for his thoughtful critiques and for past and future feedback and guidance.

I thank Logan Harriger, Sandra Gattas, Jie Zheng, Ivan Skelin, and Haoxin Zhang for assistance with data collection and for sharing their methodological brilliance with me over the years. I thank Myra Larson for assistance with electrode localization and with data preprocessing, and John Janecek for programming assistance and for helping me figure out how to code by voice. I thank Stephanie Leal for assistance with electrode localization, Olivia Kim for artifact detection, Amanda Chun for help preprocessing data, and Becca Knowles for being my hands. I thank Zach Reagh, Stephanie Leal, and Jared Roberts for their mentorship and training. I thank Liz Murray and Liv McMillan for their endless patience and support. I thank all the members of the Yassa and Lin labs for their contributions to this research and for making my time at UCI an absolute joy.

I thank Sumeet Vadera and Lilit Mnatsakanyan for patient care, the staff at the Epilepsy Monitoring Unit at the University of California Irvine Medical Center, and the patients who volunteered in this research.

I thank Robert Knight for his support and generosity, and I thank Norbert Fortin, Roemer van der Meij, and the members of the Knight lab for helpful discussions. This work was supported by NINDS T32NS45540 (PI: T.Z. Baram), NINDS R3721135 (PI: Knight), as well as NIMH R01MH102392 and NIA R21AG049220 (PI: Yassa).

CURRICULUM VITAE

EDUCATION

2013-2019	**Ph.D.**	**University of California, Irvine** Department of Neurobiology and Behavior
2001-2005	**B.A.**	**Tulane University** Bachelor of Arts *cum laude* in Latin American studies

RESEARCH EXPERIENCE

2014-	Graduate research assistant, **Yassa Lab** Principal investigator: Michael Yassa University of California, Irvine Research topics: Medial temporal and prefrontal networks in spatial memory precision and learning
2014	Graduate research assistant (rotating), **Stark Lab** Principal investigator: Craig Stark University of California, Irvine Research topic: Memory impairments associated with healthy aging
2013	Graduate research assistant (rotating**), Fortin Lab** Principal investigator: Norbert Fortin University of California, Irvine Research topic: Contributions of the hippocampus and medial prefrontal cortex to memory for sequences of events
2012-2013	Research Assistant, **Walker Lab** Principal investigator: Matthew Walker University of California, Berkeley Research topic: High density EEG of memory reactivation during sleep and the effect of sleep on anxiety
2011-2012	Research Assistant, **Shimamura Lab** Principal investigator: Art Shimamura University of California, Berkeley Research topic: The role of the posterior parietal cortex in episodic memory

TEACHING EXPERIENCE

2016-2017	Lab leader, Neurobiology Lab Instructor: Dr. Andrea Nicholas
2015	Teaching assistant, Neurobiology Lab

	Instructor: Dr. Andrea Nicholas
2015	Teaching assistant, Neurobiology and Behavior Instructors: Drs. Ian Parker, Norbert Fortin and Michael Leon
2014	Teaching assistant, From DNA to Organisms Instructors: Drs. Kim Green, Marcelo Wood, and Jorge Busciglio

ACADEMIC SERVICE

2017-	CNLM Ambassador, designing and executing outreach and educational activities for the Center for the Neurobiology of Learning and Memory (CNLM)
2014-	Reviewer, reviewed manuscripts with Dr. Yassa for multiple peer-reviewed journals, including Nature Neuroscience, Nature Communications, eLife, Current Biology, and The Journal of Neuroscience
2017-2018	Founder and coordinator, Spike Club, journal club focusing on electrophysiological papers from both human and animal studies
2015	Chair, Graduate Student Committee for the department of Neurobiology and Behavior's 50th Anniversary Retreat, UC Irvine
2015	Producer, promotional video for the department of the Neurobiology and Behavior, UC Irvine Featured on the departmental homepage: http://neurobiology.uci.edu/
2014-2015	Coordinator, Hebb Club: the journal club for the Center for the Neurobiology of Learning and Memory (CNLM)
2015	Co-coordinator, Elevator Pitch workshop, UC Irvine
2014	Member, Orange County Graduate Women in Science (OCGWIS) UC Irvine Chapter
2014	Data Blitz Chair, Center for the Neurobiology of Learning and Memory (CNLM) Spring Meeting

AWARDS AND HONORS

2019	James L. McGaugh Award for Excellence in Graduate Research in Neurobiology and Behavior
2016-2017	NIH T32 Predoctoral Training Fellowship
2016	Kavli Summer Institute of Cognitive Neuroscience Fellowship

2015	John W. Haycock Memorial Travel Award
2001-2005	Founders Scholarship, Tulane University
2001-2005	Dean's Honors, Tulane University
2001	National Merit Scholar

RELEVANT TRAINING AND COURSEWORK

2011-2017	Relevant coursework: Python Programming, Neural Computation, Analysis of Neural Time Series, Advanced Analysis of Learning and Memory, Statistics for Neurobiologists, Behavioral Neuroscience, Cellular Neuroscience, Systems Neuroscience, Molecular Neuroscience, fMRI Methods
2017	Workshop on memory consolidation, restoration, and augmentation. HRL Laboratories, LLC
2014	Workshop on Mentoring in the Research Laboratory
2014	Advanced Pedagogical Design and Educational Science Media Production, UC Irvine
2014	Teaching Assistant Training Program (TAPDP), UC Irvine
2012	fMRI Intermediate User Training, UC Berkeley

DOCUMENTARY FILMAKING EXPERIENCE (selected)

2008-2009	Editor, "Ice Stories: Dispatches from Polar Scientists", Exploratorium, San Francisco, CA http://icestories.exploratorium.edu/dispatches/
2006-2007	Researcher and production assistant, "Man Made", National Geographic Channel, Winton/duPont Films, San Francisco, CA
2005	Researcher, "The Ten Plagues of the Bible" National Geographic Channel, Winton/duPont Films, San Francisco, CA

PUBLICATIONS

Stevenson, R.F., Reagh, Z.M., Chun, A.P., Murray, E.A., Yassa, M.A., (under review, Journal of Neuroscience). Distinct hippocampal and neocortical regions support source memory and item-level pattern separation.

Stevenson, R.F., Janecek, J.T., Zheng, J., Mnatsakanyan, L., Vadera, S., Knight R.T., Lin, J.J., Yassa, M.A., (in preparation). Gamma power in the human medial temporal lobe and prefrontal cortex predicts error and learning in a spatial memory task.

Zheng, J., **Stevenson, R.F.,** Vadera, S., Knight R.T., Yassa, M.A., Lin, J.J., (2019). Multiplexing of Theta and Alpha Rhythms in the Amygdala-Hippocampal Circuit Supports Pattern Separation of Emotional Information. Neuron.

Stevenson, R.F., Zheng, J., Mnatsakanyan, L., Vadera, S., Knight R.T., Lin, J.J., Yassa, M.A., (2018). Hippocampal CA1 gamma power predicts the precision of spatial memory judgements. PNAS. doi.org/10.1073/pnas.1805724115.

Stark, S. M., **Stevenson, R**., Wu, C., & Rutledge, S., (2015). Stability of age-related deficits in the mnemonic similarity task across task variations. Behavioral Neuroscience. DOI:10.1037/bne0000055.

POSTER PRESENTATIONS

Stevenson, R.F., Mnatsakanyan, L., Vadera, S., Knight R.T., Lin, J.J., Yassa, M.A. (2018) High gamma power predicts error in a spatial learning task. International Conference on Learning and Memory, UC Irvine.

Stevenson, R.F., Zheng, J., Moon, A., Vadera, S., Knight R.T., Lin, J.J., Yassa, M.A. (2018) Gamma and theta activity in the human medial temporal lobe and prefrontal cortex predicts performance on a spatial learning task. Society for Neuroscience.

Stevenson, R.F., Zheng, J., Leal, S.L., Chun A.P., Sumeet, V., Knight, R.T., Lin, J.J., Yassa, M.A. (2016). High-frequency band activity in human hippocampal CA1 predicts the precision of spatial memory retrieval. Society for Neuroscience.

Stevenson, R., Reagh, Z.M., Chun, A.P., Murray, E.A., Yassa, M.A., (2015). High-resolution fMRI of source memory and mnemonic discrimination. Society for Neuroscience.

Lin, J.J., **Stevenson, R.F.,** Leal, S.L., Zheng, J., Roberts, J.M., Riley, J., Yassa, M.A., (2015). Intracranial EEG of hippocampal-amygdala dynamics during emotional memory discrimination. Society for Neuroscience.

Stark, S.M., **Stevenson, R.F**., Stark, C.E. (2014) Stability of age-related deficits in the Mnemonic Similarity Task across task variations. Society for Neuroscience.

Stark, S.M., **Stevenson, R.F.,** Stark, C.E. (2014) Stability of age-related deficits in the Mnemonic Similarity Task across task variations. ReMIND Emerging Scientists Symposium on Neurological Disorders, UC Irvine.

TALKS

Gamma power predicts error in a spatial learning task. Lightning talk, International Conference on Learning and Memory, UC Irvine, 2018.

Gamma and theta activity in the human medial temporal lobe and prefrontal cortex predicts performance on a spatial learning task. NeuroBlitz, UC Irvine, 2017.

Gamma power in the human medial temporal lobe and prefrontal cortex predicts performance on a spatial learning task. Progress in Neuroscience, UC Irvine, 2017.

Gamma and theta activity in human hippocampus and prefrontal cortex predicts the precision of spatial memory retrieval. EpiCenter Symposium, UC Irvine, 2017.

CA1 and MEC gamma power predicts spatial memory precision. Data Blitz presentation, Park City Winter Conference on the Neurobiology of Learning and Memory, 2016.

Depth electrode recordings in the human medial temporal lobe. Center for the Neurobiology of Learning and Memory awards ceremony, 2015.

Depth electrode recordings in the human medial temporal lobe. NeuroBlitz, UC Irvine, 2015.

The effect of task design on age-related deficits in mnemonic discrimination. NeuroBlitz, UC Irvine, 2014.

List of Figures

List of tables

Chapter 2

Chapter 3

ABSTRACT OF THE DISSERTATION

Spatial memory precision and learning in medial temporal and prefrontal networks

By

Rebecca Farwell Stevenson

Doctor of Philosophy in Biological Sciences

University of California, Irvine, 2019

Professor Michael A. Yassa, Chair

The medial temporal lobe and prefrontal cortex are known to play a critical role in tasks involving learned associations, such as between an object and a location. However, the exact neural mechanisms underlying the learning and retrieval of high-fidelity spatial associations are unknown. To address this gap, we tested presurgical epilepsy patients with bilateral depth electrodes implanted in the medial temporal lobe and prefrontal cortex on two variants of an object-location spatial learning task. In the first version of this task, subjects were shown a series of objects at random positions along the circumference of an invisible circle. At test, the same objects were shown at the top of the circle, and subjects used a dial to move the object to the location shown during encoding. Angular error between the correct location and the indicated location was recorded as a continuous measure of performance. By registering pre- and post-implantation MRI scans, we were able to localize electrodes to specific hippocampal subfields. We found a correlation between increased high-frequency gamma power (40-100 Hz), thought to reflect local excitatory activity, and the precision of spatial memory retrieval in hippocampal CA1 and dorsolateral prefrontal electrodes. Additionally, we

found a directional relationship between these regions, suggesting that the dorsolateral prefrontal cortex is involved in post-retrieval processing. In order to examine the neural activity underlying spatial learning, we then tested presurgical epilepsy patients on a variant of this task in which subjects attempted to learn object-location associations over the course of three training blocks with feedback. At retrieval, we found increased medial temporal and dorsolateral prefrontal gamma power for low error trials, consistent with the results described above. At feedback, we found the opposite pattern of activity, with increased medial temporal and dorsolateral prefrontal gamma power for high error trials. Increased medial temporal gamma activity at feedback also predicted greater decreases in error from one training block the next, indicating that these error signals are involved in updating memory representations or modifying incorrect associations during learning. Finally, we examined the contributions of low frequency oscillatory power to performance on this spatial learning task as well as the relationship between the 1/f aperiodic slope and spatial memory retrieval and learning. We found that the aperiodic slope, thought to reflect the ratio of excitation to inhibition, decreased across training blocks, but did not predict error within training blocks, suggesting that decreased excitation and/or increased inhibition is associated with increased familiarity and/or decreased novelty. Low frequency oscillatory power did not predict error within blocks and did not change across blocks. Overall, these data suggest putative mechanisms for the learning and retrieval of high-fidelity spatial associations.

INTRODUCTION

Memory for events or experiences, known as episodic memory, depends on our ability to make novel associations between the items or elements that make up each event. For instance, my memory of parking my car this morning includes a key association between the car and its location in the parking lot. Converging evidence from studies in animals and humans suggests that this ability is subserved by medial temporal and prefrontal networks. However, as these studies typically have used binary, or correct versus incorrect, measures of performance, the relationship between neural activity within these networks and memory strength, or precision, is still not well understood. Given that novel associations (e.g. face-name) are often not learned in a single episode, it is also unclear how medial temporal and prefrontal activity contribute to learning over the course of multiple episodes (e.g. learning someone's name after being reminded a few times).

In order to address these questions, we developed two variants of an object-location association task. In the first task, subjects were tested on 100 separate object-location associations, eliciting a broad range of spatial memory precision ideal for examining the neural correlates of high-fidelity spatial memory retrieval. In this task, subjects had just one shot to learn the object-location associations, i.e. the test phase immediately followed the encoding phase. In the second task, subjects attempted to learn 30 object-location associations over the course of three training blocks with feedback, allowing us

to examine how neural activity within medial temporal and prefrontal networks contribute to associative learning.

We ran both of these tasks on pre-surgical epilepsy patients with depth electrodes implanted in the medial temporal lobe and prefrontal cortex. Intracranial recordings in pre-surgical epilepsy patients provide a rare opportunity to examine medial temporal and prefrontal contributions to spatial memory precision and learning with a temporal and spatial resolution unmatched by non-invasive functional neuroimaging techniques. Unlike electroencelphalography (EEG), in which neural activity is recorded from electrodes placed on the scalp, intracranial recordings allow for reliable recording of high-frequency gamma activity (>40 Hz), a frequency range that has been an increasingly important research focus in both human and animal studies. As many of the seminal studies on episodic memory have been performed using electrophysiology in animals, intracranial recordings in humans provide a bridge to this body of research, enabling the direct testing of models and theories developed in the animal literature. The high temporal resolution that this method affords also allows us to examine the dynamics of neural processing, including the role that neural oscillations play in coordinating intra- and inter-regional neural activity. The relatively high spatial resolution of intracranial recordings enables us to determine where neural signals originate and thus make inferences about the contribution of different regions to memory processes. Finally, intracranial recordings allow us to estimate the shape of neural power spectra, or the amount of energy (power) present at different frequencies. The slope of this signal is thought to be a promising new method for estimating the balance between

excitation and inhibition, providing a new window into neural activity. Leveraging the unique features of this recording method combined with the continuous, objective measure of performance afforded by the object-location memory tasks, the overall goal of this research is to identify the neural mechanisms underlying spatial memory precision and learning. A description of specific aims follows.

Aim 1: Determine the extent to which changes in medial temporal and prefrontal high-frequency activity and network dynamics predict the precision of spatial memory retrieval.

In order to examine the neural mechanisms underlying the precision of spatial memory retrieval, we tested presurgical epilepsy patients with depth electrodes implanted in the medial temporal lobe and prefrontal cortex on an object-location memory task designed to elicit a broad range of spatial memory precision. During encoding, subjects were shown a series of 100 objects at random locations along the circumference of an invisible circle. At test, the same objects were shown at the top of the circle, and subjects were asked to use a dial to move the object to where it appeared during encoding. Angular error between the correct location and the indicated location was recorded as a continuous measure of performance. We found a correlation between increased high-frequency gamma power, thought to reflect local excitatory activity, and the precision of spatial memory retrieval in hippocampal CA1 and dorsolateral prefrontal electrodes. Additionally, we found a directional relationship between activity in the dorsolateral prefrontal cortex and CA1 region, suggesting that the dorsolateral prefrontal cortex is involved in post-retrieval processing.

Aim 2: Determine the extent to which changes in medial temporal and prefrontal high-frequency activity predict error and learning at retrieval and feedback in an object-location associative learning task.

In order to examine the neural mechanisms underlying spatial associative learning, we tested presurgical epilepsy patients with depth electrodes implanted in the medial temporal lobe and prefrontal cortex on a spatial memory task in which subjects attempted to learn object-location associations over the course of three training blocks with feedback. During encoding, subjects were shown a series of 30 objects at random locations along the circumference of an invisible circle. In each of the three training blocks, the same objects were shown at the top of the circle, and subjects were asked to use a dial to move the object to where it appeared during encoding. After the subject finished placing the object, it was shown in the correct location for 1 second as feedback. Angular error between the correct location and the indicated location was recorded as a continuous measure of performance. At retrieval, we found increased medial temporal and dorsolateral prefrontal gamma power for low error trials, consistent with the results described in aim 1. At feedback, we found the opposite pattern of activity, with increased medial temporal and dorsolateral prefrontal gamma power for high error trials. Increased medial temporal gamma activity at feedback also predicted greater decreases in error from one training block the next, indicating that these error signals are involved in updating memory representations or modifying incorrect associations during learning.

Aim 3: Determine the extent to which changes in low frequency oscillatory power and the aperiodic slope predict error and learning at retrieval and feedback in an object-location associative learning task.

In order to examine the contributions of low frequency oscillatory power to performance on the spatial learning task described above, as well as the relationship between the slope of the aperiodic component of neural power spectra and spatial learning, we used a novel algorithm to estimate low frequency oscillatory power and the aperiodic slope. We found that the aperiodic slope, thought to reflect the ratio of excitation to inhibition, decreased across training blocks, but did not predict error within training blocks, suggesting that decreased excitation and/or increased inhibition is associated with increased familiarity and/or decreased novelty. Low frequency oscillatory power did not predict error within blocks and did not change across blocks. Overall, these data suggest putative mechanisms for the learning and retrieval of high-fidelity spatial associations.

CHAPTER 1: BACKGROUND AND SIGNIFICANCE

1.1 Declarative memory and the medial temporal lobe

Interest in the medial temporal lobe (MTL) with regards to memory research began with the seminal studies on patient H.M conducted by Brenda Milner. This patient had severe bilateral MTL damage that resulted in profound amnesia. However, Milner observed that while H.M. could not remember new facts or events, he could still take in and retain some new information, such as motor skill learning. Observing similar selective deficits in other MTL patients, Cohen and Squire proposed that 'declarative memory', or the memory for facts or events, and 'procedural memory', or the memory for how to accomplish certain skills are different types of memory that can be supported by different brain structures (Cohen & Squire, 1980). While procedural memory is spared with MTL damage, declarative memory is not. Declarative memory can be further subdivided into episodic memory (Tulving, 1984), or the memory for events and experiences, and semantic memory, or the memory for facts or the meaning of words. For the purposes of this dissertation I will focus on the contributions of the MTL to episodic memory. A more complete account of theories of MTL function necessitates some knowledge of MTL anatomy. As such, a brief overview of MTL structure and connectivity follows.

1.2 Overview of medial temporal lobe anatomy

The MTL consists of the hippocampus, subiculum, and the perirhinal, parahippocampal, and entorhinal cortices. These regions are homologous across rodents, primates, and

humans, though in rodents the parahippocampal cortex is referred to as the postrhinal cortex (Allen & Fortin, 2013). The perirhinal cortex (PRC) and parahippocampal cortex (PHC) are strongly interconnected but differ in the inputs they receive from cortical association areas (Lavenex & Amaral, 2000). The PRC receives much of its input from association areas along the ventral visual processing stream (Lavenex & Amaral, 2000). This ventral stream, also known as the 'what' stream, originates in the visual cortex and is thought to process information about object or items as well as semantic information (Diana, Yonelinas, & Ranganath, 2007). The parahippocampal cortex (PHC) receives more visuospatial input from the dorsal processing stream, or the 'where' stream, including areas such as V4, and the posterior parietal and retrosplenial cortices (Lavenex & Amaral, 2000; Ranganath & Ritchey, 2012). This relative segregation of 'what' and 'where' processing streams is maintained in the EC as the lateral and medial portions of the EC receive cortical input primarily from the PRC and PHC, respectively (Burwell, 2000).

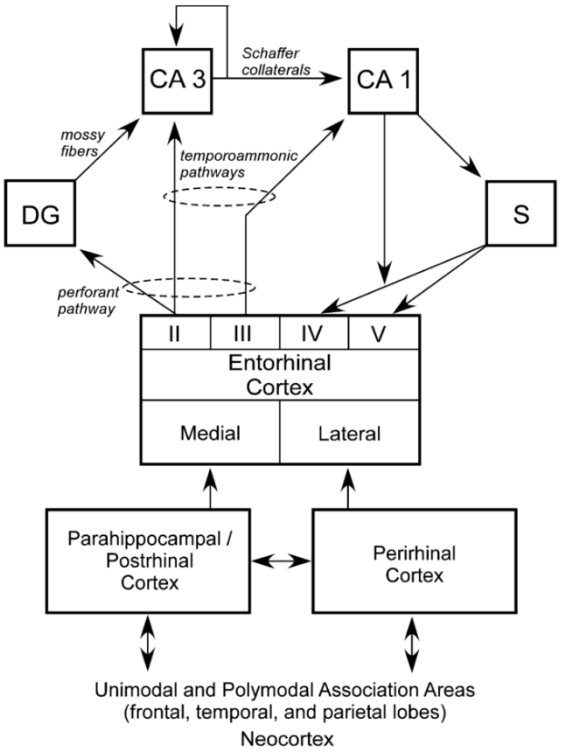

Figure 1.1. Schematic of medial temporal lobe anatomy. From Clark and Squire, 2013.

The hippocampus can be divided into the dentate gyrus (DG), CA1 and CA3 subfields. Early studies on hippocampal anatomy emphasized what was called the 'trisynaptic circuit' (Anderson, Bliss, & Skrede, 1971; Lavenex & Amaral, 2000). This largely unidirectional pathway begins with cells from layer II of the EC projecting to granule cells in the dentate gyrus via an axon bundle known as the perforant path. The granule cells in turn give rise to axons, known as mossy fibers, that synapse onto CA3 pyramidal cells. Importantly, the CA3 subfield also receives strong input from itself via recurrent collaterals. The final link in the trisynaptic pathway is the projection from CA3 pyramidal cells to the CA1 subfield via the Schaffer collaterals (Amaral & Lavenex, 2007). However, this pathway was described when it was thought that the CA1 subfield was the primary output region of the hippocampus (Amaral & Lavenex, 2007). Since it was discovered the subiculum and entorhinal cortices also serve as major sources of hippocampal output, the phrase 'trisynaptic pathway' is now thought to be outdated (Amaral & Lavenex, 2007). In addition to the connections described above, there is also a projection from EC layer II to CA3 and from EC layer III to CA1, making up what is known as the temporoammonic

pathway (Clark & Squire, 2013). It should be emphasized that this is a simplified overview of hippocampal circuitry. For instance, not included in the schematic shown in Figure 1 is the fimbria-fornix pathway, which connects the hippocampus to subcortical structures (Amaral & Lavenex, 2007).

1.3 Episodic memory and the medial temporal lobe

Long before the detailed neuroanatomical mapping of MTL circuitry described above was complete, researchers used experimental lesions in animals to try to define some broad structure-function relationships within this region (Morris, 2007). These studies showed that MTL damage resulted in severe deficits on single-trial recognition memory tasks such as the delayed non-matching to sample (DNMS) task (Morris, 2007). In this task, subjects are shown a sample object, then, after a short delay, they are shown the same object again along with a novel object. Subjects are rewarded for choosing the novel object. Using this task, researchers found that lesions to the PRC resulted in severe impairments in object, or item recognition memory (Murray & Mishkin, 1986; Ranganath, 2010; Zola-Morgan, Squire, Amaral, & Suzuki, 1989). As this task depends on memory for single events (i.e. seeing the sample object), these results were early indications that the MTL is particularly important for episodic memory, or the memory for specific events or experiences. However, converging evidence from monkey, human, and rodent studies suggested that object, or item recognition memory was relatively spared in subjects with damage limited to the hippocampus (Ranganath, 2010). As such, a number of theories emerged to try to explain the functional differences between the hippocampus and medial temporal cortices.

One of these theories, called the ‘relational memory theory’, proposed that while the PRC and PHC are involved in representing the items or elements of an event, the HC is involved in representing the relationships between items (Eichenbaum & Cohen, 2014; Eichenbaum, Otto, & Cohen, 1992). A more recent model, called the Binding of Items in Context (BIC) model, builds on the relational memory theory by incorporating information about MTL connectivity (Diana et al., 2007; Eichenbaum, Yonelinas, & Ranganath, 2007). As the PRC receives much of its input from the ventral visual ‘what’ processing stream, the model proposed that this region is involved in processing information about objects or items. Similarly, as the PHC receives more input from the dorsal ‘where’ stream, the model proposed that this region is involved in representing context. The term ‘context’ as used here means a variety of things, including memory for where or when an event took place. In this model, the HC is involved in representing the relationships, or the ‘bindings’, between items and context (Diana et al., 2007). Evidence for this model can be found in both the animal and human literature. For example, studies have shown that rodents with hippocampal damage are unimpaired on tasks that test their ability to recognizes familiar objects, but impaired on tasks that test their ability to recognize familiar objects in novel locations (Eacott, Norman, Langston, & Wood, 2004). The BIC model interprets these results as suggesting that the hippocampus mediates the association, or ‘binding’, between objects and locations. Human studies of object-location memory have found similar deficits following hippocampal damage (Hannula & Ranganath, 2008; Ryan, Althoff, Whitlow, & Cohen, 2000). Furthermore, fMRI studies have shown greater hippocampal activation during

associative memory tasks than during item recognition (Davachi et al. 2003; Diana, Yonelinas, & Ranganath, 2009).

Another influential account of the functional differences between the hippocampus and surrounding cortices (along with rest of the neocortex) was proposed by McClelland and colleagues in 1995. This model, called Complementary Learning Systems (CLS), holds that the neocortex and hippocampus mediate two 'complementary' types of learning. While the neocortex supports the gradual acquisition of knowledge about the environment, the circuitry of the hippocampus supports the rapid acquisition of information about specific events (i.e. episodic memory) (Kumaran, Hassabis, & McClelland, 2016; Mcclelland, 1995). Although the BIC and CLS models focus on different aspects of MTL function, the two models are compatible in that they both propose a critical role for the hippocampus in episodic memory and specifically in the rapid acquisition of novel associations (Ranganath, 2010).

1.4 Episodic memory and the prefrontal cortex

The MTL is not the only region important for episodic memory. Numerous studies have implicated the prefrontal cortex (PFC) in many aspects of episodic encoding and retrieval. The PFC can be divided into 6 regions: the medial PFC (mPFC; Brodmann area (BA) 10/25/32), dorsolateral PFC (dlPFC; BA 9/10/46), orbitofrontal cortex (OFC; BA 10/11/47), ventrolateral PFC (vlPFC; BA 47/45/44), anterior cingulate cortex (ACC; BA 24), and caudal PFC (cPFC; BA 6/8). However, there is no consensus on these divisions and PFC parcellation is inconsistent across studies and literature. PFC regions

are highly interconnected and have extensive and often reciprocal connections with much of the temporal and parietal cortex (Passingham & Wise, 2012). However, each PFC region has a specific pattern of connectivity that is thought to reflect its function. The mPFC receives both direct and indirect input from the hippocampus and is thought to be involved in a variety of episodic memory processes. Based on anatomical studies in rodents and primates, the direct hippocampal input to the mPFC comes from the anterior HC (ventral HC in rodents) through a white matter track known as the fornix. While this projection is unidirectional, the mPFC is densely and reciprocally connected to the medial temporal cortices, which, in turn are connected to the HC (Insausti & Amaral, 2008; Lavenex, Suzuki, & Amaral, 2002; Muñoz & Insausti, 2005). The HC and mPFC are also indirectly connected via the nucleus reuniens, one of the midline thalamic nuclei (Amaral & Cowan, 1980; Barbas, Henion, & Dermon, 1991). One of the functions associated with the mPFC is the ability to use context to guide memory retrieval (Preston & Eichenbaum, 2013). Evidence for this idea comes from studies in rodents showing that mPFC damage impairs performance on tasks that require switching between retrieval strategies (e.g. remembering an odor or a place) based on context (Preston & Eichenbaum, 2013). Furthermore, neuroimaging in human studies show mPFC activation during retrieval of contextual details (Rugg & Vilberg, 2013).

The dlPFC is also indirectly connected to the hippocampus via perirhinal and retrosplenial cortices (Passingham & Wise, 2012). In addition, it is highly connected to areas such as the posterior parietal cortex and premotor areas (Passingham & Wise, 2012). Passingham and Wise describe how the pattern of connectivity in this region

supports the ability to generate goals based on context (Passingham & Wise, 2012). Information retrieved by the MTL can be combined with visuospatial information from the posterior parietal cortex to form a representation of context, while connections to the premotor areas allow for the execution of goals relevant to this context (Passingham & Wise, 2012). Evidence for this idea comes from monkey studies using delayed response tasks, in which subjects are given a cue and then must make a response (e.g. choosing an object in a specific location) based on that cue after a short delay (Passingham & Wise, 2012). Monkeys with lesions to the dlPFC perform at chance level on this task. Electrophysiological recordings of dlPFC cells during the delay period of this task indicate that these deficits are due to the region's involvement in the prospective encoding of the response goal (i.e. the location of the object) (Passingham & Wise, 2012). Additionally, the dlPFC is thought to be involved in the monitoring and organization of information maintained in working memory as well as in the monitoring of information retrieved from episodic memory (Blumenfeld & Ranganath, 2007; Dobbins, Foley, Schacter, & Wagner, 2002; Henson, Rugg, Shallice, Josephs, & Dolan, 1999; Simons & Spiers, 2003). Other broad structure-function relationships within the PFC include the OFC's involvement in representing value and the ACC's role in conflict monitoring and error detection (Botvinick, Braver, Barch, Carter, & Cohen, 2001; Hosokawa, Kennerley, Sloan, & Wallis, 2013; Yeung & Nieuwenhuis, 2009).

1.5 Intracranial recordings in pre-surgical epilepsy patients

As noted above, intracranial recordings in pre-surgical epilepsy patients provide a rare opportunity to examine episodic memory in humans with both high spatial and temporal

resolution. The sub-millisecond temporal resolution of this method allows us to examine the role neural oscillations play in coordinating intra- and inter-regional neural activity. While most studies using this method only obtain a post-implantation CT, which somewhat limits the accuracy of electrode localization, a unique feature of the current research is that we obtain post-implantation MRIs, enabling more accurate and precise electrode localization, including on the level of hippocampal subfields.

A variety of signals can be obtained from subdural grid—termed electrocorticography (ECoG)—and depth electrode recordings in humans, including single unit activity (SUA), multi-unit activity (MUA), and the local field potential (LFP). For the purposes of this proposal, I will focus on the LFP. The LFP reflects the aggregate electrical activity generated by populations of neurons located in the vicinity of the recording electrode (Berens, Logothetis, & Tolias, 2010). The principle sources contributing to the LFP are thought to be excitatory and inhibitory post-synaptic currents, though other sources, including spiking, can also contribute (Buzsaki, Anastassiou, & Koch, 2012). Signal processing techniques can be used to transform the raw LFP time series into the frequency domain, giving a measure of energy (power) at different frequencies, called power spectra. Neural power spectra consist of narrowband peaks in power rising above a prominent “1/f” signal, where power decreases with increasing frequency following a power-law function. The narrowband peaks in power indicate the presence of neural oscillations, or rhythmic activity occurring at a particular frequency. Multiple neural oscillations have been identified at different frequency ranges, including delta (2-3 Hz), theta (3-8 Hz), alpha (8-12 Hz), beta (15-30 Hz) and gamma (>30 Hz), though the

center frequency and range of each band can vary across studies and literature (Cohen, 2014).

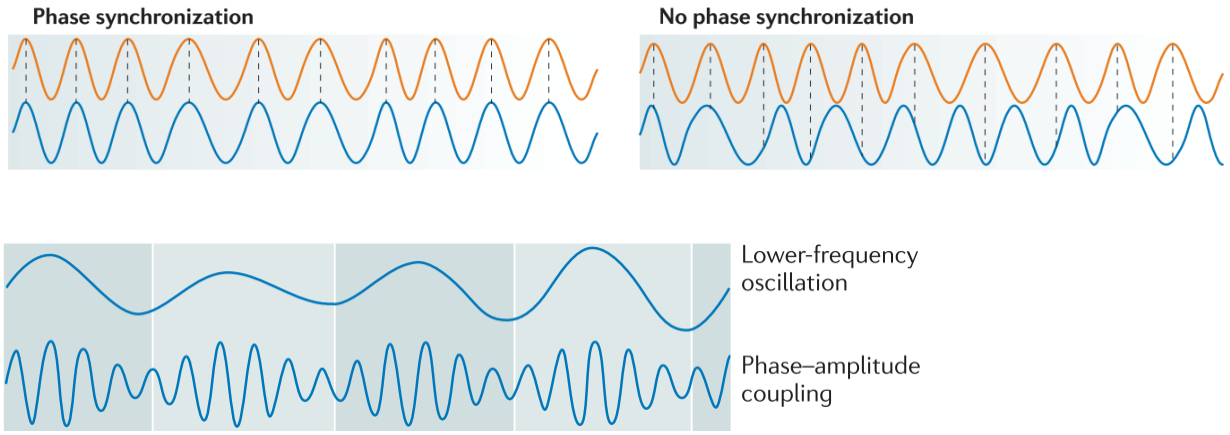

Figure 1.2. Schematic of phase synchronization and phase-amplitude coupling. Modified from Fell and Axmacher, 2011.

Much evidence suggests that neural oscillations in the theta and gamma range are involved in memory encoding and retrieval. While gamma oscillations are thought to be generated by local interactions between interneurons and pyramidal cells, theta oscillations in the rodent hippocampus are driven by interneurons projecting from the medial septum, though it was recently shown that theta rhythms can also emerge in in vitro hippocampal preparations (Buzsaki & Wang, 2012; Colgin, 2016; Colgin et al., 2009). The rhythmic properties of these oscillations play an important role in coordinating the timing of neural activity via such mechanisms as phase synchronization and phase-amplitude coupling. Phase synchronization refers to instances when there is a consistent or difference in phases between two signals (see Figure 1.2) and is thought to support neural communication and synaptic plasticity (Cohen, 2014; Fell & Axmacher, 2011). For instance, as neural spiking can preferentially occur at specific phases of an oscillation—termed spike-field coherence—this synchronization can

coordinate the timing of pre- and post-synaptic action potentials (Fell & Axmacher, 2011; Rutishauser, Ross, Mamelak, & Schuman, 2010). This temporal coordination may facilitate spike timing-dependent plasticity, in which the precise timing of pre- and post-synaptic firing is key to whether or not long-term potentiation (LTP) takes place (Fell & Axmacher, 2011). Phase-amplitude coupling, in which the phase of a low-frequency oscillation (e.g. theta) modulates the amplitude of a high-frequency oscillation (e.g. gamma; see Figure 1.2), is also thought to facilitate neural communication and synaptic plasticity (Fell & Axmacher, 2011; Igarashi, Lu, Colgin, Moser, & Moser, 2014). Compared to high-frequencies, low-frequency phase synchronization is often spread across a larger area of the brain (Buzsaki & Wang, 2012; Von Stein & Sarnthein, 2000). As such, nesting gamma oscillations within low-frequency oscillations could facilitate inter-regional gamma synchronization (Buzsaki & Wang, 2012). It is becoming increasingly clear that interactions between low- and high-frequency activity are key mechanisms underlying episodic memory encoding and retrieval.

1.6 High-frequency activity and episodic memory

Intracranial studies in pre-surgical epilepsy patients report robust increases in high frequency activity (HFA) during episodic memory encoding and retrieval (Burke, Long, et al., 2014; Greenberg, Burke, Haque, Kahana, & Zaghloul, 2015; Sederberg, Schulze-Bonhage, Madsen, Bromfield, McCarthy, et al., 2007). Moreover, increased HFA has been shown to predict performance on episodic memory tasks. For example, Sederberg et al. found that increased HFA (44-100 Hz) in regions such as the hippocampus and PFC during encoding predicted accuracy on a free recall task and that this pattern of

activity was reinstated prior to successful retrieval (Burke, Long, et al., 2014; Sederberg, Schulze-Bonhage, Madsen, Bromfield, McCarthy, et al., 2007). Increased HFA (45-95 Hz) in the PFC and temporal lobe during encoding has also been found to predict performance on an associative memory task (Greenberg et al., 2015). In a virtual navigation task in which subjects learned the locations of four objects over 8 training blocks, Park and colleagues found that hippocampal HFA (50-100 Hz) decreased over the course of the 8 blocks for high-performance but not low-performance sessions. These results indicate that hippocampal HFA is related to the successful encoding of the object locations (Park et al., 2014).

A prominent question in the field is what neurophysiological processes HFA in humans represents. One possibility is that HFA reflects gamma oscillations that coordinate the firing activity of populations of neurons. As described above, gamma oscillations are generated by local interactions between interneurons and pyramidal neurons. They have a well-defined frequency and phase, and appear as narrowband ‘peaks’ in the power spectrum (Lachaux, Axmacher, Mormann, Halgren, & Crone, 2012). As gamma phase synchronization can enhance spike-timing dependent plasticity, these oscillations are thought play a mechanistic role in memory processing (Fell & Axmacher, 2011; Igarashi et al., 2014). Another possibility is that HFA does not reflect oscillatory activity, but rather a broadband increase in the power spectra stemming from increased neuronal spiking (Buzsaki & Wang, 2012; Miller, Sorensen, Ojemann, & den Nijs, 2009). While it was originally thought that action potentials don’t contribute much to the LFP at frequencies below 500 Hz since the field generated by action potentials only lasts ~2ms,

recent studies have shown that spiking can result in increased broadband power that can be detected as low as 40 Hz (Buzsaki & Wang, 2012; Lachaux et al., 2012). Support for this view comes from studies in primates (Ray & Maunsell, 2011) and humans (Manning, Jacobs, Fried, & Kahana, 2009) showing that broadband increases in power are highly correlated with firing rate. These broadband increases in power are aperiodic, as they are not dominated by any particular frequency. In this view, HFA is non-oscillatory and does not play a mechanistic role in memory processing, but can be thought of as biomarker for local activity. Given that the frequency range of this broadband shift overlaps with that of 'true' gamma oscillations, a third possibility is that HFA reflects a combination of these processes (Burke, Long, et al., 2014). While it is difficult to rule out this third possibility, since most studies on HFA and memory in humans report broadband effects, this signal is thought to primarily reflect increased spiking (Burke, Ramayya, et al., 2014).

1.7 Theta oscillations and episodic memory

Theta in the rodent hippocampus is very prominent in freely moving rats and has been widely studied over the years. These studies have revealed a critical role for theta in encoding and retrieval (Berry & Thompson, 1978; Hyman, Wyble, Goyal, Rossi, & Hasselmo, 2003; Mitchell, Rawlins, Steward, & Olton, 1982; Winson, 1978). Hippocampal theta has also been linked to spatial navigation (e.g. theta phase precession) and representation (e.g. theta sequences) (see Colgin, 2016 for review). Furthermore, theta is correlated with sniffing and whisking (in rats) and eye movements

(in monkeys), leading some researchers to hypothesize that theta rhythms are important for coordinating the intake of sensory information (Colgin, 2016).

Theta oscillations in humans are also thought to play an important role in memory encoding and retrieval. Several studies in pre-surgical epilepsy patients have found increased theta power in the medial temporal lobe during episodic memory retrieval (Burke, Long, et al., 2014; Watrous, Tandon, Conner, Pieters, & Ekstrom, 2013). While these studies did not find that theta power during retrieval predicted performance, alterations in theta power during encoding has been shown to predict subsequent memory (Burke et al., 2013; Lega, Jacobs, & Kahana, 2012). Furthermore, using single unit and LFP recordings in the MTL, Rutishauser and colleagues found that theta phase-locking of neural firing during encoding predicted subsequent memory on a recognition memory task as well as subjects' confidence in their responses (Rutishauser et al., 2010). Lastly, theta power preceding the onset of an encoding stimulus or retrieval cue has been shown to predict successful encoding and retrieval (Addante, Watrous, Yonelinas, Ekstrom, & Ranganath, 2011; Fell et al., 2011; Merkow, Burke, Stein, & Kahana, 2014). Researchers have interpreted this pre-stimulus theta as reflecting a neural state that facilitates mnemonic processes.

In rodents, theta phase synchronization has been shown to coordinate neural activity within the MTL and between the MTL and PFC during a wide variety of memory tasks, while theta-gamma phase-amplitude coupling within the MTL has repeatedly been shown to track learning of novel associations (Igarashi et al., 2014; Tort, Komorowski,

Manns, Kopell, & Eichenbaum, 2009). Though fewer in number, studies in humans suggest that theta plays a similar mechanistic role in mnemonic processes. For instance, MTL-PFC theta synchronization has been shown to increase during free recall and predict successful retrieval of spatial context (Anderson, Rajagovindan, Ghacibeh, Meador, & Ding, 2010; Watrous et al., 2013). As noted above, this inter-regional coupling is thought to facilitate neural communication and support neural plasticity within distributed memory networks.

1.8 1/f aperiodic signal and neural excitation/inhibition

While neural oscillations are, by definition, periodic, the 1/f component of the LFP is thought to arise from aperiodic neural activity (Haller et al., 2018b; Miller et al., 2009). 1/f signals are observed in many natural phenomena (e.g. earthquakes) and are indicative of "scale-free" activity, meaning that they are not dominated by any particular frequency or time scale (He, 2014). Although more attention has been given to neural oscillations in the literature, recent work has highlighted the ways in which the aperiodic component of the LFP can be used as a window into neural activity. As noted above, neuronal spiking can shift the broadband aperiodic signal upwards, meaning that the offset of the aperiodic signal can reflect overall neural activity (Miller et al., 2014). More recently, results from computational modeling of the LFP signal demonstrated that the 1/f shape of the aperiodic signal can arise from a combination of excitatory and inhibitory postsynaptic currents (Gao, Peterson, & Voytek, 2017). Interestingly, this model showed that the slope of this simulated aperiodic signal reflected the balance between excitation and inhibition, and that increasing the ratio of excitation to inhibition

increased (flattened) the slope. The results from this model were corroborated by experimental data showing that the aperiodic slope measured in the CA1 region of the rat hippocampus was correlated with the excitatory (AMPA) to inhibitory (GABA) synapse ratio. In addition, ECOG recordings in monkeys have shown decreases in the aperiodic slope following administration of propofol, a general anesthetic that positively modulates the effect of GABA receptors (Gao et al., 2017).

Imbalances in excitation and inhibition have been implicated in multiple neurological and psychiatric disorders, such as schizophrenia, epilepsy, and age-related cognitive decline (Gao et al., 2017). Other measures of excitation/inhibition ratios are restricted to small populations of cells (e.g. intracellular or single unit recordings) or have low temporal resolution (e.g. magnetic resonance spectroscopy). As the aperiodic slope can be measured through LFP, ECOG, or EEG, this offers a novel method for estimating excitation/inhibition ratios with high temporal resolution from relatively large populations of neurons. A recent demonstration of the potential uses for this method showed that age-related impairments in working memory were mediated by a flattening of the aperiodic slope (Voytek et al., 2015). However, the links between the aperiodic slope and memory processing have yet to be fully explored.

CHAPTER 2: SPATIAL MEMORY PRECISION IN MEDIAL TEMPORAL AND PREFRONTAL NETWORKS

2.1 Abstract

The hippocampus plays a critical role in spatial memory. However, the exact neural mechanisms underlying high-fidelity spatial memory representations are unknown. We report findings from pre-surgical epilepsy patients with bilateral hippocampal depth electrodes performing an object-location memory task that provided a broad range of spatial memory precision. During encoding, patients were shown a series of objects along the circumference of an invisible circle. At test, the same objects were shown at the top of the circle (0 degrees) and patients used a dial to move the object to where it appeared during encoding. Angular error between the correct location and the indicated location was recorded as a continuous measure of performance. By registering pre- and post-implantation MRI scans, we were able to localize the electrodes to specific hippocampal subfields. We found a correlation between increased gamma power, thought to reflect local excitatory activity, and the precision of spatial memory retrieval in hippocampal CA1 electrodes. Additionally, we found a similar relationship between gamma power and memory precision in the dorsolateral prefrontal cortex, and a directional relationship between activity in this region and in the CA1, suggesting that the dorsolateral prefrontal cortex is involved in post-retrieval processing. These results indicate that local processing in hippocampal CA1 and dorsolateral prefrontal cortex supports high-fidelity spatial memory representations.

2.2 Introduction

A critical feature of episodic memory is the ability to form associations between the elements of an experience. This ability is known to rely on the medial temporal lobe (MTL), consisting of the hippocampus and surrounding cortices. Neuroimaging and lesion studies have demonstrated that the hippocampus plays a crucial role in tasks involving learned associations, such as between an object and a location (Eichenbaum et al., 2007). While the involvement of the hippocampus in the successful encoding and storage of associative memories is well-established, a major gap in our understanding stems from the use of binary (correct vs. incorrect) measures of performance, which do not allow for a detailed examination of the factors underlying the precision of learned associations. For example, associative memory can be highly precise in some cases (e.g. I parked my car in the far right corner of the parking lot), or more general (e.g. I parked my car in the parking lot) (Harlow & Yonelinas, 2016). As such, the contributions of the hippocampus to the precision of remembered associations remain poorly understood.

To address this gap, we developed an incidental object-location memory encoding task designed to elicit a broad range of spatial memory precision. We used a mixture modeling approach to analyze performance on the task, which allowed us to estimate which trials were remembered with some degree of precision and which trials were likely guesses. Testing pre-surgical epilepsy patients with bilateral depth electrodes implanted in the hippocampus and surrounding cortices, we used the objective, continuous measure of performance afforded by this task to examine the

electrophysiological correlates of spatial memory precision. Previous studies using intracranial recordings in humans have shown that MTL gamma power (> 40 Hz), which is thought to reflect local neural processing (Burke, Long, et al., 2014; Burke, Ramayya, & Kahana, 2015; Kucewicz et al., 2017), is associated with correct memory judgments (Burke, Long, et al., 2014; Greenberg et al., 2015; Sederberg, Schulze-Bonhage, Madsen, Bromfield, Litt, et al., 2007). Here, we predicted that increases in hippocampal gamma power during retrieval would track increases in spatial memory precision. Furthermore, by co-registering pre- and post-implantation MRI scans, we were able to localize electrodes within hippocampal subfields. This approach allowed us to estimate subfield-level gamma power and to examine how this activity related to performance on the task. Additionally, as the prefrontal cortex has also been shown to be involved in associative memory, we tested the relationship between gamma power and precision in this region. Leveraging the high temporal resolution of intracranial recordings, we also examined the relative timing and directionality of the observed effects across regions.

2.3 Material and methods

Participants

Subjects were 4 patients (3 Female, 1 Male, Age 32-58) who had stereotactically implanted intracranial depth electrodes (Integra or Ad-Tech, 5-mm inter-electrode spacing) placed at the University of California, Irvine Medical Center to localize the seizure onset zone for possible surgical resection. Informed consent was obtained from each subject prior to testing and the research protocol was approved by the IRB of the

University of California, Irvine. Electrode placement was exclusively guided by clinical needs.

Spatial precision task

One hundred images of common objects were selected from a set previously used by our group and (S. M. Stark, R. Stevenson, C. Wu, S. Rutledge, & C. E. L. Stark, 2015). Images were presented on a laptop computer screen set at a comfortable distance from the patient. Three hundred and sixty locations on the computer screen were generated along the circumference of a circle centered on the screen with a spacing of 1°. During encoding, the 100 objects appeared one at a time at pseudorandomly assigned circle locations and subjects were asked to judge whether each object would more likely be found indoors or outdoors (Figure 1; 1.2 +/- 0.2 second ITI; .5 second ISI). Following a short (~1 minute) delay, subjects were shown each object again in pseudorandom order, this time at the top of the screen. Subjects were instructed to wait 1 second (until text that read 'Wait…' disappeared from the screen) before using a mouse wheel to move the object to where it appeared during encoding. Subjects pressed the space bar to indicate that they were finished placing the object. If subjects performed more than one session, new objects and locations were used. No more than one session was performed on each day.

Behavioral analysis

Error on the spatial precision task was measured as the number of degrees between where subjects placed the object and the correct location. Histograms were used to

examine the distribution of error values. We used mixture modeling, as implemented by the MemFit function of Memtoolbox (Suchow, Brady, & Alvarez, 2013), to obtain an estimate of two parameters describing these distributions: the guess rate (g), which reflects the area under the uniform distribution, and the standard deviation of the von Mises distribution (SDMem). We used the cumulative distribution function of the von Mises distribution estimated for each session to split trials into three conditions: High precision, Low precision, and Guess. Trials that had less than a 10% chance of being remembered with some degree of precision were placed in the Guess condition. The remaining trials were sorted by error and split evenly into the High and Low precision conditions.

Electrode localization

The electrode localization was performed using pre- and post-implantation structural T1-weighted 1mm isotropic MRI scans as well as post-implantation CT scans. For each participant, the post-implantation MRI and CT scans were registered to the pre-implantation scan using a 6-parameter rigid body transformation implemented with Advanced Normalization Tools – ANTs (Avants et al., 2011). Electrodes were localized within MTL subregions using a high-resolution (.55 mm) in-house anatomical template with manual tracings of hippocampal subfields and parahippocampal gyrus subregions (M. A. Yassa & C. E. L. Stark, 2009). Regions of interest (ROIs) included the CA1, DG/CA3, subiculum (Sub), lateral and medial entorhinal cortex (LEC, MEC), and the perirhinal (PrC) and parahippocampal (PHC) cortices. Hippocampal subfield segmentation followed our previously published protocols (M. A. Yassa & C. E. L. Stark,

2009). The labeled template was resampled and aligned to each subject's pre-implantation scan using ANTs Symmetric Normalization, so that the labels could be used to guide localization. Each electrode location was determined by examining the co-registered pre- and post-implantation MRIs and identifying the ROI that corresponded to the center of the electrode artifact in the post-implantation MRI and CT. Cases in which electrodes were on the border between ROI's or between gray matter and white matter were noted as such. Outside the MTL, electrode localization was guided by a FreeSurfer cortical parcellation of the pre-implantation MRI (Fischl et al., 2004).

Data collection and preprocessing

Intracranial EEG data were recorded using a Nihon Khoden recording system, analog-filtered above 0.01 Hz and digitally sampled at 5000 Hz. After acquisition, data were demeaned and band-pass filtered from 0.3 Hz to 350 Hz using a two pass zero phase delay Butterworth infinite impulse response (IIRR) filter. Power spectra were examined to identify line noise and a Butterworth notch filter was used to remove 60 Hz noise and harmonics. All electrodes were re-referenced to a white matter electrode located on the same depth electrode probe. A neurologist (J.L.) with subspecialty training in epilepsy visually inspected continuous recordings from each session to identify all data with interictal epileptiform discharges. Data were also inspected for excessive noise, including broadband electromagnetic noise from hospital equipment. To avoid potentially biasing the results, the neurologist was blinded to trial information (e.g. stimulus onset and behavioral performance) as well as to electrode location. Only data

from recordings contralateral to the seizure source or outside of the seizure onset zone were used in subsequent analyses.

Gamma Power Analyses

Intracranial recordings were broken into event-related epochs (3 seconds pre-stimulus onset and 3 seconds post-stimulus offset) and convolved with complex Morlet wavelets, implemented using the FieldTrip toolbox, to obtain a measure of instantaneous power (Oostenveld, Fries, Maris, & Schoffelen, 2011). Center frequencies ranged from 1 to 150 Hz, with a spacing of 1 Hz and a variable cycle number of 4-15. Power was baseline corrected to the average pre-stimulus power across all trials (0.5 to 0.2 prior to stimulus onset), resulting in a measure of relative power per frequency (power divided by pre-stimulus power) at each time point. While we examined a wider range of power in the spectrograms (up to 150 Hz), we used an a priori gamma frequency range of 40-100 Hz for our gamma power analyses. This frequency range was based on prior literature showing MTL gamma activity in this range (Burke, Long, et al., 2014; Greenberg et al., 2015; Sederberg, Schulze-Bonhage, Madsen, Bromfield, Litt, et al., 2007) and reflected the dominant gamma frequency range that was influenced by task performance (Fig. S2.3). For the within-session analysis, we then averaged baseline corrected power over our gamma frequency range (40-100 Hz) and retrieval window (0.25-1 second post-stimulus onset). The start of the retrieval window was based on the time at which stimulus-evoked activity has been shown to emerge in the hippocampus following stimulus onset (Mormann et al., 2005; Staresina, Fell, Do Lam, Axmacher, & Henson, 2012). The end of the retrieval window (1 second post-stimulus onset) is the

time at which subjects were able to start moving the object. We took the absolute value of the angular error and logged the resulting values to account for the non-normal distribution of error. Pearson correlation was used to test the relationship between single trial power in each MTL electrode and error. P values from these correlations were then Bonferroni-corrected for the number of MTL electrodes in each patient (see Table 2.1 for the number of electrodes).

For the across-session analysis, electrodes were divided into nine regions: 1) the CA1 subfield, 2) the hippocampus, including the CA1, 3) the entorhinal, and parahippocampal cortices, 4) the lateral temporal cortex, 5) the insula, 6) the caudal prefrontal cortex (broadman area (BA) 6/8), orbitofrontal cortex, and dorsolateral prefrontal cortex (BA 9/10/46). Electrodes that were on the border between the CA1 subfield and other hippocampal subfields were included in the hippocampal region but not in the CA1 region. Regions where we had electrode contacts in fewer than three subjects (e.g. amygdala) were excluded from the analysis. There were not enough electrodes across subjects in either the DG/CA3 or subiculum to be able to look at activity separately within these regions. Power was baseline corrected to the average pre-stimulus power (as described above), and subsequently z-transformed separately within each session to account for differences in power and noise across sessions.

We used a cluster-based permutation approach implemented using the FieldTrip toolbox to examine the correlation between gamma power and error (including Guess condition) and precision (excluding Guess condition) at each time point within each

region (Oostenveld et al., 2011; Seth, 2010). T-statistics derived from regression coefficients were calculated at each time point (-.5 to 1.5 seconds post-stimulus onset) and then thresholded at an αlevel of 0.05. Adjacent time points that survived this thresholding were grouped into clusters, and cluster-level test statistics were calculated as the sum of the t-statistics within each cluster. A null distribution was formed by randomly shuffling the correspondence between gamma power and error (or precision) 1,000 times and taking the largest cluster-level test statistic produced by each iteration. P values of the observed, experimental clusters were calculated as the proportion of random shuffles that produced a test statistic larger that the test statistic of the observed clusters. We also used this method to examine the relationship between theta (3-8 Hz) power and error in each region and found a significant negative correlation between theta power and error during the retrieval window in CA1 and a significant positive correlation that emerged after the retrieval window in dlPFC (Fig. S2.5). Neither of these regions showed a significant correlation between theta power and precision. For Figures 2.5d-f and 2.6b, trials were divided into High precision, Low precision, and Guess conditions, then z-transformed power was averaged over the retrieval time window (0.25- 1s post-stimulus onset) and a one-way ANOVA was performed across the three conditions. In regions where we found a main effect of error, we tested for pairwise differences between conditions using post hoc Holm-Sidak tests.

The number of expected guesses in the High and Low precision conditions (S2.6) was balanced using the following method. The number of degrees spanned by each condition was calculated for each session and used to determine the number of

expected guesses in each condition as predicted by the uniform distribution. If there were more expected guesses in the Low precision condition, we added simulated ‘guesses’ to the High precision condition so that the number of High and Low precision guesses would be equal. These simulated ‘guesses’ were generated by taking the mean power in the Guess condition during the retrieval window. We also added the same number of simulated ‘null’ trials to the Low precision condition to keep trial count balanced across conditions. These ‘null’ trials were generated by taking the mean power in the Low precision condition during the retrieval window.

Granger Prediction Analysis

The preprocessed LFP was first downsampled to 250 Hz before obtaining the mean gamma power time series (40-100 Hz) during the full retrieval period (0-1s post stimulus onset). These data were epoched, detrended, and normalized over time and across trials to increase stationarity (Barnett & Seth, 2014). A model order of five was chosen for each session. This order was determined by the Bayesian information criteria, which was calculated using the Multivariate Granger Causality (MGVC) Matlab Toolbox (Solomon et al., 2017). The MGVC toolbox was also used to calculate the time-domain Granger prediction index for High precision, Low precision, and Guess trials for each CA1 and dlPFC electrode pair. The difference in Granger prediction values between conditions (e.g. High-Guess) was calculated for each electrode pair, averaged over electrode pairs within each session for each direction (CA1 to dlPFC and dlPFC to CA1), and then averaged across sessions. A null average difference distribution was created by shuffling the trial labels 500 times before calculating the difference in

Granger prediction values between conditions. These distributions of permuted difference values were then averaged first over electrode pairs and then across sessions, as described above (Solomon et al., 2017). The observed average Granger difference value was compared to this null average Granger difference distribution. P-values were calculated as the fraction of times the null average Granger difference values were equal to or more extreme than the observed average Granger difference value.

2.4 Results

***Task performance*.** Subjects (7 sessions from 4 patients) performed an object-location memory task as we recorded intracranial electroencephalogram (EEG). During the encoding phase, 100 objects were presented, one at a time, at random positions around the circumference of an invisible circle while subjects performed an incidental encoding task (Fig. 2.1). At test, the same objects were presented at the top of the circle, and subjects were instructed to use the mouse wheel to rotate the object to where it had appeared during encoding. Performance was measured as angular error, or the difference (in degrees) between where the subjects placed the object and its correct initial location.

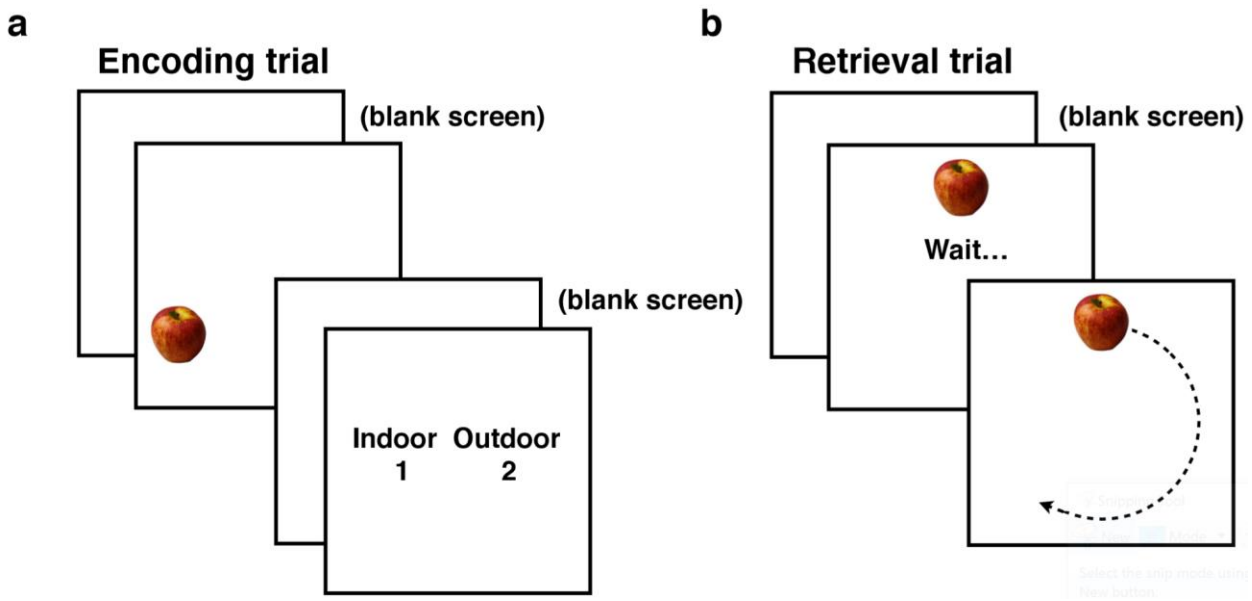

Figure 2.1. Spatial precision task. (a) During encoding, 100 objects were presented at random positions around the circumference of an invisible circle while subjects performed an incidental encoding task in which they were asked if each object was more likely to be found indoors or outdoors. ITI: 1.2 +/- 0.2 seconds ISI: 0.5 seconds. **(b)** At test, the same objects were presented at the top of the screen. After a 1 second wait period, subjects used the mouse wheel to rotate the object to where it appeared during encoding.

Across sessions, the distribution of angular error was centered around zero degrees (the correct location) and spanned the range of possible responses (-180° to 180°) (Fig. 2.2a). These error distributions can be modeled as a mixture of two distributions: a uniform distribution of errors and a von Mises distribution of errors (Fig. 2.2b) (Sutterer & Awh, 2016; Zhang & Luck, 2008). The uniform distribution reflects trials on which the subject had no memory for the location of the object and guessed randomly. The von Mises distribution, which is the circular analog of a Gaussian distribution, reflects trials on which the subject remembered the location of the object with some degree of precision.

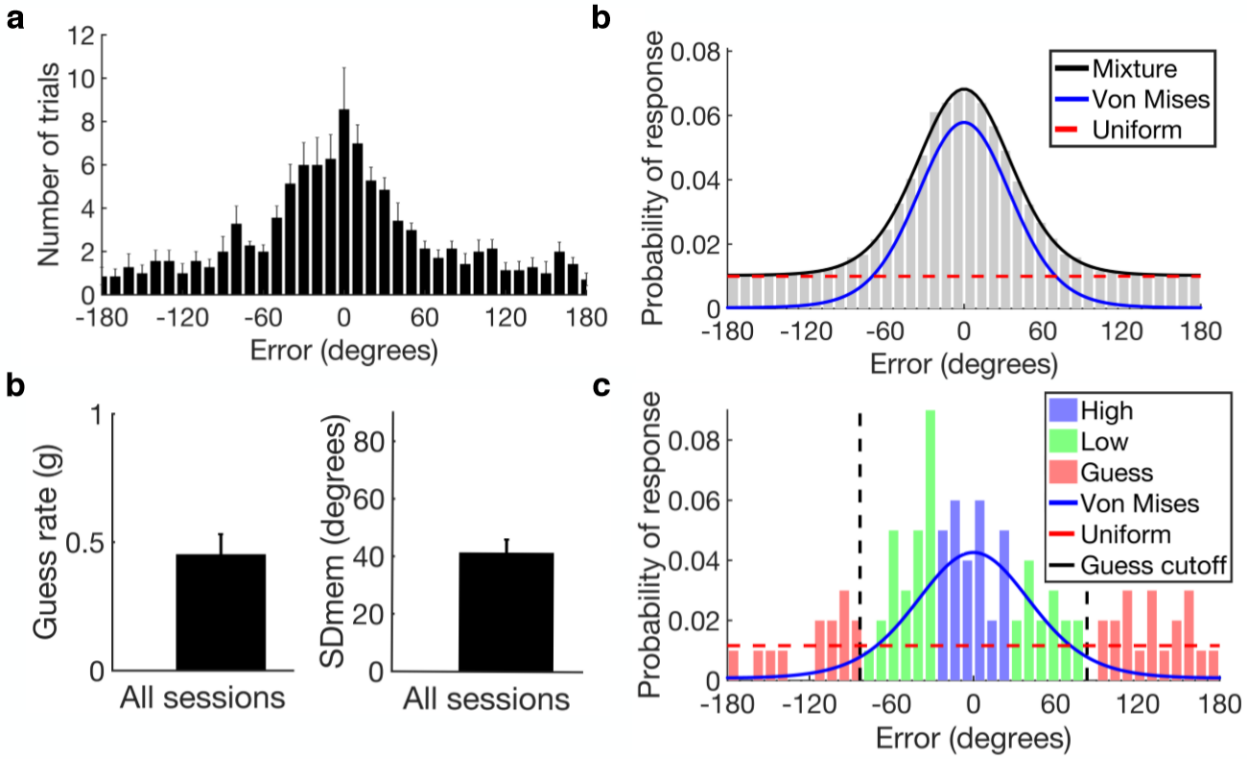

Figure 2.2. Mixture model and performance. (a) Histogram of errors across all sessions. **(b)** Example of a mixture model fit to simulated data. **(c)** Mean guess rate and SDmem across all sessions. **(d)** Example of a mixture model fit to the data from subject 1. The cutoff for trials placed in the Guess condition (+/-83; black dashed line) was derived from the cumulative distribution function of the von Mises distribution, i.e. 90% of trials that were remembered with some degree of precision fell within +/-83 (see text). Error bars indicate s.e.m.

We used the MemFit function of Memtoolbox in MATLAB (Jordan W Suchow et al., 2013), to obtain an estimate of two parameters describing these distributions: the guess rate (g), which reflects the area under the uniform distribution, and the standard deviation of the von Mises distribution (SDMem), which reflects the overall precision of responses that were not guesses. Figure 2.2C shows the mean value of these parameters across sessions (see Fig. S2.1 for parameter values for all sessions). The upper limit of the 95% credibility interval for each subject's guess rate was less than one, indicating that performance was above chance for all subjects. An example of the

mixture model fit of Subject 1's angular error is shown in Figure 2.2d. In addition to using a continuous measure

Patient information, hemisphere included in the analyses, number of MTL contacts, and number of dlPFC contacts.

Subject	Hand	Epileptogenic region	Coverage	Hemisphere analyzed	Number of sessions	MTL contacts	dlPFC contacts
1	R	Right TLE	Bilateral	L	1	7 (6 CA1)	7
2	L	Right medial frontal/supplementary motor area	Bilateral	Bilateral	3	9 (2 CA1)	6
3	R	Left TLE	Bilateral	R	1	5 (2 CA1)	10
4	R	Right TLE	Bilateral	L	2	11 (0 CA1)	8
Total						32	31

L, left; R, right; TLE, temporal lobe epilepsy.

of error, in subsequent analyses we also divided trials into three conditions, High precision, Low precision, and Guess. We used the cumulative distribution function of the von Mises distribution estimated for each session to determine which trials to place in the Guess condition. Trials that had less than a 10% chance of being remembered with some degree of precision were placed in the Guess condition. For example, in subject 1, the middle 90% of the von Mises distribution spans +/-83°, so trials with error greater/less than +/-83° were placed in the Guess condition (Fig. 2.2d). As such, across sessions most of the Guess trials were likely guesses. The remaining trials were sorted by error and split evenly into the High and Low precision conditions.

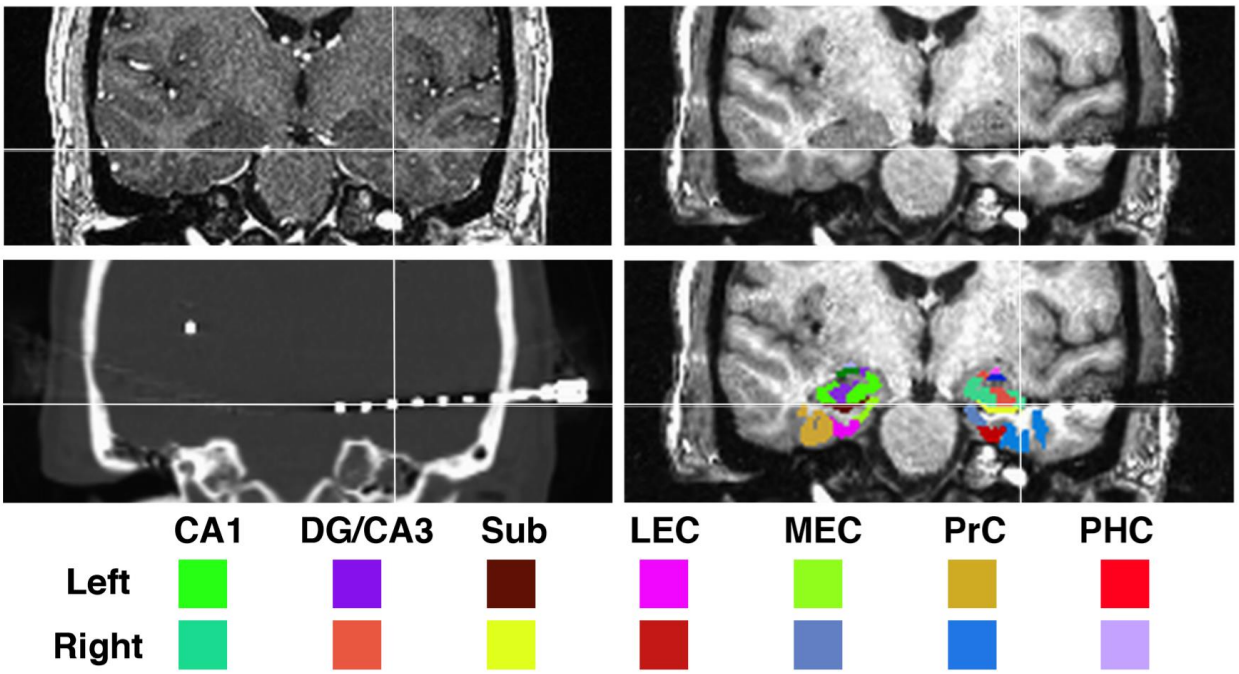

Figure 2.3. Example MRIs, CT, and template for a single subject. Electrodes were localized in each subject using co-registered pre-implantation (top left), post-implantation MRI (top right), and CT (bottom left) scans. A high-resolution template labeled with medial temporal lobe (MTL) subregions was aligned to each subject's pre-implantation scan to guide electrode localization. Regions of interest (ROIs) in the MTL included the CA1, DG/CA3, subiculum (Sub), lateral and medial entorhinal cortex (LEC, MEC), and the perirhinal (PRC) and parahippocampal (PHC) cortices. The template also provided labels for amygdala nuclei, which can be seen in the figure but were not included in the analysis.

***Electrode localization*.** Depth electrodes were localized using co-registered pre- and post-implantation MRIs, as well as registration to a high resolution anatomical atlas with manual tracings of hippocampal subfields and MTL subregions (Fig. 2.3) (Zheng et al., 2017). Co-registered post-implantation CTs were also used to help determine the center of each electrode artifact. All subjects had electrodes localized to the hippocampus and dlPFC, and three out of four subjects had electrodes localized to the CA1 subfield (see Table 2.1 for number of CA1 and dlPFC contacts for each subject; see S2.2 for number of contacts in each MTL subregion across subjects). Only data from recordings contralateral to the seizure source or outside of the seizure onset zone were used in subsequent analyses.

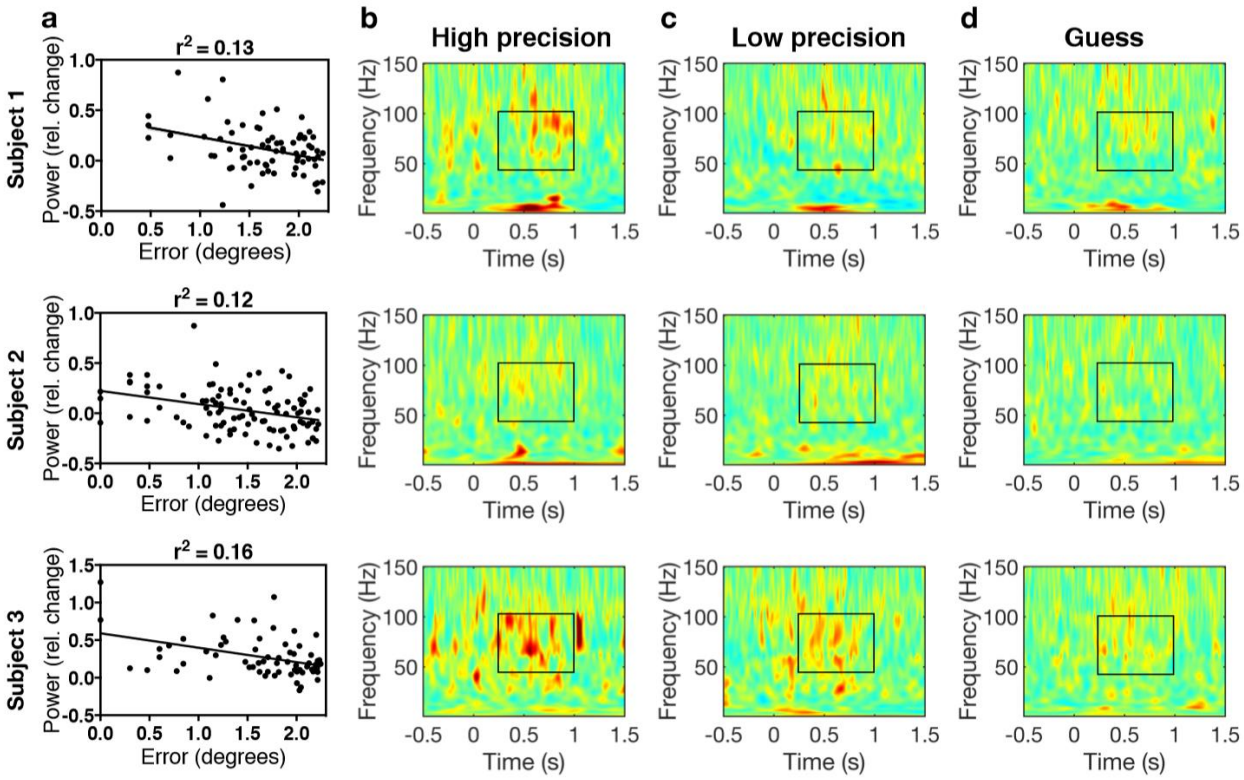

Figure 2.4. Within session CA1 gamma power predicts error. a, Trial-by-trial Pearson correlation between mean gamma power and angular error. **b-d**, Spectrograms showing mean power across High Precision **(b)**, Low Precision **(c)**, and Guess **(d)** trials for the CA1 electrodes shown in (A). Stimulus onset is at time zero and the frequency range (40-100 Hz) and time period (0.25-1 second post-stimulus onset) of interest are indicated by the black rectangle.

***CA1 gamma power predicts error within sessions*.** We first examined mean gamma power (40-100 Hz) over the retrieval window (0.25-1 second post-stimulus onset) within each session. The start of the a-priori retrieval window was based on the time at which stimulus-evoked activity has been shown to emerge in the hippocampus following stimulus onset (Mormann et al., 2005; Staresina et al., 2012), while the end of the retrieval window (1 second post-stimulus onset) is the time at which subjects were able to start moving the object. The absolute value of the angular error was logged to account for the non-normal distribution of error. We found a correlation between gamma power and logged error in all three subjects that had electrodes localized to the CA1

subfield (Subject 1: P = 0.002, n = 74; Subject 2: P = 0.0003, n = 98; Subject 3: P = 0.0008, n = 63; all P < .05, Bonferroni corrected for number of MTL electrodes) (Fig. 2.4a, see Table 2.1 for number of MTL electrodes tested). To better visualize the relationship between gamma power and error, spectrograms for High precision, Low precision, and Guess trials for the CA1 electrodes shown in Figure 2.4a are included in Figure 2.4b-d. While there is a smaller increase in gamma power relative to baseline across trials in subject 2, a correlation between gamma power and error is observed in the trial-by-trial analysis. In the within session analysis, the correlations in the CA1 subfield were the only ones that survived Bonferroni correction. However, the specificity of this effect should be interpreted with caution, as effects in other regions could be present but not strong enough to surpass the stringent statistical threshold for multiple comparison correction.

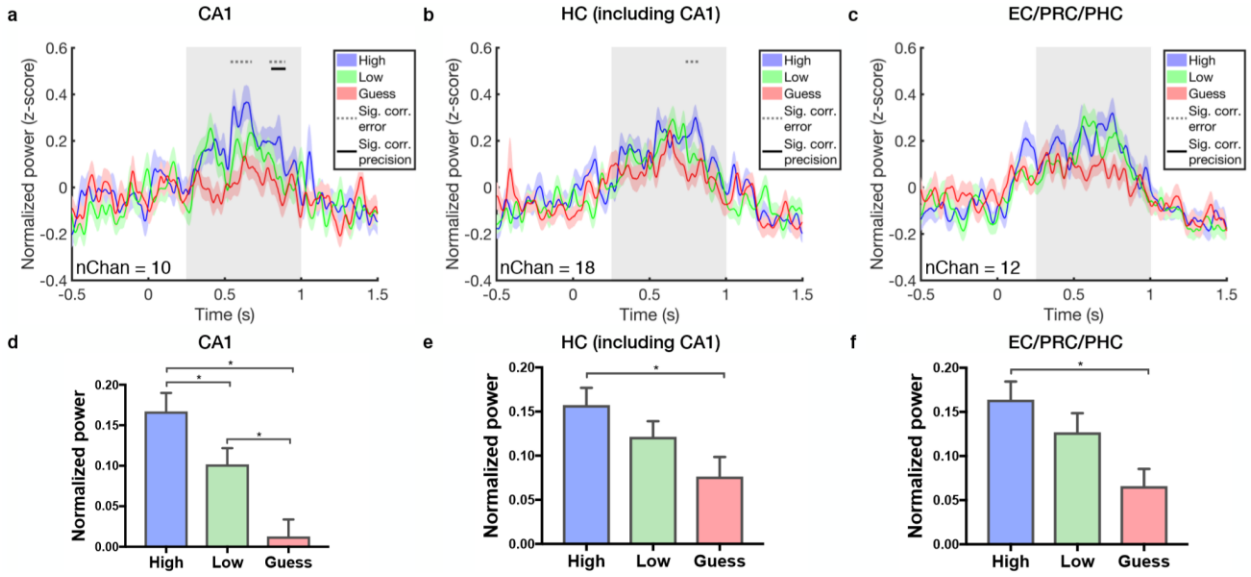

Figure 2.5. **Across session gamma power in the MTL. A-C,** Time course of gamma power in the CA1 subfield **(a)**, hippocampus (HC), including CA1, CA3/DG, and subiculum **(b),** and entorhinal (EC), perirhinal (PRC), and parahippocampal cortices (PHC) **(c).** Stimulus onset is at time zero and the retrieval window (0.25 to 1 second post-stimulus onset) is shaded in gray. Dotted gray horizontal lines indicate time points where there are significant correlations between gamma power and error ($p < 0.05$, cluster-corrected). Solid gray horizontal lines indicate time points where there are significant correlations between gamma power and precision (excluding Guess trials; $p < 0.05$, cluster-corrected). Colored

shaded regions indicate s.e.m. **d-f**, Mean gamma power over the retrieval window (0.25 to 1 second post-stimulus onset) for High precision, Low precision, and Guess conditions. Error bars indicate s.e.m. and * indicates $P < 0.05$.

Across sessions, CA1 gamma power predicts spatial memory precision. Figure 2.5a-c shows the time course of gamma power in the CA1 subfield, the hippocampus (HC, including CA1, DG/CA3, and subiculum), and the entorhinal, perirhinal, and parahippocampal cortices (EC/PRC/PHC) for High precision, Low precision, and Guess trials. First, we pooled trials from all conditions across sessions and tested for a correlation between gamma power and error in each MTL region. Using a cluster-based permutation approach to correct for multiple comparisons across time points, we found significant negative correlations between gamma power and error during the retrieval window in the CA1 subfield and HC (Fig. 2.5 a-c). To address the concern that these correlations were driven by a binary effect of retrieval success versus failure, we excluded trials that were likely guesses (i.e. the Guess condition) and reran the analyses. In this, as well as in subsequent analyses, we refer to correlations with 'precision' in analyses where the Guess condition was excluded. We found a significant correlation between gamma power and precision in the CA1 subfield beginning at 804 ms post-stimulus onset (Fig. 2.5a). In a complementary analysis, we averaged gamma power over the retrieval window (0.25-1s post-stimulus onset) and ran a two-way ANOVA with error (High Precision, Low Precision, and Guess) and region (CA1, HC, and EC/PRC/PHC) as fixed factors. We found a significant effect of error ($F(2, 1595) = 21.6$; $p = 5 \times 10^{-10}$), but no significant effect of region ($F(2, 1595) = 1.3$; $p = 0.28$) and no interaction between region and error ($F(4, 1595) = 0.81$; $p = 0.51$). Post hoc t-tests revealed a significant difference between High precision and Guess conditions in all

MTL regions (CA1 High vs. Guess: mean difference = 0.15, P < .05, corrected; HC High vs. Guess: mean difference = 0.08, P < .05, corrected; MTL High vs. Guess: mean difference = 0.1, P < .05, corrected) (Fig. 5d-f). We also found a significant difference between High and Low precision as well as between Low precision and Guess in the CA1 subfield (High vs. Low: mean difference = 0.07, P < .05, corrected; Low vs. Guess: mean difference = .09, P < .05, corrected). While the CA1 subfield was the only region to show significant correlations between gamma power and precision as well as a significant difference between High and Low precision, we do not mean to imply that there are not similar effects in other MTL regions.

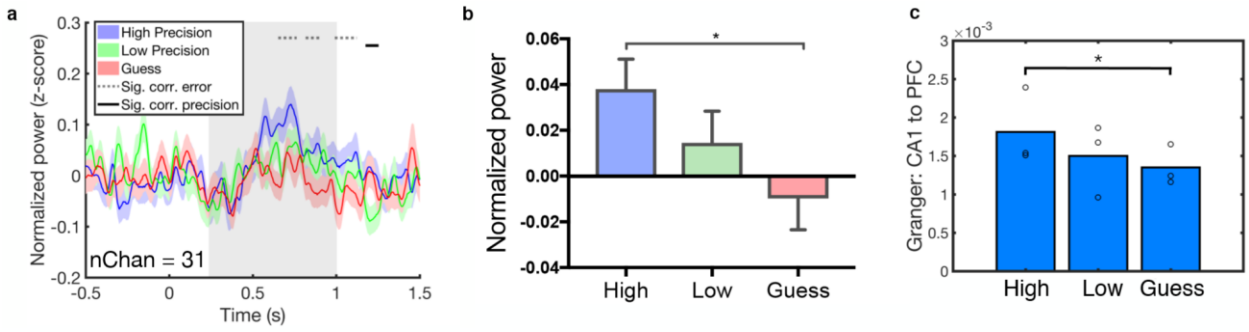

Figure 2.6. dlPFC gamma power predicts the precision of spatial memory retrieval. (a) Time course of gamma power in the dorsolateral prefrontal cortex (dlPFC). Stimulus onset is at time zero and the retrieval window (0.25 to 1 second post-stimulus onset) is shaded in gray. Dotted gray horizontal lines indicate time points where there are significant correlations between gamma power and error (p < 0.05, cluster-corrected). Solid gray horizontal lines indicate time points where there are significant correlations between gamma power and precision (excluding Guess trials; p < 0.05, cluster-corrected). Colored shaded regions indicate s.e.m. **(b)** Mean gamma power over the retrieval window for High precision, Low precision and Guess conditions. **(c)** Mean CA1 to dlPFC Granger prediction values for each condition. * indicates significantly greater CA1 to dlPFC directionality for High precision versus Guess trials as determined by permutation testing (P < 0.05). **(d)** Mean dlPFC to CA1 Granger prediction values for each condition.

***PFC gamma power lags CA1 in predicting spatial memory precision*.** We also found a negative correlation between gamma power and error during the retrieval window in dlPFC contacts (p < 0.05 cluster corrected) (Fig 2.6a). There was no effect of error during the retrieval window or at any time period post-stimulus onset in any of the

other regions we recorded from (see Fig. S2.4). Excluding the Guess condition, we found a significant correlation between gamma power and precision starting at 1175 ms post-stimulus onset (Fig 2.6a). Averaging power over the retrieval window, we found a main effect of error ($F(2, 613) = 3.17$, $P = 0.04$) and a significant difference between High precision and Guess conditions (mean difference = 0.05, $P < .05$, corrected) (Fig. 2.6b). Interestingly, we found that the significant correlations between gamma power and error as well as between gamma power and precision appeared later in the dlPFC than in the CA1 subfield (error effect: CA1 = 538 ms post-stimulus onset, dlPFC = 652 ms; precision effect: CA1 = 804 ms, PFC = 1175 ms). However, the timing of these effects should be interpreted with caution, as they might be subject to statistical thresholding effects resulting from the cluster-based correction over time points. For instance, while the dlPFC precision effect doesn't reach cluster-corrected significance until after the end of the retrieval period (i.e. after 1000ms), the effect is also present ($p < 0.05$, uncorrected) during the retrieval window. To further examine the relative timing and directionality of CA1 and dlPFC activity at retrieval, we performed a time-domain Granger prediction analysis using the gamma power time series for all sessions showing a significant correlation between gamma power and error ($P < 0.05$) in both CA1 and dlPFC electrodes (n = 3 subjects). Granger prediction provides a measure of directionality by testing if activity from region A (for example, the dlPFC) at one time point can be better predicted by knowing activity from region B (for example, the CA1) at past time points. We first calculated Granger prediction values for all CA1-dlPFC electrode pairs for High precision, Low precision, and Guess trials during the full retrieval period (0-1s post-stimulus onset), and then calculated the difference between

conditions (e.g. High-Guess) for each electrode pair. We then averaged these Granger difference values first over electrode pairs within sessions, then across sessions (n = 3), and then compared this averaged difference value to a null distribution (see Methods). We found greater CA1 to dlPFC directionality for High precision trials than for Guess trials ($P < 0.05$, permutation test; see Methods), indicating that activity associated with high precision spatial memory judgments starts earlier in the CA1 subfield (Fig. 2.6c). There was no significant difference between conditions (High vs. Guess, High vs. Low, Low vs. Guess) in dlPFC to CA1 Granger prediction values ($P > 0.05$, permutation test)(Fig. 2.6d).

Since the Low precision condition tended to cover a greater proportion of the estimated uniform distribution (see Figure 2.2d), the number of expected guesses in the Low precision condition was slightly higher than in the High precision condition (on average, there were 2.8 more expected guesses per session in the Low precision condition than in the High precision condition). As such, it is possible that the observed differences in CA1 gamma power across the High and Low precision conditions were driven by a slightly higher number of guesses in the Low precision condition. However, balancing the number of expected guesses in the High and Low precision conditions using simulated 'guesses' derived from the mean power in the Guess condition (see SI Materials and Methods) produced similar results (Main effect of error: $F(2, 462) = 12.5$, $p = 5 \times 10^{-6}$; High vs. Guess: mean diff. = 0.14, $p = 3 \times 10^{-6}$; High vs. Low: mean diff. = 0.05, $p = 0.06$; Low vs. Guess: mean diff. = 0.09, $p = 0.004$) (Fig. S2.6). Since PFC activity is known to be modulated before the initiation of action, another possible

confound is that the dlPFC gamma effect is due to differences in movement onset after the delay period (0-1s post-stimulus onset) as patients may start moving the object earlier for more precise trials (Harlow & Yonelinas, 2016; Miller & Cohen, 2001). However, we found no significant correlation between angular error and movement onset, indicating that this factor was not driving the effects (Kendall's Tau = -0.006; p = 0.86; the data from session 1 was not included in this analysis as we did not record mouse movements for this session). Gamma power at encoding also did not predict subsequent performance on the task (Fig. S2.8). We additionally performed control analyses to ascertain that the gamma effects in the CA1 and dlPFC were not associated with the distance the object was moved on the screen or trial order (Fig. S2.7, S2.9).

2.5 Discussion

Prior studies have shown that the hippocampus and PFC are involved in associative memory retrieval. However, the contributions of these regions to the precision of remembered associations are poorly understood. One possibility is that activity within these regions reflects a binary signal of retrieval success versus failure. Alternatively, activity within these regions could track the precision, or fidelity, of the retrieved memory. When we included guess trials in our analyses, we found increased hippocampal and prefrontal gamma power in highly precise trials vs. trials that were likely guesses (i.e. the Guess condition). This is consistent with prior work showing increased activity in these regions associated with retrieval success (Blumenfeld & Ranganath, 2007; Burke et al., 2015; Eichenbaum et al., 2007). However, we additionally showed negative correlations between hippocampal and prefrontal gamma

power and error magnitude, suggesting that increased activity in these regions tracks representational fidelity. Our additional analyses after excluding the Guess condition further indicated that activity in these regions was associated with the precision of the spatial judgments. Overall, these results suggest that these regions are not only involved in retrieval success, but also in indexing the precision of retrieved memories.

Across sessions, we found significant correlations between CA1 gamma power and precision and significant differences between the High and Low precision conditions. The CA1 subfield has long been known to be involved in spatial processing and memory. For instance, CA1 place cells provide precise representations of specific locations in an environment and can code for associations between objects and locations (Komorowski, Manns, & Eichenbaum, 2009; Moser, Rowland, & Moser, 2015). While the current task does not involve subjects physically moving through space, studies in primates have shown that the CA1 also contains spatial 'view cells' that respond whenever a monkey looks towards specific locations in the environment (Rolls, 1999). More recently, studies in rats have found increased place cell firing and gamma power (60-100 Hz) in the CA1 as animals explored familiar objects in novel locations (Larkin, Lykken, Tye, Wickelgren, & Frank, 2014; Zheng, Bieri, Hwaun, & Colgin, 2016). However, while the CA1 subfield was the only region to show significant correlations between gamma power and precision as well as a significant difference between High and Low precision, we do not mean to imply that there are not similar effects in other MTL regions.

The neural mechanisms generating high frequency gamma activity in humans remains a prominent question in the field. One possibility is that high frequency gamma activity reflects gamma oscillations generated by local interactions between interneurons and pyramidal neurons (Buzsaki & Wang, 2012). As gamma phase synchronization can enhance spike-timing dependent plasticity, these oscillations are thought to play a mechanistic role in memory processing (Buzsaki & Wang, 2012). Accumulating evidence from the rodent literature suggests that oscillatory gamma can be split into two types, ‘slow gamma’ (25-55 Hz) and ‘fast gamma’ (60-100 Hz), that play distinct roles in memory encoding and retrieval (Colgin, 2016). As such, we examined the dominant frequency range influenced by task performance and found significant effects across our a priori frequency range (40-100 Hz) with peaks in the slow and fast gamma ranges (Fig. S2.3). The significance of these peaks remains unclear and whether two different neural mechanisms may give rise to these effects remains an outstanding question. Another possibility is that the high frequency activity observed in humans does not reflect oscillatory activity, but rather a broadband shift of the power spectrum stemming from increased neuronal spiking (Buzsaki & Wang, 2012; Miller et al., 2009). In this view, high frequency activity is non-oscillatory and does not play a mechanistic role in memory processing, but can be thought of as a biomarker for local activity (Rich & Wallis, 2017; Watson, Ding, & Buzsaki, 2018). Given that the frequency range of this broadband shift overlaps with that of oscillatory gamma activity, a third possibility is that high frequency gamma power reflects a combination of these processes (Burke et al., 2015; Kucewicz et al., 2017). In each view, however, gamma power can be thought of as a spatially precise indicator of local excitatory activity. In light of our results, this

suggests that increasing excitatory activity in the CA1 and dlPFC is associated with increasing memory precision.

A number of recent studies have implicated the extended hippocampal network in spatial memory precision (Koen, Borders, Petzold, & Yonelinas, 2017; Kolarik et al., 2016; Nilakantan, Bridge, Gagnon, VanHaerents, & Voss, 2017). For example, Nilakantan et al. found that stimulation of the posterior cortical-hippocampal network using TMS in humans increased precision on an object-location memory task similar to the one used in the current study. In a case study that examined the performance of a patient with MTL damage on a virtual Morris water maze, Kolaric et al. found that while the patient tended to search in the general vicinity of the correct location, the precision of her search path was significantly lower than controls. These findings provide convergent evidence that the hippocampus facilitates the precise recall of learned associations. Our findings are consistent with these studies but further propose a role specifically for hippocampal CA1 and dlPFC as well as a temporal relationship between the two that may be an important facet of spatial memory retrieval.

Our results also are convergent with findings from studies that have shown that hippocampal activity tracks *subjective* measures of memory strength (e.g. confidence or vividness) (Geib, Stanley, Wing, Laurienti, & Cabeza, 2017; Rutishauser et al., 2010; Rutishauser et al., 2015). While subjective ratings are associated with performance accuracy (Harlow & Yonelinas, 2016), these measures could be influenced by a variety of factors including subject bias. Here, we fit a mixture model to an objective measure of

precision to estimate the probability of guessing. This approach is less likely to be contaminated by subjective biases.

In addition to hippocampal CA1, we also observed that gamma power in the dlPFC at retrieval was associated with spatial memory precision. The dlPFC is reciprocally connected to the MTL and has been implicated in a wide variety of memory processes (Blumenfeld & Ranganath, 2007). For instance, fMRI studies have shown increased activity in the dlPFC when subjects retrieve contextual details about a cue, such as the location of a studied object (Dobbins et al., 2002). A common interpretation of these findings is that the dlPFC is involved in maintaining, or monitoring information retrieved from episodic memory (Dobbins et al., 2002), which is consistent with the dlPFC's well recognized role in working memory (Passingham & Wise, 2012). The precision effect observed in the CA1 region preceded the onset of the effect in dlPFC, which is consistent with this interpretation of the dlPFC's role, as it involves post-retrieval processes. The Granger prediction analysis further corroborated this finding, indicating that activity associated with highly precise spatial memory judgments appears earlier in the CA1 than in the dlPFC.

Overall, our results suggest a role for local processing within the hippocampus and dlPFC in indexing the precision of spatial associative memory. The correlations between gamma power and the precision of spatial memory judgments raise the possibility that disrupting gamma activity in CA1 and/or dlPFC may reduce the precision of memory

judgments, thereby establishing a causal link. Future studies using electrical disruption in humans or more invasive techniques in rodents can test these hypotheses directly.

CHAPTER 3: MEDIAL TEMPORAL AND PREFRONTAL HIGH FREQUENCY ACTIVITY DURING SPATIAL LEARNING

3.1 Abstract

The ability to learn novel associations is thought to depend on local processing within the medial temporal lobe (MTL) and prefrontal cortex (PFC) as well as functional interactions between these two regions. However, the ways in which the MTL and PFC contribute to associative learning in humans remain poorly understood. We tested pre-surgical epilepsy patients with depth electrodes implanted in both the MTL and PFC using a spatial memory task in which subjects attempted to learn object-location associations over the course of three training blocks. During encoding, subjects were shown objects at random locations along the circumference of an invisible circle. For each training block, the same objects were shown at the top of the circle and subjects used a dial to rotate the object to where it appeared during encoding. After subjects finished placing each object, the object was shown in the correct location for one second as feedback. At retrieval, we found greater high frequency gamma (40-100 Hz) power in the MTL and dorsolateral PFC (dlPFC) for low error trials. The opposite pattern of activity was observed at feedback, with greater MTL and dlPFC gamma power for high error trials. Increased MTL activity at feedback also predicted greater decreases in error from one training block to the next, indicating that these error signals are involved in updating memory representations or modifying incorrect associations during learning. Overall, these data suggest putative mechanisms for the learning of object-location associations.

3.2 Introduction

The ability to learn novel associations is a critical feature of episodic memory. A wealth of evidence indicates that medial temporal and prefrontal networks play a crucial role in tasks involving learned associations, such as between an object and a location. Convergent studies in rodents, monkeys, and humans have found that activity within the medial temporal lobe (MTL) during retrieval tracks the acquisition of novel associations (Igarashi et al., 2014; Ison, Quian Quiroga, & Fried, 2015; Law et al., 2005; Rutishauser, 2008; Suthana et al., 2015; Wirth et al., 2009). Likewise, single unit recordings in monkeys have shown that neurons in the prefrontal cortex (PFC) at retrieval change their firing in parallel with learning (Brincat & Miller, 2015; Histed, Pasupathy, & Miller, 2009). As novel associations are often not learned in a single episode, the ability to process and incorporate information about feedback is an important component of associative learning. Both MTL and PFC activity has been found to signal trial outcome at feedback, with single unit recordings showing cells that selectively increase firing for both correct and incorrect trials (Brincat & Miller, 2015; Wirth et al., 2009). However, the ways in which activity within these networks reflects trial outcome in humans is poorly understood. Additionally, whether feedback signals in these regions predict subsequent associative learning performance has not been previously shown.

To address this question, we tested pre-surgical epilepsy patients with depth electrodes implanted in both the MTL and dorsolateral PFC (dlPFC) on a variant of a commonly used object-location memory task (Reagh & Yassa, 2014; Rudoy, Voss, Westerberg, &

Paller, 2009). During encoding, 30 objects were presented at random locations along the circumference of an invisible circle. For each of the three training blocks, the same objects were shown one at a time at the top of the circle and subjects used a dial to rotate the object to where it appeared during encoding. After subjects finished placing each object, it was shown in the correct location for one second as feedback. After the final training block, a final test was given with no feedback. Performance was measured in angular error, or the distance (in degrees) between where subjects placed the object and the correct location. Using a variant of this task in which subjects were given only one shot to learn the object-location associations (i.e. no training), we found a negative correlation between MTL and dlPFC gamma power (40-100 Hz), thought to reflect local excitatory activity, and error at retrieval, indicating that activity within these regions tracks representational fidelity (Stevenson et al., 2018). Here, we predicted that we would replicate these results, showing increased MTL and dlPFC gamma power at retrieval for low error trials. In addition, we predicted that MTL and dlPFC gamma power at feedback would predict error, and that the magnitude of this response would predict subsequent performance on that object-location association.

3.3 Materials and methods

Participants

Subjects were 9 patients (5 female, 4 male, age 21-69) who had stereotactically implanted intracranial depth electrodes (Integra or Ad-Tech, 5-mm inter-electrode spacing) placed at the University of California, Irvine Medical Center to localize the seizure onset zone for possible surgical resection. Informed consent was obtained from

each subject prior to testing and the research protocol was approved by the IRB of the University of California, Irvine. Electrode placement was exclusively guided by clinical needs.

Spatial learning task

Thirty images of common objects were selected from a set previously used by our group (S. M. Stark, R. Stevenson, C. Wu, S. Rutledge, & C. E. Stark, 2015). Images were presented on a laptop computer screen set at a comfortable distance from the patient. Three hundred and sixty locations on the computer screen were generated along the circumference of a circle centered on the screen with a spacing of 1°. Prior to encoding, subjects were told that they would be shown objects at different locations on the computer screen and were asked to try to remember the location of each object. During encoding, the 30 objects appeared one at a time at pseudorandomly assigned circle locations (Figure 1; 1.2 +/- 0.2 second ITI). During each of the 3 training blocks, subjects were shown the same objects again in pseudorandom order, this time at the top of the screen. Subjects were instructed to wait 1 second (until text that read 'Wait…' disappeared from the screen) before using a mouse wheel to move the object to where it appeared during encoding. Subjects pressed the space bar to indicate that they were finished placing the object. The object was then shown in the correct location for one second as feedback. After the third training block, there was a final test block in which no feedback was given. There was a short (<1 minute) break after the encoding phase and between each training/test block during which task instructions were read. If

subjects performed more than one session, new objects and locations were used. No more than one session was performed on each day.

Behavioral analysis

Error on the spatial learning task was measured as the number of degrees between where subjects placed the object and the correct location. Histograms were used to examine the distribution of error values across and within task blocks. We used mixture modeling, as implemented by the MemFit function of Memtoolbox (Suchow, Brady, Fougnie, & Alvarez, 2013), to obtain an estimate of two parameters describing these distributions: the guess rate (g), which reflects the area under the uniform distribution, and the standard deviation of the von Mises distribution (SDMem). We first fit the model using trials from all training and test blocks. Trials that had less than a 10% chance of being remembered with some degree of precision based on the von Mises distribution of this model were placed in the high error condition. The remaining trials were sorted by error and split evenly into the medium and low error conditions. We then fit the model using trials within each block (i.e. the model was fit separately for training blocks 1 and 2) to determine how the guess rate and precision (SDMem) changed across task blocks.

Electrode localization

The electrode localization was performed using pre- and post-implantation structural T1-weighted 1mm isotropic MRI scans as well as post-implantation CT scans. For each participant, the post-implantation MRI and CT scans were registered to the pre-

implantation scan using a 6-parameter rigid body transformation implemented with Advanced Normalization Tools – ANTs (Avants et al., 2011). Electrodes were localized within MTL subregions using a high-resolution (.55 mm) in-house anatomical template with manual tracings of hippocampal subfields and parahippocampal gyrus subregions (M. A. Yassa & C. E. Stark, 2009). Hippocampal subfield segmentation followed our previously published protocols (M. A. Yassa & C. E. Stark, 2009). The labeled template was resampled and aligned to each subject's pre-implantation scan using ANTs Symmetric Normalization, so that the labels could be used to guide localization. Each electrode location was determined by examining the co-registered pre- and post-implantation MRIs and identifying the ROI that corresponded to the center of the electrode artifact in the post-implantation MRI and CT. Cases in which electrodes were on the border between ROI's or between gray matter and white matter were noted as such. Outside the MTL, electrode localization was guided by a FreeSurfer cortical parcellation of the pre-implantation MRI (Fischl et al., 2004).

Data collection and preprocessing

Intracranial EEG data were recorded using a Nihon Khoden recording system, analog-filtered above 0.01 Hz and digitally sampled at 5000 Hz. After acquisition, data were demeaned and band-pass filtered from 0.3 Hz to 350 Hz using a two pass zero phase delay Butterworth infinite impulse response (IIRR) filter. Power spectra were examined to identify line noise and a Butterworth notch filter was used to remove 60 Hz noise and harmonics. All electrodes were re-referenced to a white matter electrode located on the same depth electrode probe. A neurologist (J.L.) with subspecialty training in epilepsy

visually inspected continuous recordings from each session to identify all data with interictal epileptiform discharges. Data were also inspected for excessive noise, including broadband electromagnetic noise from hospital equipment. To avoid potentially biasing the results, the neurologist was blinded to trial information (e.g. stimulus onset and behavioral performance) as well as to electrode location. Only data from recordings contralateral to the seizure source or outside of the seizure onset zone were used in subsequent analyses.

Gamma Power Analyses

Intracranial recordings were broken into event-related epochs (3 seconds pre-stimulus onset and 3 seconds post-stimulus offset) and convolved with complex Morlet wavelets, implemented using the FieldTrip toolbox, to obtain a measure of instantaneous power (Oostenveld et al., 2011). Center frequencies ranged from 1 to 150 Hz, with a spacing of 1 Hz and a variable cycle number of 4-15. Power was baseline corrected to the average pre-stimulus power across all trials (0.5 to 0.2 prior to stimulus onset), resulting in a measure of relative power per frequency (power divided by pre-stimulus power) at each time point. Power was then z-transformed separately within each session to account for differences in power and noise across sessions. We then averaged normalized power over our a priori gamma frequency range of 40-100 Hz, based on prior literature showing MTL and dlPFC gamma activity in this range (Burke, Long, et al., 2014; Greenberg et al., 2015; Sederberg, Schulze-Bonhage, Madsen, Bromfield, McCarthy, et al., 2007; Stevenson et al., 2018). Next, we averaged gamma power across electrodes located within the MTL, including electrodes in the hippocampus as

well as the entorhinal, perirhinal, and parahippocampal cortices, and within the dlPFC (Broadman area (BA) 9/10/46). To examine the specificity of effects, we also ran analyses on regions outside of the MTL and dlPFC including the lateral temporal cortex, the insula, the caudal prefrontal cortex (BA 6/8), orbitofrontal cortex, and anterior cingulate cortex.

We used a cluster-based permutation approach implemented using the FieldTrip toolbox to test for differences in gamma power across task blocks (T1-T3, test) and conditions (high, medium, and low error) at each time point within each region (Oostenveld et al., 2011). In order to test for correlations between gamma power and error, we averaged gamma power over 100ms sliding windows and calculated the Pearson correlation between gamma power and angular error at intervals of 20ms. For this analysis, angular error was logged to account for the non-normal distribution of error. We used permutation testing to ensure that the observed correlations were not driven by outliers or other biases in the data. A null distribution of r values was created by shuffling the trial labels between conditions 1000 times. We derived p-values for the observed r values using the cumulative distribution function of these distributions. We used partial correlations to test for associations between gamma power at feedback for high error trials and the subsequent change in error from one block the next, controlling for error on the earlier task block (i.e. the association between gamma power at feedback on a high error trial at T1 and the change in error for that object-location association from T1 to T2, controlling for error on that trial at T1). P-values for the observed rho values were obtained via permutation testing as described above.

3.4 Results

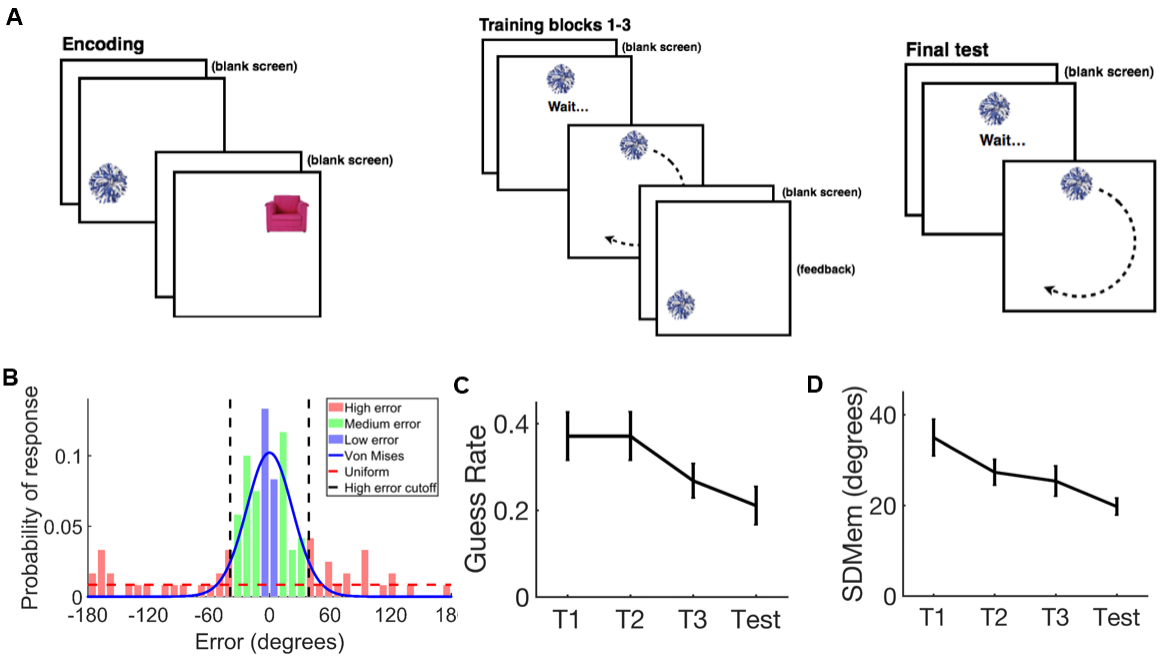

Figure 3.1. Task schematic and performance. A. During encoding, 30 objects were presented at random positions along the circumference of an invisible circle. During the 3 training blocks, the same objects were presented at the top of the screen. After a 1 second wait period, subjects rotated the object to where it appeared during encoding. After subjects finished placing the object, it was shown in the correct location for 1 second as feedback. No feedback was given during the final test phase. B. Example of a mixture model fit of all trials for subject 1. The cut off for high error trials across blocks was derived from the cumulative distribution function of the von Mises distribution, i.e. 90% of trials estimated to be remembered fell within +/-38 degrees of the correct location. C-D, Mean guess rate (C), and SDMem across sessions for training blocks 1-3 (T1-T3) and test.

Task performance. Subjects (21 sessions from 9 patients) performed a spatial learning task as we recorded intracranial electroencephalogram (EEG). During the encoding phase, 30 objects were presented, one at a time, at random positions around the circumference of an invisible circle (Fig. 3.1). Prior to the encoding phase, subjects were told that they would be tested on the location of each object. Following encoding, there were three training blocks during which each object was shown again, this time at the top of the circle, and subjects were instructed to use the mouse wheel to rotate the

object to where it appeared during encoding. Subjects were asked to wait 1 second (until text that read ‘Wait…’ disappeared from the screen) before beginning to rotate the object and to press the space bar when they were finished placing the object. After each trial, the object appeared on the screen in the correct location for 1 second as feedback. During the final test phase, subjects were again asked to rotate each object to the correct location, though this time no feedback was given. The inter-trial interval (ITI) was 1.2 +/- 0.2 seconds and the interstimulus interval (ISI), meaning the time between when the subjects finished placing the object and when it was shown in the correct location as feedback was fixed at 0.5 seconds for subjects 1-2 and variable (0.4 +/- 0.2 seconds) for subjects 3-9. Performance was measured in angular error, or the distance (in degrees) between where subjects placed the object and the correct location. If subjects performed more than one session, new objects and locations were used. No more than one session was performed on each day.

Figure 3.1B shows the distribution of error across all trials for subject 9 (session 21) (see S3.1 for error distributions for all sessions). These error distributions can be modeled as a mixture of two distributions: a uniform distribution of errors and a von Mises distribution of errors (Fig. 3.1B) (Sutterer & Awh, 2016; Zhang & Luck, 2008). The uniform distribution reflects trials on which the subject had no memory for the location of the object and guessed randomly. The von Mises distribution, which is the circular analog of a Gaussian distribution, reflects trials on which the subject remembered the location of the object with some degree of precision. We used the cumulative distribution function of the von Mises distribution estimated for each session to

determine which trials to place in the high error condition. Trials that had less than a 10% chance of being remembered with some degree of precision were put into the high error condition. For example, in subject 1, the middle 90% of the von Mises distribution spans +/-38°, so trials with error greater/less than +/-38° were designated as high error trials (Fig. 3.2B). The remaining trials were sorted by error and split evenly into the medium and low error conditions.

We used the MemFit function of Memtoolbox in MATLAB (J. W. Suchow et al., 2013), to obtain an estimate of two parameters describing these distributions: the guess rate (g), which reflects the area under the uniform distribution, and the standard deviation of the von Mises distribution (SDMem), which reflects the overall precision of responses that were not guesses. Figure 3.1C-D shows the mean value of these parameters for T1-3 and for the final test (see Fig. S3.1 for error histograms and parameter values across blocks for all sessions). Guess rate, SDMem, and angular error all decreased over task blocks, indicating learning of the object-location associations (linear trend analysis, guess rate: $F(1, 60) = 14.6$, $p = 0.0003$, SDMem: $F(1, 60) = 23$, $p < 0.0001$; error: $F(1, 60) = 173$, $p < 0.0001$).

Patient information, hemisphere included in the MTL analyses, number of sessions, number of MTL contacts, number of dlPFC contacts.							
Subject	**Hand**	**Epileptogenic region**	**Coverage**	**MTL Hemisphere analyzed**	**Number of sessions**	**MTL contacts**	**dlPFC contacts**
1	R	Right TLE	SEEG	L	1	4 (1 HC)	4
2	R	Right TLE	SEEG	N/A	3	0	3
3	L	Right medial frontal/SMA	SEEG	Bilateral	4	9 (6 HC)	6
4	R	Left TLE	SEEG	R	4	5 (4 HC)	7
5	A	Bilateral TLE	SEEG	N/A	2	0	7
6	R	Right TLE	SEEG	L	3	4 (1 HC)	7
7	R	Right TLE	SEEG	L	1	6 (6 HC)	3
8	R	Right TLE	SEEG	N/A	1	0	5
9	R	Not determined	SEEG	N/A	2	0	2
Total					21	28	44
L, left; R, right; A, ambidextrous; TLE, temporal lobe epilepsy; SEEG, stereoelectroencephalography; SMA, supplementary motor area; HC, hippocampus							

Electrode localization. Electrodes were localized using co-registered pre- and post-implantation MRIs, as well as registration to a high resolution anatomical atlas with manual tracings of MTL subregions (Zheng et al., 2017). Co-registered post-implantation CTs were also used to help determine the center of each electrode artifact. Five subjects had electrodes localized to the MTL and 9 subjects had electrodes localized to the dlPFC (see Table 3.1 for number of MTL and dlPFC contacts for each subject; see S3.2 for number of contacts in each MTL subregion across subjects). Only data from recordings contralateral to the seizure source or outside of the seizure onset zone were used in subsequent analyses.

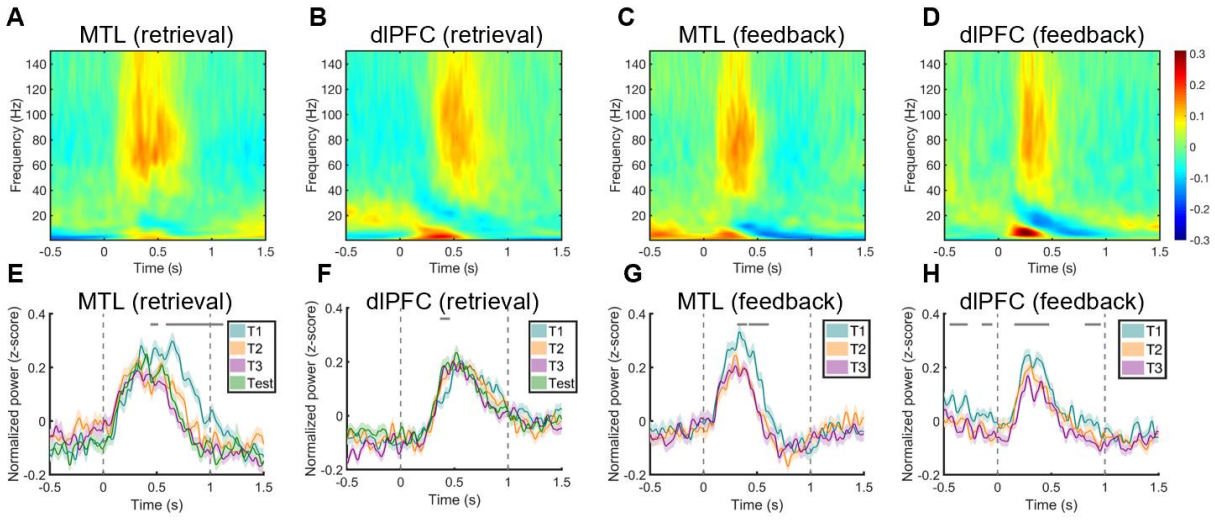

Figure 3.2. Gamma power decreases across task blocks. Spectrograms showing mean MTL and dlPFC power across all trials at retrieval (A-B) and feedback (C-D). Time course of gamma (40-100 Hz) power for each task block (T1-3, and Test for retrieval, T1-3 for feedback). Gray horizontal lines indicate time points where there are significant differences between task blocks (ANOVA, $p < 0.05$, cluster-corrected). Colored shaded regions indicate s.e.m.

Gamma power decreases across task blocks. We first examined how gamma power (40-100 Hz) changed over the course of the task during retrieval and feedback. Spectrograms for MTL and dlPFC power across all trials at retrieval (A-B) and feedback (C-D) are shown in Figure 3.2A-D. The time course of mean MTL and dlPFC gamma power (40-100 Hz) for all task blocks at retrieval and feedback is shown in Figure 3.2E-H. Using a cluster-based permutation approach to correct for multiple comparisons across time points, we found that gamma power decreased across blocks in the MTL at both retrieval and feedback (Fig. 3.2E, G) and in the dlPFC at feedback (Fig. 3.2H) (ANOVA $p < 0.05$, cluster-corrected). The decreases in gamma power at feedback were present in nearly all brain regions we recorded from, including the lateral temporal, orbitofrontal cortex, and anterior cingulate cortex (see S3.3-4 for results from all recording sites at retrieval and feedback). However, there were regions (e.g. the insula) and time periods where there was no significant difference in gamma power across

blocks suggesting that these changes were not driven by non-neural sources such as changes in electrode impedance over time. In order to determine if these decreases in gamma power predicted decreases in error from one task block to the next for specific object-location associations we averaged gamma power across time for the retrieval and feedback windows for each task block, then calculated the difference in power from one block to the next for specific object-location associations (e.g. gamma power during 2 retrieval for object 1 at T1 versus gamma power during retrieval for the same object at T2). At feedback, we found a positive correlation between the change in MTL gamma power from one block the next (e.g. T2-T1) and the change in error, indicating that decreases in gamma power predicted decreases in error for specific object-location associations in this region (Spearman's rho = 0.09, p = 0.02). However, these decreases in gamma power could also have been driven by increased familiarity with the objects themselves or with the task environment rather than by learning of the object-location associations. Furthermore, although MTL gamma power at retrieval also decreased across blocks, the correlation between the change in gamma power and change in error at retrieval in this region was trending in the opposite direction (Spearman's rho = -0 .05, p = 0.12). These results suggest that multiple, and perhaps opposing, factors were driving the changes in power across blocks.

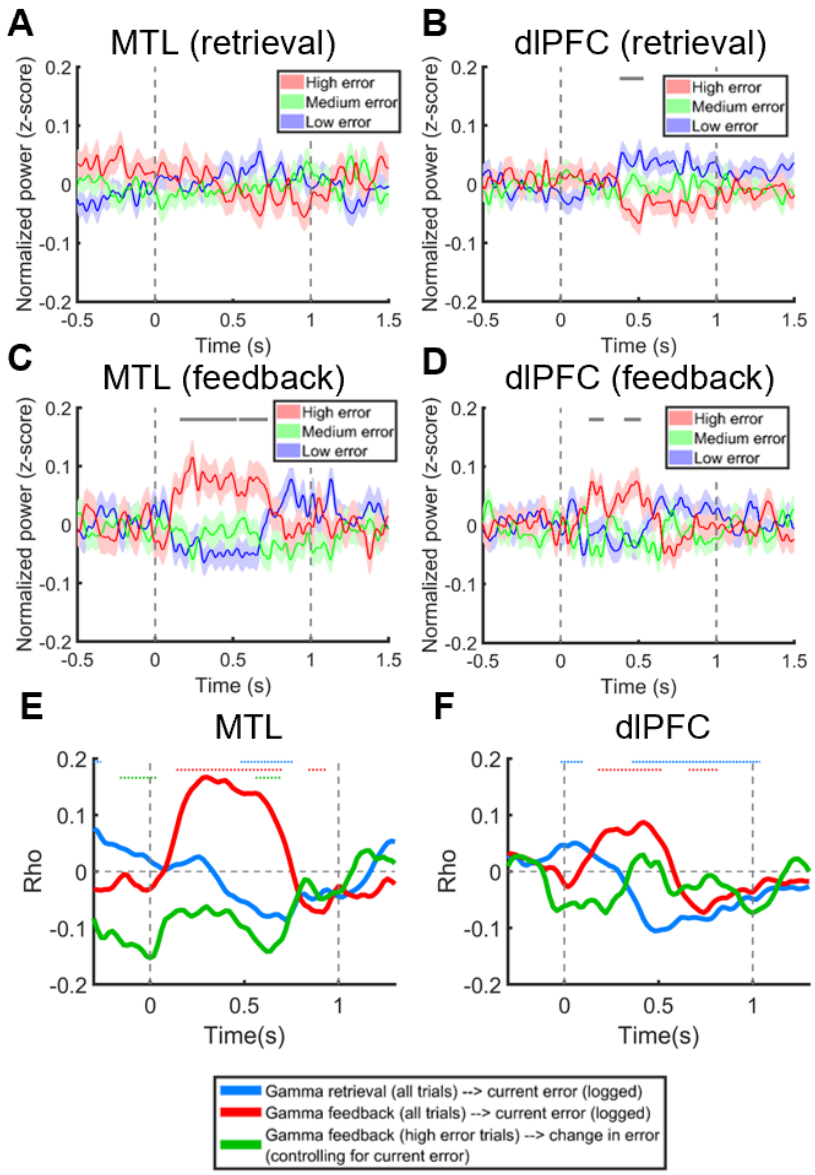

Figure 3.3. MTL gamma power predicts error within blocks and learning across blocks. A-D, Time course of MTL and dlPFC gamma power, normalized within blocks, for high, medium, and low error trials at retrieval (A-B) and feedback (C-D). Gray horizontal lines indicate time points where there are significant differences between conditions (ANOVA, $p < 0.05$, cluster-corrected). Colored shaded regions indicate s.e.m. **E-F,** Correlations between MTL (E) and dlPFC (F) gamma power and current error for at retrieval (blue), and at feedback (red), and partial correlations between gamma power at feedback and the subsequent change in error for high error trials from one task block to the next (green, controlling for current error).

MTL and dlPFC gamma power at retrieval and feedback predicts error within blocks. In order to examine the relationship between gamma power and error within

blocks we first normalized gamma power within each block (T1-3 and test) to control for changes in gamma power across blocks. Using a cluster-based permutation approach to correct for multiple comparisons across time points, we found greater gamma power for lower error trials in the dlPFC at retrieval (ANOVA, $p < 0.05$, cluster-corrected). We found the opposite pattern of activity during feedback, with greater gamma power for high error trials in both regions (Fig. 3C-F). No other region we recorded from showed a significant difference in gamma power between high, medium, and low error trials during the retrieval window (S3.5). However, multiple regions, including the anterior cingulate cortex and caudal prefrontal cortex, showed increased gamma power for high error trials at feedback, indicating that this effect was relatively widespread (ANOVA, $p < 0.05$, cluster-corrected) (S3.6). We also found a marginal effect of increased gamma power at encoding for trials that were subsequently designated low error trials at training block 1 (ANOVA cluster p-value = 0.09, cluster corrected) (S3.7).

Since there were fewer high error trials then there were medium or low error trials, we performed control analyses to make sure observed differences between conditions were not due to differing numbers of trials across conditions. To address this issue, we sorted trials within each block by error and split them into thirds, putting the top 1/3 trials with the highest error from each block into the high error condition, the middle 1/3 trials into the medium error condition, and the bottom 1/3 trials with the least error from each block into the low error condition. We observed the same pattern of effects in both regions for both retrieval and feedback when trials were sorted evenly in this way (S3.8). We additionally performed control analyses to ascertain that the gamma effects

in the MTL and dlPFC at retrieval and feedback were not associated with the distance the object was moved on the screen (Fig. S3.9).

As an alternative analysis, we also tested for correlations between gamma power and error in the MTL and DLPFC at retrieval and feedback. Figure 3.3 shows the correlation between gamma power, averaged over 100ms siding time windows, and angular error, logged to account for the non-normal distribution of error. We found negative correlations between gamma power and logged error in the MTL and DLPFC at retrieval, and positive correlations in both regions at feedback, replicating the results from the ANOVA analyses described above (Fig. 3.3E-F) (Pearson, $p < 0.05$, permutation corrected).

MTL gamma power at feedback predicts accuracy on subsequent trials. We then wanted to determine if gamma error signals on particular trials predicted learning and improved performance on subsequent trials. We found a significant partial correlation between MTL gamma power at feedback for high error trials and the change in error from one block to the next (e.g. T1 to T2) for specific object-location associations, controlling for error on the trial occurring in the earlier block (current error) (partial correlation, Pearson, $p < 0.05$, permutation corrected) (Fig. 3.3E-F). This was a negative correlation, indicating that the bigger the gamma error signal in the MTL was, the bigger the decrease in error from one block to the next. Importantly, this partial correlation controls for the amount current error, indicating that this effect is not due to ceiling/floor effects stemming from the amount of current error (i.e the larger the current

error is, the more room there is for decreases in error). In addition, this correlation remained significant when controlling for changes in power across blocks by adding task block as a factor in the partial correlation instead of by normalizing power within blocks (S3.8).

3.5 Discussion

Prior work has shown that MTL and dlPFC activity at feedback signals trial outcome (correct vs. incorrect). However, the contributions of these signals to performance on subsequent trials (i.e. learning) are poorly understood. Here, we found that increased MTL and dlPFC gamma power, thought to reflect local excitatory activity, signaled increased error at feedback in an object-location associative learning task. Increased MTL activity at feedback also predicted greater decreases in error from one training block to the next for specific object-location associations, indicating that MTL error signals are involved in updating incorrect or imprecise associations during learning.

A variety of processes could contribute to the observed error signals at feedback. Accumulating evidence suggests that the hippocampus plays a crucial role in developing models, or predictions, about the environment. Numerous studies have shown that hippocampal activity increases when predictions about the environment are violated, resulting in what has been termed a ‘match/mismatch’ signal (Duncan, 2012). These ‘match/mismatch’ signals might contribute to the observed error signals if subjects’ placement of an object was less accurate than they had expected. Similarly, prediction errors signal discrepancies between actual and expected outcomes and are

thought to drive learning by updating expectations to make predictions more accurate (Mattar & Daw, 2018; Stachenfeld, Botvinick, & Gershman, 2017). Given that it is generally preferable to do well on any given task, reward prediction errors, or the difference between an actual and expected reward might contribute to the observed error signals. In this case, the reward would be good performance on the task (low error), and a reward prediction error would occur if subjects' placement of an object was less accurate than they had expected. State prediction errors, which respond to incorrect predictions of both neutral and affective stimuli could also contribute (Glascher, Daw, Dayan, & O'Doherty, 2010). The increased activity for high error trials might also reflect encoding (or re-encoding) of the correct location if the location of the object was forgotten, misremembered, or imprecise. Regardless of whether subjects had a specific prediction about where the object would be when it was shown in the correct location at feedback, there would likely be a measure of increased surprise and novelty for higher error trials since the object would appear at an unexpected location. As such, attentional effects that accompany surprise or novelty might also contribute to these signals (Corbetta & Shulman, 2002). However, the error signal observed in the MTL at feedback predicted subsequent performance on specific object-location associations, indicating that this signal is not just reflecting surprise or novelty but that it is contributing to associative learning.

Previous studies in rodents and monkeys have found cells that increase firing at feedback for both correct and error trials (Brincat & Miller, 2015; Wirth et al., 2009). However, the ways in which these cells contribute to population activity as recorded by

the local field potential or by BOLD fMRI in animals and humans is poorly understood. In a cross-species study that examined feedback signals in both monkeys (using LFP) and humans (using fMRI), increased MTL gamma (30-100 Hz) power was found for error trials (incorrect > correct) in monkeys (Hargreaves, Mattfeld, Stark, & Suzuki, 2012). The BOLD fMRI signal in humans at feedback showed the opposite polarity, with increased MTL activity for correct trials (correct > incorrect). High frequency gamma power is thought to be generated by increased spiking, gamma oscillations, or by a combination of these two processes (Burke et al., 2015). In each case, this would mean that the observed error signals reflect increased local excitatory activity, as noted above. Although the BOLD signal has been found to be correlated with the local field potential, this signal is thought to be generated by complex neurovascular coupling, making the polarity of this signal difficult to interpret (Logothetis, 2001). The results from the current study support the idea that, at a population level, MTL excitatory activity is driven by increased error at feedback, though other task designs could result in differing effects.

At retrieval, we found negative correlations between increased MTL and dlPFC gamma power and error, replicating results from our previous study (Stevenson et al., 2018). These results provide additional evidence that MTL and dlPFC activity does not just reflect a binary signal of retrieval success versus failure, but rather that activity within these regions tracks representational fidelity. This adds to a growing body of literature implicating the extended hippocampal network in spatial memory precision (Koen et al., 2017; Kolarik et al., 2016; Nilakantan et al., 2017).

We also observed decreases in MTL and dlPFC gamma power across task blocks at retrieval and feedback. Although these decreases in activity paralleled decreases in error across blocks, low error trials within blocks were associated with *increased* MTL and dlPFC activity at retrieval, indicating that these shifts in power were not driven solely by object-location associative learning. Interestingly, multiple other studies have shown decreases in gamma activity over the course of experimental sessions, linking these gradual shifts to decreases in novelty and increases in familiarity as well as to decreases in attention (Park et al., 2014; Sederberg et al., 2006; Serruya, Sederberg, & Kahana, 2014). Decreases in gamma power have also been linked to repetition suppression, where activity elicited by a stimulus decreases from the first to the second presentation (Rodriguez Merzagora et al., 2014). Additionally, these decreases in activity could be related to increases in processing efficiency or learning of the task environment and/or stimuli. Future work will be needed to determine how shifts in gamma power relate to changes in novelty, attention, processing efficiency, or item recognition.

A limitation of the current study is that the research was conducted with patients with epilepsy, whose brains may undergo epilepsy-related changes. However, in line with recommendations put forth in a review by human and nonhuman primate intracranial researchers, we excluded trials that contained epileptiform discharges and only included recordings from non-epileptic tissues (Parvizi & Kastner, 2018).

The ability to update incorrect or imprecise representations of the environment based on negative feedback is critical for the formation of accurate predictions that can be used to guide behavior. These results suggest a role for the MTL in signaling error at feedback and in updating representations of object-location associations. We also provide additional evidence for the involvement of the MTL and dlPFC in high-fidelity spatial memory retrieval. Future studies will be needed to determine if the MTL is involved in non-spatial associative learning via feedback (e.g. face-name) and in indexing the precision of non-spatial memory judgments.

CHAPTER 4: MEDIAL TEMPORAL LOW FREQUENCY ACTIVITY AND APERIODIC SLOPE DURING SPATIAL LEARNING

4.1 Abstract

Neural power spectra consist of narrowband peaks in power, reflecting putative oscillations, rising above the aperiodic 1/f signal. Low frequency neural oscillations in the theta range (~3-8 Hz) are thought to play a critical role in memory encoding and retrieval by coordinating the timing of neural activity. Oscillatory power is often estimated via narrowband filtering, giving a measure of total power in a specific bandwidth. However, since this measure reflects a combination of oscillatory power (if present) and the aperiodic signal, apparent changes in oscillatory power can be driven by shifts in the aperiodic signal. As such, oscillatory power is better defined as power relative to the aperiodic signal, or 'peak amplitude'. Although it has received less attention in the literature, the aperiodic signal is also thought to reflect aspects of neuronal function important for memory processing. Accumulating evidence suggests that the slope of the aperiodic signal reflects the balance between excitatory and inhibitory synaptic currents, and that decreasing the ratio of excitation to inhibition decreases (steepens) the slope. In order to examine low-frequency oscillations in the theta range and the slope of the aperiodic signal during associative learning, we tested presurgical epilepsy patients with depth electrodes implanted in the medial temporal lobe on a spatial learning task in which subjects attempted to learn object-location associations over the course of three training blocks with feedback. We used a novel algorithm to parameterize the recorded power spectra, providing an estimate of theta

peak amplitude as well as an estimate of the slope of the aperiodic signal. We found that total theta power, estimated using narrowband filtering, increased across training blocks at retrieval and feedback. However, there was no change in theta peak amplitude. Rather, the increases in total theta power were driven by decreases in the aperiodic slope. These results suggest that there was a decrease in the ratio of excitation to inhibition across training blocks, indicating decreases in excitatory activity or increases in inhibition that could reflect increased familiarity or decreased novelty with training.

4.2 Introduction

Neural oscillations in the theta range (~3-8 Hz) are thought to play a critical role in memory encoding and retrieval. These oscillations appear as narrowband peaks in the power spectrum rising above the aperiodic 1/f signal. The rhythmic properties of these oscillations have been shown to play an important role in coordinating the timing of neural activity via such mechanisms as phase synchronization and phase amplitude coupling (Fell & Axmacher, 2011; Rutishauser et al., 2010). Studies in presurgical epilepsy patients have found increased theta power in the medial temporal lobe (MTL) during episodic memory retrieval, though these studies did not find that theta power predicted memory performance (Burke, Sharan, et al., 2014; Watrous et al., 2013). Alterations in MTL theta power during encoding have been shown to predict subsequent memory, though there is conflicting evidence as to the directionality of this effect, with both increases and decreases in theta power predicting subsequent performance (Burke et al., 2013; Lega et al., 2012). A possible explanation for these conflicting

results is that oscillatory power is often estimated via narrowband filtering, giving a measure of total power in a specific bandwidth. However, since this measure reflects a combination of oscillatory power (if present) and the aperiodic signal, apparent changes in oscillatory power can be driven by shifts in the aperiodic signal. As such, the contributions of theta oscillations to memory processing are still unclear.

Although it has received less attention in the literature, the 1/f signal is also thought to reflect aspects of neuronal function critical to memory processing. This signal follows a power-law function, in which power decreases with increasing frequency ($P \sim 1/f^x$), giving it its “1/f” shape (He, 2014; Miller et al., 2009). The slope of the 1/f signal is defined by the power-law exponent (x), which typically ranges between 0-4 for neural spectra (He, 2014; Miller et al., 2009). In contrast to neural oscillations, which are, by definition, periodic, this signal is not dominated by any particular time scale or frequency and is thought to arise from aperiodic neural activity. Recent results from computational modeling suggest that the 1/f aperiodic signal is generated by a combination of excitatory and inhibitory postsynaptic currents (Gao et al., 2017). In this model, decreasing the ratio of excitation to inhibition decreased (steepened) the slope of the simulated aperiodic signal. These modeling results were corroborated by experimental data showing that increasing levels of inhibition predicted aperiodic slope decreases in rodent LFP and monkey ECOG recordings (Gao et al., 2017). The balance between excitation to inhibition is thought to be important for neural homeostasis, numerous neural computations, and normal neural processing such as the generation of neural oscillations (Atallah & Scanziani, 2009; Turrigiano & Nelson, 2004; Vogels & Abbott,

2009). Imbalances in the ratio of excitation to inhibition have been linked to multiple neurological and psychiatric disorders, such as epilepsy, schizophrenia, and autism (Gao et al., 2017). Accumulating evidence suggests that hyperactivity within the hippocampus is linked to age-related impairments in memory, perhaps reflecting excitatory/inhibitory imbalances (Bakker et al., 2012; Yassa et al., 2011). Additionally, a recent study found that age-related impairments in working memory were mediated by increases in the aperiodic slope, which could reflect increases in “neural noise” produced by excitatory/inhibitory imbalances (Voytek et al., 2015). However, the links between the aperiodic slope and memory processing are still poorly understood.

In order to examine how low-frequency theta oscillations and changes in the aperiodic slope contribute to associative learning in humans, we tested presurgical epilepsy patients on a spatial learning task in which subjects attempted to learn object-location associations over the course of three training blocks with feedback. We used a novel algorithm developed by Haller and colleagues to model the recorded power spectra, giving us an estimate of theta power relative to the aperiodic signal (peak amplitude), as well as an estimate of the aperiodic slope (Haller et al., 2018a). We predicted that theta peak amplitude and the aperiodic slope would be modulated across the three training blocks at retrieval and feedback and that peak amplitude and the aperiodic slope would predict error within training blocks.

4.3 Materials and methods

Participants. Subjects were 5 patients (3 female, 1 male, age 24-58) who had stereotactically implanted intracranial depth electrodes (Integra or Ad-Tech, 5-mm inter-electrode spacing) placed at the University of California, Irvine Medical Center to localize the seizure onset zone for possible surgical resection. These patients were a subset of the subjects included in chapter 3 (subjects 3, 4, 6, and 7). Informed consent was obtained from each subject prior to testing and the research protocol was approved by the IRB of the University of California, Irvine. Electrode placement was exclusively guided by clinical needs.

Spatial learning task and behavioral analyses. The spatial learning task was the same used in chapter 3. Briefly, during encoding subjects were shown 30 objects one at a time at random locations along the circumference of an invisible circle. For each training block, the same objects were shown at the top of the circle and subjects used a mouse wheel to rotate the object to where it appeared during encoding. After subjects finished placing each object, it was shown in the correct location for one second as feedback. Performance was measured as angular error, or the difference in degrees between where subjects placed the object and its correct location. In order to examine the relationship between total theta power, theta peak amplitude, and error, as well as the relationship between the aperiodic slope and error, we sorted trials within each block by error and split them into thirds, putting the top 1/3 trials with the highest error from each block into the high error condition and the bottom 1/3 trials with the least error from each block into the low error condition. See chapter 3 for a more detailed description of the spatial learning task and in-depth behavioral analyses.

Electrode localization, data collection and preprocessing. Electrode localization, data collection, and preprocessing were performed as in chapter 3. See Table 3.1 for number of MTL contacts for each subject.

Total theta (3-8 Hz) power analyses (narrowband filtering). Intracranial recordings were broken into event-related epochs (3 seconds pre-stimulus onset and 4 seconds post-stimulus onset) at retrieval and feedback. At retrieval, stimulus onset refers to the time at which the object appears at the top of the circle. At feedback, stimulus onset refers to the time at which the object appears at the correct location as feedback. These raw time series data were then convolved with complex Morlet wavelets, implemented using the FieldTrip toolbox, to obtain a measure of instantaneous power (Oostenveld et al., 2011). Center frequencies ranged from 1 to 150 Hz, with a spacing of 1 Hz and a variable cycle number of 4-15. Power was baseline corrected to the average pre-stimulus power across all trials (0.5 to 0.2 prior to stimulus onset), resulting in a measure of relative power per frequency (power divided by pre-stimulus power) at each time point. Power was then z-transformed separately within each session to account for differences in power and noise across sessions. We used an a priori theta frequency range of 3-8 Hz in order to examine total theta power, based on prior literature showing MTL theta activity in this range. We then averaged baseline corrected power over this theta frequency range (3-8 Hz) and across MTL electrodes. We used a cluster-based permutation testing to compare theta power across task blocks, as in chapter 3. To examine the specificity of effects, we also ran analyses on regions outside of the MTL

including the lateral temporal cortex, the insula, the caudal prefrontal cortex (BA 6/8), orbitofrontal cortex, anterior cingulate cortex, and dorsolateral prefrontal cortex (BA 9/10/46).

Power spectral densities (PSDs). Intracranial recordings were broken into event-related epochs (0 to 1 second poststimulus onset) at retrieval and feedback. We applied a Hanning window to these data epochs and then used Fourier transform to derive power spectral densities (Fieldtrip toolbox function ft_freqanalysis ('mtmfft', Hanning window)) (Oostenveld et al., 2011). Center frequencies ranged from 2 to 40 Hz with a spacing of 1 Hz.

Parameterizing the neural power spectra. In order to decompose these PSDs into aperiodic signals and peaks, or putative oscillations, we used a novel algorithm developed by Haller and colleagues called Fitting Oscillations and One Over F (1/f) (FOOOF) (Haller et al., 2018a). This algorithm first finds an initial fit for the aperiodic signal, which is then subtracted from the original PSD creating a flattened spectrum. An amplitude threshold is applied to this flattened spectrum in order to find low amplitude points that are most likely to represent the aperiodic signal. The aperiodic signal is then refit using these low amplitude points. After the resulting aperiodic signal is regressed out, the algorithm iteratively searches for peaks that are each individually fit with a Gaussian. A multi-Gaussian model is then fit to these peaks, minimizing the squared error between the flattened spectrum and the number of Gaussian. This multi-Gaussian model is then subtracted from the original PSD, and the aperiodic signal is refit. The

final fit for the aperiodic signal is then combined with the Gaussian model. Since changes in broadband gamma (>40 Hz) could potentially skew the model fit, we cut off the frequency range at 40 Hz. As such, the PSDs analyzed by the model had a frequency range of 2-40 Hz.

Permutation testing. We used permutation testing to statistically compare parameters across conditions. Trials were pooled across sessions and the difference in aperiodic slope between conditions (e.g. T1 vs. T3) was calculated. A null difference distribution was created by shuffling the trial labels 500 times before calculating the difference in slopes between conditions. The observed slope difference value was then compared to this null average difference distribution. P-values were calculated as the fraction of times the null difference values were equal to or more extreme than the observed difference value. In order to compare theta peak amplitudes between conditions, we found the difference between the highest amplitude peaks detected between 2-11 Hz in each condition. A null difference distribution was created by shuffling the trial labels 500 times before calculating the difference in peak amplitudes between conditions. If no peak was detected in one of the permuted iterations, the aperiodic signal was subtracted from the PSD creating a flattened spectrum, and the peak amplitude for that iteration was set as the highest amplitude point between 2-11 Hz in this flattened spectrum.

4.4 Results

Task performance. Subjects (11 sessions from 4 patients) performed a spatial learning task as we recorded intracranial electroencephalogram (EEG). During the encoding phase, 30 objects were presented, one at a time, at random positions around the circumference of an invisible circle (see Fig. 3.1). Prior to the encoding phase, subjects were told that they would be tested on the location of each object. Following encoding, there were three training blocks during which each object was shown again, this time at the top of the circle, and subjects were instructed to use the mouse wheel to rotate the object to where it appeared during encoding. Subjects were asked to wait 1 second (until text that read 'Wait…' disappeared from the screen) before beginning to rotate the object and to press the space bar when they were finished placing the object. After each trial, the object appeared on the screen in the correct location for 1 second as feedback. During the final test phase, subjects were again asked to rotate each object to the correct location, though this time no feedback was given. The inter-trial interval (ITI) was 1.2 +/- 0.2 seconds and the interstimulus interval (ISI), meaning the time between when the subjects finished placing the object and when it was shown in the correct location as feedback was fixed at 0.5 seconds. Performance was measured in angular error, or the distance (in degrees) between where subjects placed the object and the correct location. If subjects performed more than one session, new objects and locations were used. No more than one session was performed on each day.

We used the MemFit function of Memtoolbox in MATLAB (J. W. Suchow et al., 2013), to obtain an estimate of two parameters describing these distributions: the guess rate (g), which reflects the area under the uniform distribution, and the standard deviation of the

von Mises distribution (SDMem), which reflects the overall precision of responses that were not guesses. Guess rate, SDMem, and angular error all decreased over task blocks, indicating learning of the object-location associations (linear trend analysis, guess rate: $F(1, 30) = 10.3$, $p = 0.003$, SDMem: $F(1, 30) = 14$, $p = 0.0007$; error: $F(1, 30) = 90.6$, $p < 0.0001$).

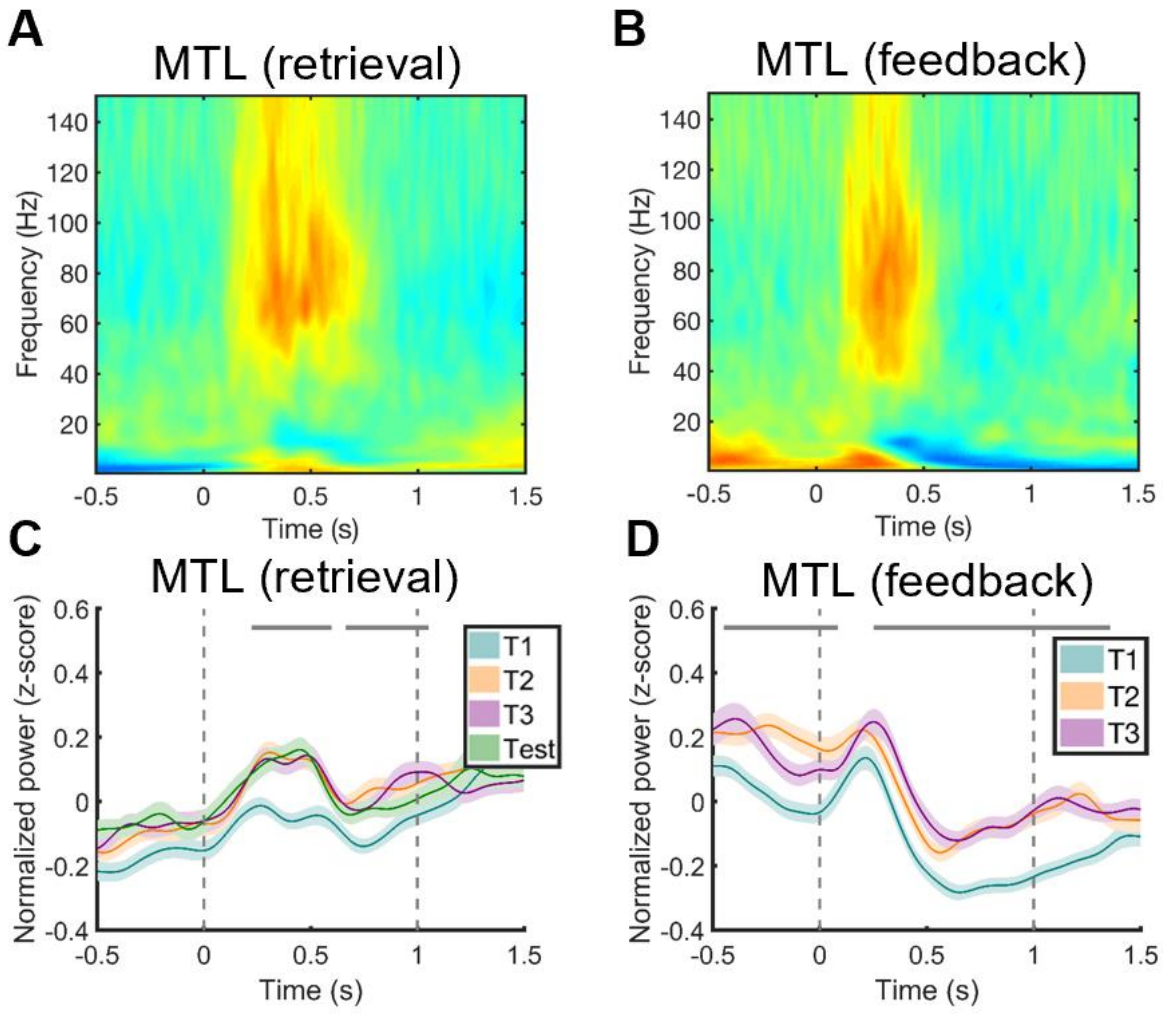

Figure 4.1. Total theta power (3-8 Hz) increases across task blocks. A-B, Spectrograms showing mean MTL power across all trials at retrieval (A) and feedback (B). C-D, Time course of total theta (3-8 Hz) power for each task block at retrieval (C) and feedback (D) (T1-3, and Test for retrieval, T1-3 for feedback). Gray horizontal lines indicate time points where there are significant differences between task blocks (ANOVA, $p < 0.05$, cluster-corrected). Colored shaded regions indicate s.e.m. T1-3: training blocks 1-3.

Total theta power (3-8 Hz) increases across task blocks. We first examined how total, narrowband filtered power in the theta range (3-8 Hz) changed across task blocks during retrieval and feedback. Spectrograms for MTL power across all trials at retrieval and feedback are shown in Figure 4.1A-B. The time course of mean MTL total theta power for each task block at retrieval and feedback (including the test block for retrieval but not feedback since feedback was not given during the final test) is shown in Figure 4.1C-D. Using a cluster-based permutation approach to correct for multiple comparisons across time points, we found significant differences in total theta power across blocks in both regions for both retrieval and feedback (ANOVA $p < 0.05$, cluster-corrected). These increases in total theta power were not specific to the MTL but were present in nearly all brain regions we recorded from, including the orbitofrontal cortex, anterior cingulate, and dorsolateral prefrontal cortex (see S4.1-2 for results from all recording sites at retrieval and feedback). However, there were regions (e.g. the insula) and time periods where there was no significant difference in total theta power across blocks suggesting that these changes were not driven by non-neural sources such as changes in electrode impedance over time.

To determine if these increases in total theta power reflected increases in oscillatory power, we pooled trials across sessions and applied the Fourier transform to the 1 second period following stimulus onset at retrieval and feedback to obtain power spectral densities (PSDs) between 2-40 Hz. We used a novel algorithm developed by Haller and colleagues (2018), called Fitting Oscillations and One Over F (1/f) (FOOOF),

to disentangle putative oscillatory peaks present in these PSDs from the aperiodic signal. This algorithm first finds an initial fit for the aperiodic signal, which is then subtracted from the original PSD. The algorithm then iteratively searches for peaks in this flattened spectrum which are each fit with a Gaussian curve. A multi-Gaussian model is then fit to these peaks, minimizing the squared error between the flattened spectrum and the number of Gaussian curves. This multi-Gaussian model is then subtracted from the original PSD, and the aperiodic signal is refit. The final fit for the aperiodic signal is then combined with the Gaussian model. The parameters estimated by the final model include the center frequencies and bandwidth of the detected peaks (if present), the amplitude of these peaks relative to the aperiodic signal, as well as the broadband offset and slope of the aperiodic signal (Fig. 4.2A). The model fit of the MTL PSDs averaged over all trials at retrieval and feedback was highly accurate, with an r^2 of 0.9989 and a root mean squared error of 0.0198 at retrieval (Fig. 4.2B) and an r^2 of 0.9986 and a root mean squared error of 0.0201 at feedback. Peaks were detected in the theta range at both retrieval and feedback, with a center frequency of 8.8 Hz and bandwidth of 2.6 Hz at retrieval and a center frequency of 8.9 Hz and bandwidth of 2.1 Hz at feedback. We then used permutation testing to statistically compare theta peak amplitudes across task blocks. First, we took the difference in MTL theta peak amplitudes between training block 1 (T1) and training block 3 (T3). A null difference distribution was created by shuffling the trial labels 500 times before calculating the difference between the highest amplitude peaks detected between 2-11 Hz in each condition. If no peak was detected in one of the permuted iterations, the aperiodic signal was subtracted from the PSD creating a flattened spectrum, and the peak amplitude for

that iteration was set as the highest amplitude point between 2-11 Hz in this flattened spectrum. P-values were calculated as the fraction of times the null difference values were equal to or more extreme than the observed difference in peak amplitudes. We found no significant difference in MTL theta peak amplitudes for T1 versus T3 at retrieval or feedback, indicating that the differences in total theta power were driven by alterations in the aperiodic signal (permutation testing, $p > 0.05$).

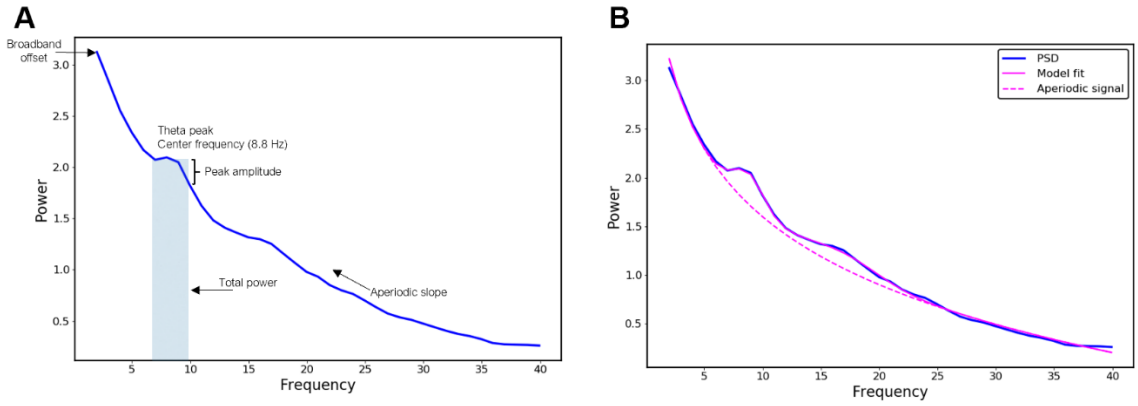

Figure 4.2. Parameterizing neural power spectra. A. Neural power spectra consist of narrowband peaks in power, reflecting putative oscillations, rising above the aperiodic signal. Each peak has a center frequency and bandwidth, while the aperiodic signal is defined by its slope and broadband offset. Oscillatory power is better defined as power relative to the aperiodic signal (peak amplitude) rather than total power. **B.** Model fit of the MTL PSD averaged over all trials at retrieval. Two peaks were found, one with a center frequency of 8.8 Hz and a bandwidth of 2.6 Hz, and one with a center frequency of 16.9 Hz and a bandwidth of 6.2 Hz. The r^2 of the model fit was 0.9989 and that the root mean squared error was 0.0198. The offset of the aperiodic signal was estimated to be at 3.9, and the slope was estimated to be 2.3.

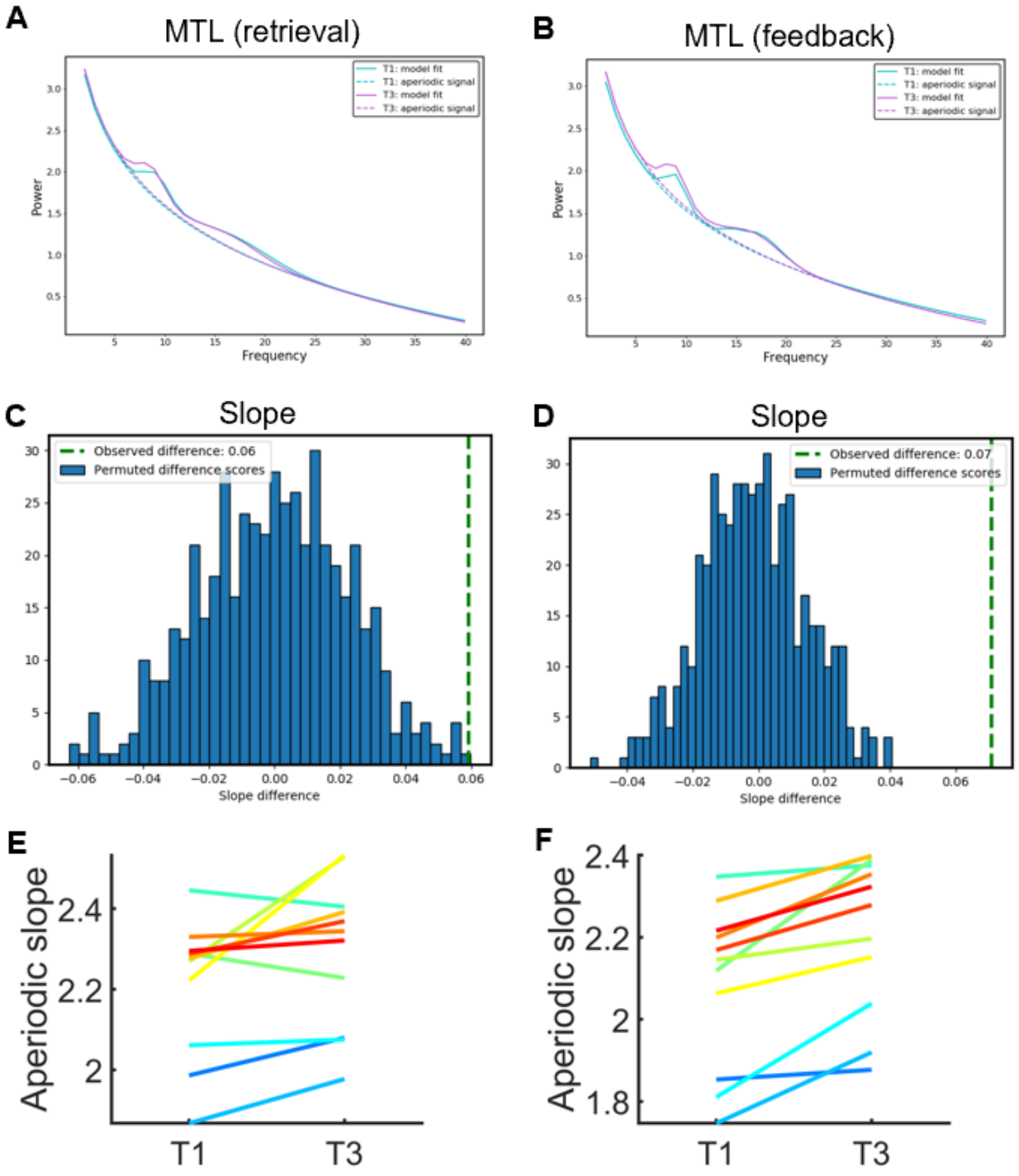

Figure 4.3. Aperiodic slope decreases across training blocks. A, C. Model fit of the MTL PSDs at training block 1 (T1) training block 3 (T3) at retrieval (A) and feedback (C). B, D. A null distribution was formed by randomly shuffling trials between conditions in order to test for differences in slope. E, F. Aperiodic slope for T1 and T3 at retrieval (E) and feedback (C) for each session.

Aperiodic slope decreases across training blocks. Using the estimates of aperiodic slope derived from the FOOOF model, we used permutation testing to compare slopes across training blocks. We found that the aperiodic slope significantly decreased (i.e. the power-law exponent significantly increased, making the slope steeper) from training blocks 1 to 3 at retrieval (permutation test, $p = 0.004$) and feedback (permutation test, $p = 0.002$) (Fig. 4.3A-D). To determine how consistent the slope change was across sessions, we fit each session individually using the FOOOF algorithm and found a significant difference in slopes at the group level for T1 and T3 at retrieval (Wilcoxon signed rank test, $p = 0.03$) and feedback (Wilcoxon signed rank test, $p = 0.001$). Although this decrease in aperiodic slope parallels the decrease in error from T1 to T3, this slope decrease across training blocks could also have been driven by increased familiarity with the objects themselves or with the task environment rather than by learning of the object-location associations. As such, we next examined the relationship between the aperiodic slope and error within blocks.

Error within blocks not predicted by total theta power, theta peak amplitude, or aperiodic slope. We sorted trials within each block by error and split them into thirds, putting the top 1/3 trials with the highest error from each block into the high error condition and the bottom 1/3 trials with the least error from each block into the low error condition. We found no significant difference in total theta power between high and low error trials at retrieval or feedback ($p > 0.05$, cluster-corrected), nor did we find a significant difference in theta peak amplitude between conditions for retrieval or feedback ($p > 0.05$, permutation testing). We also did not find significant differences in

aperiodic slope between high and low error trials, indicating that the decreases in slope across blocks were driven by increases in familiarity or decreases in novelty ($p > 0.05$, permutation testing) (Fig. 4.4).

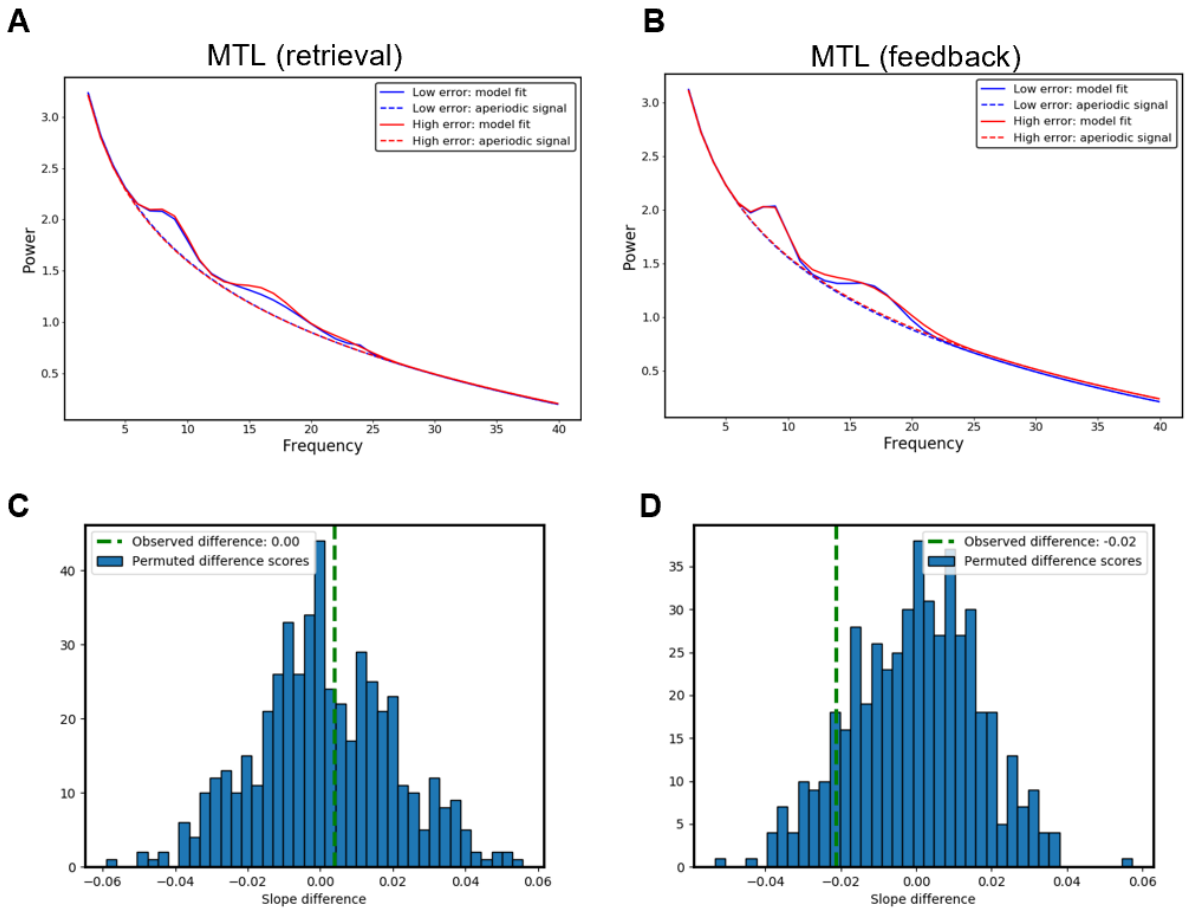

Figure 4.4. Error within blocks not predicted by aperiodic slope. Model fit of the MTL PSD for high and low error trials at retrieval (A) and feedback (B). C-D, A null distribution was formed by randomly shuffling trials between high and low error conditions in order to test for differences in slope.

4.5 Discussion

Testing presurgical epilepsy patients with depth electrodes implanted in the medial temporal lobe, we found that total theta power, estimated using narrowband filtering, increased across training blocks in a spatial learning task. However, using a novel algorithm to disentangle putative oscillatory power from the aperiodic signal, we found

that these increases in total theta power were driven, at least in part, by decreases in the aperiodic slope, and that theta peak amplitude, likely reflecting oscillatory power, showed no change across training blocks. Neither total theta power, theta peak amplitude, nor aperiodic slope predicted error within blocks, suggesting that the decreases in aperiodic slope across training blocks reflected decreases in novelty or increases in familiarity rather than object-location associative learning. Since decreases in aperiodic slope are thought to reflect decreases in the ratio of excitation to inhibition, these results suggest that decreases in excitation and/or increases in inhibition might underlie the changes in neural processing that accompany increased familiarity or decreased novelty, such as decreased attention, increased processing efficiency, or learning of the task environment and/or stimuli.

These increases in total theta power parallel the decreases in gamma power across test blocks described in chapter 3, suggesting these processes both reflect a tilt in the aperiodic signal. Interestingly, multiple studies from other groups have also shown simultaneous increases in theta power and decreases in gamma over the course of experimental sessions (Park et al., 2014; Sederberg et al., 2006; Serruya et al., 2014). We also observed decreases in gamma power across a single test session in a variant of the spatial learning task used in the current experiment (see Chapter 2) (Stevenson et al., 2018) . The current results indicate that these shifts in power are driven by changes in the aperiodic slope rather than by alterations in oscillatory power, indicating that changes in the ratio of excitation to inhibition commonly occur over the course of experimental sessions.

The gradual power shifts seen in previous studies during encoding have been shown to predict subsequent memory and have been interpreted as reflecting a primacy effect whereby earlier stimuli receive increased attention/processing power, or as reflecting increased familiarity/decreased novelty with the task environment/stimuli. In addition to the gradual shifts in power across experimental sessions, trial-by-trial increases in gamma power and decreases in theta power at encoding have been shown to be strong predictors of subsequent memory (Burke et al., 2013; Ezzyat et al., 2017). In a study that directly examined the relationship between aperiodic slope and memory, age-related changes in working memory were found to be mediated by increases in aperiodic slope (Voytek et al., 2015). Although we did not find that the aperiodic slope predicted object-location associative error at retrieval or feedback within blocks, the decreased slope across training blocks could reflect increases in processing efficiency or learning of the task environment and/or stimuli.

Although we observed a prominent peak in the theta range at both retrieval and feedback, indicating the presence of theta oscillations, we found no difference in theta peak amplitude between high and low trials at retrieval or feedback. This is consistent with results from previous studies, in which theta power was estimated using narrowband filtering, that showed no relationship between theta power and memory performance at retrieval. However, the differing results obtained across blocks when measuring total theta power versus theta peak amplitude in the current study highlight the need to take into account the aperiodic signal when measuring oscillatory power.

Future work could examine if changes in theta peak amplitude during feedback predict performance on specific object-location associations from one training block to the next. Although theta peak amplitude did not predict error on the object-location associative memory task, theta oscillations during retrieval or feedback could still play a role in memory processing. For instance, theta phase synchronization or theta-gamma phase amplitude coupling could facilitate reactivation at retrieval or memory updating at feedback by coordinating the timing of neural activity.

Using a novel method for parameterizing neural power spectra combined with intracranial recordings in humans, these results suggest that decreases in excitation and/or increases in inhibition might underlie the changes in neural processing that accompany increased familiarity or decreased novelty. Future work using single unit recordings in rodents and/or magnetic resonance spectroscopy in humans to examine levels of glutamate, an excitatory neurotransmitter, might be able to parse whether these changes are driven by decreases in excitation or increases in inhibition, and how they relate to changes in attention, processing efficiency, or item recognition.

CHAPTER 5: CONCLUSION AND FUTURE DIRECTIONS

5.1 Overview of findings

Prior studies have shown that the medial temporal lobe and prefrontal cortex are involved in associative memory learning and retrieval. However, the contributions of these regions to the precision of spatial memory retrieval and to associative learning via feedback are poorly understood. To address this gap, we tested presurgical epilepsy patients with bilateral depth electrodes implanted in the medial temporal lobe and prefrontal cortex on two variants of an object-location associative memory task designed to probe spatial memory precision and learning. In chapter 2, we show that increased hippocampal and dlPFC high-frequency gamma power, thought to reflect local excitatory activity, predicted the precision of spatial memory retrieval. We replicate these results in chapter 3, showing negative correlations between medial temporal and prefrontal activity at retrieval and error magnitude. We also show a directional relationship between CA1 and dlPFC activity in chapter 2 indicating that the dlPFC is involved in post-retrieval processing. These results suggest that medial temporal and prefrontal networks are not only involved in retrieval success, but also in indexing the precision of retrieved memories.

Using a variant of the spatial memory task in which object-location associations are learned over the course of 3 training blocks with feedback, we show the opposite pattern of activity at feedback in chapter 3, with increased MTL and dlPFC activity predicting increases in error. Increased MTL activity at feedback also predicted greater

decreases in error from one training block to the next for specific object-location associations, indicating that MTL error signals are involved in updating incorrect or imprecise associations during learning. We also show decreases in MTL and dlPFC gamma power across task blocks at retrieval and feedback which might reflect decreases in novelty or increases in familiarity as task environment/stimuli are learned.

In chapter 4 we describe how the increases in total theta power across task blocks observed in the spatial learning task are driven by decreases in the aperiodic slope, thought to reflect decreases in the ratio of excitation to inhibition. These decreases in aperiodic slope parallel the decreases in gamma power across test blocks described in chapter 3, suggesting these processes both reflect a seesaw-like tilt in the aperiodic signal (i.e. low frequency power goes up, high frequency power goes down). These results suggest that decreases in excitation and/or increases in inhibition might underlie the changes in neural processing that accompany increased familiarity or decreased novelty, such as decreased attention, increased processing efficiency, or learning of the task environment and/or stimuli.

A limitation of the current study is that the research was conducted with patients with epilepsy, whose brains may undergo epilepsy-related changes. However, in line with recommendations put forth in a review by human and nonhuman primate intracranial researchers, we excluded trials that contained epileptiform discharges and only included recordings from non-epileptic tissues (Parvizi & Kastner, 2018). Working with a clinical population also meant that subject sample sizes were relatively small (4-9) and that

electrode recordings were sparsely and inconsistently distributed throughout the brain given that electrode placement was solely driven by clinical need.

5.2 Conceptual framework for the role of the medial temporal lobe and prefrontal cortex in spatial memory precision and learning

Overall, these results are consistent with the proposed role for the hippocampus in relational memory and in forming and retrieving associations between the items or elements of an experience (e.g. an object and a location) (Diana et al., 2007; Eichenbaum et al., 1992). Chapter 2 adds to this framework by proposing a further role for hippocampal CA1 in facilitating the precise recall of learned associations. Multiple recent studies have implicated the extended hippocampal network in spatial memory precision, which, combined with the current results, provide convergent evidence that the hippocampus is important for the formation and retrieval of precise spatial representations. These results are also consistent with the Complementary Learning Systems framework in that the hippocampus is important for the rapid acquisition of novel associations (McClelland, McNaughton, & O'Reilly, 1995). Although we did not have enough electrodes in other hippocampal subfields or in surrounding cortices to be able to examine activity within these regions separately, we found that increased activity within the combined regions of the MTL predicted decreased error at retrieval in both versions of the object-location association task. As the perirhinal and parahippocampal cortices are thought to be involved in object and spatial/contextual processing, respectively, each of these regions would presumably be important for the retrieval of

highly precise object-location associations. The decreases in activity observed across task blocks in chapter 3 are consistent with the proposed role for the medial temporal lobe in processing changes in familiarity and novelty (Diana et al., 2007; Yonelinas, Aly, Wang, & Koen, 2010). As described in chapter 4, we additionally find that shifts in the balance between excitation and inhibition might drive the modulations in MTL activity that accompany changes in familiarity and novelty. Our results further propose a role for the MTL in signaling errors in object-location associative memory at feedback as well as in updating spatial memory representations or modifying incorrect associations.

In chapter 2 we describe how the gamma-precision effect observed at retrieval appeared earlier in the CA1 than in the dlPFC. This is consistent with the proposed role of the dlPFC in post-retrieval processing and in maintaining goals active in working memory (Passingham & Wise, 2012). In this case, the dlPFC could be involved in maintaining the retrieved location in mind as subjects prepare to move the object. We also observed increased dlPFC activity for high error trials at feedback, indicating a role for this region in signaling errors in associative memory retrieval. Although we did not find a relationship between error signals in the dlPFC and subsequent performance, given the sparse distribution of electrode recordings it is possible that other regions of the prefrontal cortex or even different areas of the dlPFC contribute to associative learning via feedback. Overall, these data suggest putative mechanisms for the learning and retrieval of high-fidelity special associations.

5.3 Future directions

In the current study, we describe a role for the hippocampus and dlPFC in indexing the precision of object-location associative memory. An important question that remains is whether these regions are important for *non-spatial* associative memory precision. A recent study from our group that tested subjects on their memory for the precise timing of specific events found that BOLD fMRI activity in the hippocampus and lateral entorhinal cortex predicted high versus low temporal precision (Montchal, Reagh, & Yassa, 2019). Running this task on pre-surgical epilepsy patients would provide a trial-by-trial measure of activity within these regions, allowing us to determine if these regions are involved in tracking temporal precision. In addition, it would be interesting to determine if hippocampal activity tracks the precision of item memory in addition to associative memory. In prior studies examining memory precision subjects were tested on their memory for the color of an item by having them select the color on a 360° color wheel, providing a continuous, objective measure of item detail memory (Sutterer & Awh, 2016). As with the temporal precision task, running this task on pre-surgical epilepsy patients would allow us to determine if hippocampal activity tracks the fidelity of item memory representations.

Accumulating evidence suggests that deep brain stimulation of the medial and lateral temporal cortices during encoding can improve subsequent memory (Ezzyat et al., 2017; Ezzyat et al., 2018; Suthana & Fried, 2014). However, it is currently unclear if stimulation can improve the precision of remembered associations. In addition, multiple studies have found that decreased gamma power and increased theta power reflect a ‘poor encoding state’ and that stimulation specifically during these time periods can

improve subsequent memory (Ezzyat et al., 2017). Since novel associations are often not learned in a single episode, an important question regarding the translational implications of this research is whether ‘poor updating/re-encoding states’ during feedback exist, and if stimulation during these time periods would predict learning.

Although we did not find associations between oscillatory power in the theta range and associative error in the current study, future work could determine if coupling between gamma power and specific phases of low frequency oscillations predicts error/precision. Researchers have just begun to leverage the aperiodic signal in examining memory processes and there are many promising lines of investigation using this method. As discussed in chapter 4, age-related impairments in working memory has been shown to be mediated by increases in the aperiodic slope, thought to reflect an increase in the ratio between excitation and inhibition (Voytek et al., 2015). Future work can examine the relationship between aging and spatial memory precision/learning and examine if age-related increases in the aperiodic slope predict impairments on these tasks.

REFERENCES

Addante, R. J., Watrous, A. J., Yonelinas, A. P., Ekstrom, A. D., & Ranganath, C. (2011). Prestimulus theta activity predicts correct source memory retrieval. *Proc Natl Acad Sci U S A, 108*(26), 10702-10707. doi:10.1073/pnas.1014528108

Allen, T. A., & Fortin, N. J. (2013). The evolution of episodic memory. *Proc Natl Acad Sci U S A, 110 Suppl 2*, 10379-10386. doi:10.1073/pnas.1301199110

Amaral, D. G., & Cowan, W. M. (1980). Subcortical afferents to the hippocampal formation in the monkey. *Journal of Comparative Neurology, 189*, 573-591. doi:10.1002/cne.901890402

Amaral, D. G., & Lavenex, P. (Eds.). (2007). *Hippocampal Neuroanatomy*. New York, NY: Oxford University Press.

Anderson, K. L., Rajagovindan, R., Ghacibeh, G. A., Meador, K. J., & Ding, M. (2010). Theta oscillations mediate interaction between prefrontal cortex and medial temporal lobe in human memory. *Cereb Cortex, 20*(7), 1604-1612. doi:10.1093/cercor/bhp223

Anderson, P., Bliss, T. V. P., & Skrede, K. K. (1971). Lamellar Organization of Hippocampal Excitatory Pathways. *Exp. Brain Res, 13*, 222-238.

Atallah, B. V., & Scanziani, M. (2009). Instantaneous modulation of gamma oscillation frequency by balancing excitation with inhibition. *Neuron, 62*(4), 566-577. doi:10.1016/j.neuron.2009.04.027

Avants, B. B., Tustison, N. J., Song, G., Cook, P. A., Klein, A., & Gee, J. C. (2011). A reproducible evaluation of ANTs similarity metric performance in brain image registration. *Neuroimage, 54*(3), 2033-2044. doi:10.1016/j.neuroimage.2010.09.025

Bakker, A., Krauss, G. L., Albert, M. S., Speck, C. L., Jones, L. R., Stark, C. E., . . . Gallagher, M. (2012). Reduction of hippocampal hyperactivity improves cognition in amnestic mild cognitive impairment. *Neuron, 74*, 467-474. doi:10.1016/j.neuron.2012.03.023

Barbas, H., Henion, T. H. H., & Dermon, C. R. (1991). Diverse thalamic projections to the prefrontal cortex in the rhesus monkey. *Journal of Comparative Neurology, 313*, 65-94. doi:10.1002/cne.903130106

Barnett, L., & Seth, A. K. (2014). The MVGC multivariate Granger causality toolbox: A new approach to Granger-causal inference. *Journal of Neuroscience Methods, 223*, 50-68. doi:10.1016/j.jneumeth.2013.10.018

Berens, P., Logothetis, N. K., & Tolias, A. S. (2010). Local field potentials, BOLD and spiking activity: Relationships and physiological mechanisms. *Nature Precedings, 2010*, 1-27. doi:10101/npre.2010.5216.1

Berry, S. D., & Thompson, R. F. (1978). Prediction of learning rate from the hippocampal electroencephalogram. *Science (New York, N.Y.), 200*, 1298-1300.

Blumenfeld, R., & Ranganath, C. (2007). Prefrontal cortex and long-term memory encoding: an integrative review of findings from neuropsychology and neuroimaging. *The Neuroscientist, 13*, 280-291. doi:10.1177/1073858407299290

Botvinick, M. M., Braver, T. S., Barch, D. M., Carter, C. S., & Cohen, J. D. (2001). Conflict monitoring and cognitive control. *Psychological Review, 108*, 624-652.

Brincat, S. L., & Miller, E. K. (2015). Frequency-specific hippocampal-prefrontal interactions during associative learning. *Nat Neurosci, 18*(4), 576-581. doi:10.1038/nn.3954

Burke, J. F., Long, N. M., Zaghloul, K. A., Sharan, A. D., Sperling, M. R., & Kahana, M. J. (2014). Human intracranial high-frequency activity maps episodic memory formation in space and time. *Neuroimage, 85 Pt 2*, 834-843. doi:10.1016/j.neuroimage.2013.06.067

Burke, J. F., Ramayya, A. G., & Kahana, M. J. (2015). Human intracranial high-frequency activity during memory processing: neural oscillations or stochastic volatility? *Current Opinion in Neurobiology, 31*, 104-110. doi:10.1016/j.conb.2014.09.003

Burke, J. F., Sharan, A. D., Sperling, M. R., Ramayya, A. G., Evans, J. J., Healey, M. K., . . . Kahana, M. J. (2014). Theta and high-frequency activity mark spontaneous recall of episodic memories. *J Neurosci, 34*(34), 11355-11365. doi:10.1523/JNEUROSCI.2654-13.2014

Burke, J. F., Zaghloul, K. A., Jacobs, J., Williams, R. B., Sperling, M. R., Sharan, A. D., & Kahana, M. J. (2013). Synchronous and asynchronous theta and gamma activity during episodic memory formation. *J Neurosci, 33*(1), 292-304. doi:10.1523/JNEUROSCI.2057-12.2013

Burwell, R. D. (2000). The parahippocampal region: corticocortical connectivity. *Annals of the New York Academy of Sciences, 911*, 25-42.

Buzsaki, G., Anastassiou, C. A., & Koch, C. (2012). The origin of extracellular fields and currents--EEG, ECoG, LFP and spikes. *Nat Rev Neurosci, 13*(6), 407-420. doi:10.1038/nrn3241

Buzsaki, G., & Wang, X. J. (2012). Mechanisms of gamma oscillations. *Annu Rev Neurosci, 35*, 203-225. doi:10.1146/annurev-neuro-062111-150444

Clark, R. E., & Squire, L. R. (2013). Similarity in form and function of the hippocampus in rodents, monkeys, and humans. *Proc Natl Acad Sci U S A, 110 Suppl 2*, 10365-10370. doi:10.1073/pnas.1301225110

Cohen, M. X. (2014). Analyzing Neural Time Series Data: Theory and Practice.

Cohen, N., & Squire, L. (1980). Preserved learning and retention of pattern-analyzing skill in amnesia: dissociation of knowing how and knowing that. *Science, 210*.

Colgin, L. L. (2016). Rhythms of the hippocampal network. *Nat Rev Neurosci, 17*(4), 239-249. doi:10.1038/nrn.2016.21

Colgin, L. L., Denninger, T., Fyhn, M., Hafting, T., Bonnevie, T., Jensen, O., . . . Moser, E. I. (2009). Frequency of gamma oscillations routes flow of information in the hippocampus. *Nature, 462*(7271), 353-357. doi:10.1038/nature08573

Corbetta, M., & Shulman, G. L. (2002). Control of goal-directed and stimulus-driven attention in the brain. *Nat Rev Neurosci, 3*(3), 201-215. doi:10.1038/nrn755

Diana, R. A., Yonelinas, A. P., & Ranganath, C. (2007). Imaging recollection and familiarity in the medial temporal lobe: a three-component model. *Trends Cogn Sci, 11*(9), 379-386. doi:10.1016/j.tics.2007.08.001

Dobbins, I. G., Foley, H., Schacter, D. L., & Wagner, A. D. (2002). Executive control during episodic retrieval: multiple prefrontal processes subserve source memory. *Neuron, 35*, 989-996. doi:10.1016/S0896-6273(02)00858-9

Eacott, M. J., Norman, G., Langston, R. F., & Wood, E. R. (2004). Integrated Memory for Object, Place, and Context in Rats: A Possible Model of Episodic-Like Memory? *Journal of Neuroscience, 24*, 1139-1153. doi:10.1002/hipo.20714

Eichenbaum, H., & Cohen, N. J. (2014). Can we reconcile the declarative memory and spatial navigation views on hippocampal function? *Neuron, 83*(4), 764-770. doi:10.1016/j.neuron.2014.07.032

Eichenbaum, H., Otto, T., & Cohen, N. J. (1992). The hippocampus—what does it do? *Behavioral and Neural Biology, 57*, 2-36. doi:10.1016/0163-1047(92)90724-I

Eichenbaum, H., Yonelinas, A. P., & Ranganath, C. (2007). The medial temporal lobe and recognition memory. *Annu Rev Neurosci, 30*, 123-152. doi:10.1146/annurev.neuro.30.051606.094328

Ezzyat, Y., Kragel, J. E., Burke, J. F., Levy, D. F., Lyalenko, A., Wanda, P., . . . Kahana, M. J. (2017). Direct Brain Stimulation Modulates Encoding States and Memory Performance in Humans. *Curr Biol, 27*(9), 1251-1258. doi:10.1016/j.cub.2017.03.028

Ezzyat, Y., Wanda, P. A., Levy, D. F., Kadel, A., Aka, A., Pedisich, I., . . . Kahana, M. J. (2018). Closed-loop stimulation of temporal cortex rescues functional networks and improves memory. *Nat Commun, 9*(1), 365. doi:10.1038/s41467-017-02753-0

Fell, J., & Axmacher, N. (2011). The role of phase synchronization in memory processes. *Nat Rev Neurosci, 12*(2), 105-118. doi:10.1038/nrn2979

Fell, J., Ludowig, E., Staresina, B. P., Wagner, T., Kranz, T., Elger, C. E., & Axmacher, N. (2011). Medial temporal theta/alpha power enhancement precedes successful memory encoding: evidence based on intracranial EEG. *J Neurosci, 31*(14), 5392-5397. doi:10.1523/JNEUROSCI.3668-10.2011

Fischl, B., van der Kouwe, A., Destrieux, C., Halgren, E., Segonne, F., Salat, D. H., . . . Dale, A. M. (2004). Automatically parcellating the human cerebral cortex. *Cereb Cortex, 14*(1), 11-22. doi:10.1093/cercor/bhg087

Gao, R., Peterson, E. J., & Voytek, B. (2017). Inferring synaptic excitation/inhibition balance from field potentials. *Neuroimage, 158*, 70-78. doi:10.1016/j.neuroimage.2017.06.078

Geib, B. R., Stanley, M. L., Wing, E. A., Laurienti, P. J., & Cabeza, R. (2017). Hippocampal Contributions to the Large-Scale Episodic Memory Network Predict Vivid Visual Memories. *Cereb Cortex, 27*(1), 680-693. doi:10.1093/cercor/bhv272

Glascher, J., Daw, N., Dayan, P., & O'Doherty, J. P. (2010). States versus rewards: dissociable neural prediction error signals underlying model-based and model-free reinforcement learning. *Neuron, 66*(4), 585-595. doi:10.1016/j.neuron.2010.04.016

Greenberg, J. A., Burke, J. F., Haque, R., Kahana, M. J., & Zaghloul, K. A. (2015). Decreases in theta and increases in high frequency activity underlie associative memory encoding. *Neuroimage, 114*, 257-263. doi:10.1016/j.neuroimage.2015.03.077

Haller, M., Donoghue, T., Peterson, E., Varma, P., Sebastian, P., Gao, R., . . . Voytek, B. (2018a). doi:10.1101/299859

Haller, M., Donoghue, T., Peterson, E., Varma, P., Sebastian, P., Gao, R., . . . Voytek, B. (2018b). Parameterizing neural power spectra. *bioRxiv*, 299859. doi:10.1101/299859

Hannula, D. E., & Ranganath, C. (2008). Medial Temporal Lobe Activity Predicts Successful Relational Memory Binding. *Journal of Neuroscience, 28*, 116-124. doi:10.1523/JNEUROSCI.3086-07.2008

Hargreaves, E. L., Mattfeld, A. T., Stark, C. E., & Suzuki, W. A. (2012). Conserved fMRI and LFP signals during new associative learning in the human and macaque monkey medial temporal lobe. *Neuron, 74*(4), 743-752. doi:10.1016/j.neuron.2012.03.029

Harlow, I. M., & Yonelinas, A. P. (2016). Distinguishing between the success and precision of recollection. *Memory, 24*(1), 114-127. doi:10.1080/09658211.2014.988162

He, B. J. (2014). Scale-free brain activity: past, present, and future. *Trends Cogn Sci, 18*(9), 480-487. doi:10.1016/j.tics.2014.04.003

Henson, R. N., Rugg, M. D., Shallice, T., Josephs, O., & Dolan, R. J. (1999). Recollection and familiarity in recognition memory: an event-related functional magnetic resonance imaging study. *The Journal of neuroscience : the official journal of the Society for Neuroscience, 19*, 3962-3972.

Histed, M. H., Pasupathy, A., & Miller, E. K. (2009). Learning substrates in the primate prefrontal cortex and striatum: sustained activity related to successful actions. *Neuron, 63*(2), 244-253. doi:10.1016/j.neuron.2009.06.019

Hosokawa, T., Kennerley, S. W., Sloan, J., & Wallis, J. D. (2013). Single-Neuron Mechanisms Underlying Cost-Benefit Analysis in Frontal Cortex. *Journal of Neuroscience, 33*, 17385-17397. doi:10.1523/JNEUROSCI.2221-13.2013

Hyman, J. M., Wyble, B. P., Goyal, V., Rossi, C. A., & Hasselmo, M. E. (2003). Stimulation in hippocampal region CA1 in behaving rats yields long-term potentiation when delivered to the peak of theta and long-term depression when delivered to the trough. *The Journal of neuroscience : the official journal of the Society for Neuroscience, 23*, 11725-11731.

Igarashi, K. M., Lu, L., Colgin, L. L., Moser, M. B., & Moser, E. I. (2014). Coordination of entorhinal-hippocampal ensemble activity during associative learning. *Nature, 510*(7503), 143-147. doi:10.1038/nature13162

Insausti, R., & Amaral, D. G. (2008). Entorhinal cortex of the monkey: IV. Topographical and laminar organization of cortical afferents. *J Comp Neurol, 509*(6), 608-641. doi:10.1002/cne.21753

Ison, M. J., Quian Quiroga, R., & Fried, I. (2015). Rapid Encoding of New Memories by Individual Neurons in the Human Brain. *Neuron, 87*(1), 220-230. doi:10.1016/j.neuron.2015.06.016

Koen, J. D., Borders, A. A., Petzold, M. T., & Yonelinas, A. P. (2017). Visual short-term memory for high resolution associations is impaired in patients with medial temporal lobe damage. *Hippocampus, 27*(2), 184-193. doi:10.1002/hipo.22682

Kolarik, B. S., Shahlaie, K., Hassan, A., Borders, A. A., Kaufman, K. C., Gurkoff, G., . . . Ekstrom, A. D. (2016). Impairments in precision, rather than spatial strategy, characterize performance on the virtual Morris Water Maze: A case study. *Neuropsychologia, 80*, 90-101. doi:10.1016/j.neuropsychologia.2015.11.013

Komorowski, R. W., Manns, J. R., & Eichenbaum, H. (2009). Robust conjunctive item-place coding by hippocampal neurons parallels learning what happens where. *J Neurosci, 29*(31), 9918-9929. doi:10.1523/JNEUROSCI.1378-09.2009

Kucewicz, M. T., Berry, B. M., Kremen, V., Brinkmann, B. H., Sperling, M. R., Jobst, B. C., . . . Worrell, G. A. (2017). Dissecting gamma frequency activity during human memory processing. *Brain, 140*(5), 1337-1350. doi:10.1093/brain/awx043

Kumaran, D., Hassabis, D., & McClelland, J. L. (2016). What Learning Systems do Intelligent Agents Need? Complementary Learning Systems Theory Updated. *Trends in Cognitive Sciences, 20*, 512-534. doi:10.1016/j.tics.2016.05.004

Lachaux, J. P., Axmacher, N., Mormann, F., Halgren, E., & Crone, N. E. (2012). High-frequency neural activity and human cognition: past, present and possible future of intracranial EEG research. *Prog Neurobiol, 98*(3), 279-301. doi:10.1016/j.pneurobio.2012.06.008

Larkin, M. C., Lykken, C., Tye, L. D., Wickelgren, J. G., & Frank, L. M. (2014). Hippocampal output area CA1 broadcasts a generalized novelty signal during an object-place recognition task. *Hippocampus, 24*(7), 773-783. doi:10.1002/hipo.22268

Lavenex, P., & Amaral, D. G. (2000). Hippocampal-neocortical interaction: a hierarchy of associativity. *Hippocampus, 10*, 420-430. doi:10.1002/1098-1063(2000)10:4<420::AID-HIPO8>3.0.CO;2-5

Lavenex, P., Suzuki, W. A., & Amaral, D. G. (2002). Perirhinal and parahippocampal cortices of the macaque monkey: projections to the neocortex. *J Comp Neurol, 447*(4), 394-420. doi:10.1002/cne.10243

Law, J. R., Flanery, M. A., Wirth, S., Yanike, M., Smith, A. C., Frank, L. M., . . . Stark, C. E. (2005). Functional magnetic resonance imaging activity during the gradual acquisition and expression of paired-associate memory. *J Neurosci, 25*(24), 5720-5729. doi:10.1523/JNEUROSCI.4935-04.2005

Lega, B. C., Jacobs, J., & Kahana, M. (2012). Human hippocampal theta oscillations and the formation of episodic memories. *Hippocampus, 22*(4), 748-761. doi:10.1002/hipo.20937

Manning, J. R., Jacobs, J., Fried, I., & Kahana, M. J. (2009). Broadband shifts in local field potential power spectra are correlated with single-neuron spiking in humans. *J Neurosci, 29*(43), 13613-13620. doi:10.1523/JNEUROSCI.2041-09.2009

Mattar, M. G., & Daw, N. D. (2018). Prioritized memory access explains planning and hippocampal replay. *Nat Neurosci, 21*(11), 1609-1617. doi:10.1038/s41593-018-0232-z

McClelland, J. L., McNaughton, B. L., & O'Reilly, R. C. (1995). Why there are complementary learning systems in the hippocampus and neocortex: insights from the successes and failures of connectionist models of learning and memory. *Psychological Review, 102*, 419-457.

Mcclelland, J. L., O'Reilly Randall C., McNaughton, Bruce L. (1995). Why there are Complementary Learning Systems in the Hippocampus and Neocortex:Insights from the Successes and Failures of Connectionist Models of Learning and Memory. *Psychological Review*, 1-47.

Merkow, M. B., Burke, J. F., Stein, J. M., & Kahana, M. J. (2014). Prestimulus theta in the human hippocampus predicts subsequent recognition but not recall. *Hippocampus, 24*(12), 1562-1569. doi:10.1002/hipo.22335

Miller, E. K., & Cohen, J. D. (2001). An Integrative Theory of Prefrontal Cortex Function. 167-202.

Miller, K. J., Honey, C. J., Hermes, D., Rao, R. P., denNijs, M., & Ojemann, J. G. (2014). Broadband changes in the cortical surface potential track activation of functionally diverse neuronal populations. *Neuroimage, 85 Pt 2*, 711-720. doi:10.1016/j.neuroimage.2013.08.070

Miller, K. J., Sorensen, L. B., Ojemann, J. G., & den Nijs, M. (2009). Power-law scaling in the brain surface electric potential. *PLoS Comput Biol, 5*(12), e1000609. doi:10.1371/journal.pcbi.1000609

Mitchell, S. J., Rawlins, J. N., Steward, O., & Olton, D. S. (1982). Medial septal area lesions disrupt theta rhythm and cholinergic staining in medial entorhinal cortex and produce impaired radial arm maze behavior in rats. *The Journal of neuroscience : the official journal of the Society for Neuroscience, 2*, 292-302.

Montchal, M. E., Reagh, Z. M., & Yassa, M. A. (2019). Precise temporal memories are supported by the lateral entorhinal cortex in humans. *Nat Neurosci, 22*(2), 284-288. doi:10.1038/s41593-018-0303-1

Mormann, F., Fell, J., Axmacher, N., Weber, B., Lehnertz, K., Elger, C. E., & Fernández, G. (2005). Phase/amplitude reset and theta-gamma interaction in the human medial temporal lobe during a continuous word recognition memory task. *Hippocampus, 15*, 890-900. doi:10.1002/hipo.20117

Theories of Hippocampal Function (Oxford University Press 2007).

Moser, M. B., Rowland, D. C., & Moser, E. I. (2015). Place cells, grid cells, and memory. *Cold Spring Harb Perspect Biol, 7*(2), a021808. doi:10.1101/cshperspect.a021808

Muñoz, M., & Insausti, R. (2005). Cortical efferents of the entorhinal cortex and the adjacent parahippocampal region in the monkey (Macaca fascicularis). *European Journal of Neuroscience, 22*, 1368-1388. doi:10.1111/j.1460-9568.2005.04299.x

Murray, E. A., & Mishkin, M. (1986). Visual recognition in monkeys following rhinal cortical ablations combined with either amygdalectomy or hippocampectomy. *The Journal of neuroscience : the official journal of the Society for Neuroscience, 6*, 1991-2003.

Nilakantan, A. S., Bridge, D. J., Gagnon, E. P., VanHaerents, S. A., & Voss, J. L. (2017). Stimulation of the Posterior Cortical-Hippocampal Network Enhances Precision of Memory Recollection. *Curr Biol, 27*(3), 465-470. doi:10.1016/j.cub.2016.12.042

Oostenveld, R., Fries, P., Maris, E., & Schoffelen, J. M. (2011). FieldTrip: Open source software for advanced analysis of MEG, EEG, and invasive electrophysiological data. *Comput Intell Neurosci, 2011*, 156869. doi:10.1155/2011/156869

Park, J., Lee, H., Kim, T., Park, G. Y., Lee, E. M., Baek, S., . . . Kang, J. K. (2014). Role of low- and high-frequency oscillations in the human hippocampus for encoding environmental novelty during a spatial navigation task. *Hippocampus, 24*(11), 1341-1352. doi:10.1002/hipo.22315

Parvizi, J., & Kastner, S. (2018). Promises and limitations of human intracranial electroencephalography. *Nat Neurosci, 21*(4), 474-483. doi:10.1038/s41593-018-0108-2

Passingham, R. E., & Wise, S. P. (2012). The Neurobiology of the Prefrontal Cortex: Anatomy, Evolution, and the Origin of Insight.

Preston, A. R., & Eichenbaum, H. (2013). Interplay of hippocampus and prefrontal cortex in memory. *Curr Biol, 23*(17), R764-773. doi:10.1016/j.cub.2013.05.041

Ranganath, C. (2010). A unified framework for the functional organization of the medial temporal lobes and the phenomenology of episodic memory. *Hippocampus, 20*, 1263-1290. doi:10.1002/hipo.20852

Ranganath, C., & Ritchey, M. (2012). Two cortical systems for memory-guided behaviour. *Nature Reviews Neuroscience, 13*, 713-726. doi:10.1038/nrn3338

Ray, S., & Maunsell, J. H. (2011). Different origins of gamma rhythm and high-gamma activity in macaque visual cortex. *PLoS Biol, 9*(4), e1000610. doi:10.1371/journal.pbio.1000610

Reagh, Z. M., & Yassa, M. A. (2014). Object and spatial mnemonic interference differentially engage lateral and medial entorhinal cortex in humans. *Proc Natl Acad Sci U S A, 111*(40), E4264-4273. doi:10.1073/pnas.1411250111

Rich, E. L., & Wallis, J. D. (2017). Spatiotemporal dynamics of information encoding revealed in orbitofrontal high-gamma. *Nat Commun, 8*(1), 1139. doi:10.1038/s41467-017-01253-5

Rodriguez Merzagora, A., Coffey, T. J., Sperling, M. R., Sharan, A., Litt, B., Baltuch, G., & Jacobs, J. (2014). Repeated stimuli elicit diminished high-gamma electrocorticographic responses. *Neuroimage, 85 Pt 2*, 844-852. doi:10.1016/j.neuroimage.2013.07.006

Rolls, E. T. (1999). Spatial view cells and the representation of place in the primate hippocampus. *Hippocampus, 9*, 467-480. doi:10.1002/(SICI)1098-1063(1999)9:4<467::AID-HIPO13>3.0.CO;2-F

Rudoy, J. D., Voss, J. L., Westerberg, C. E., & Paller, K. a. (2009). Strengthening individual memories by reactivating them during sleep. *Science (New York, N.Y.), 326*, 1079. doi:10.1126/science.1179013

Rugg, M. D., & Vilberg, K. L. (2013). Brain networks underlying episodic memory retrieval. *Curr Opin Neurobiol, 23*(2), 255-260. doi:10.1016/j.conb.2012.11.005

Rutishauser, U. (2008). Activity of human hippocampal and amygdala neurons during retrieval of declarative memories. *105*.

Rutishauser, U., Ross, I. B., Mamelak, A. N., & Schuman, E. M. (2010). Human memory strength is predicted by theta-frequency phase-locking of single neurons. *Nature, 464*(7290), 903-907. doi:10.1038/nature08860

Rutishauser, U., Ye, S., Koroma, M., Tudusciuc, O., Ross, I. B., Chung, J. M., & Mamelak, A. N. (2015). Representation of retrieval confidence by single neurons in the human medial temporal lobe. *Nat Neurosci, 18*(7), 1041-1050. doi:10.1038/nn.4041

Ryan, J. D., Althoff, R. R., Whitlow, S., & Cohen, N. J. (2000). Amnesia is a deficit in relational memory. *Psychological science : a journal of the American Psychological Society / APS, 11*, 454-461. doi:10.1111/1467-9280.00288

Sederberg, P. B., Gauthier, L. V., Terushkin, V., Miller, J. F., Barnathan, J. A., & Kahana, M. J. (2006). Oscillatory correlates of the primacy effect in episodic memory. *Neuroimage, 32*(3), 1422-1431. doi:10.1016/j.neuroimage.2006.04.223

Sederberg, P. B., Schulze-Bonhage, A., Madsen, J. R., Bromfield, E. B., Litt, B., Brandt, A., & Kahana, M. J. (2007). Gamma oscillations distinguish true from false memories. *Psychological science, 18*, 927-932. doi:10.1111/j.1467-9280.2007.02003.x

Sederberg, P. B., Schulze-Bonhage, A., Madsen, J. R., Bromfield, E. B., McCarthy, D. C., Brandt, A., . . . Kahana, M. J. (2007). Hippocampal and neocortical gamma oscillations predict memory formation in humans. *Cereb Cortex, 17*(5), 1190-1196. doi:10.1093/cercor/bhl030

Serruya, M. D., Sederberg, P. B., & Kahana, M. J. (2014). Power shifts track serial position and modulate encoding in human episodic memory. *Cereb Cortex, 24*(2), 403-413. doi:10.1093/cercor/bhs318

Seth, A. K. (2010). A MATLAB toolbox for Granger causal connectivity analysis. *Journal of Neuroscience Methods, 186*, 262-273. doi:10.1016/j.jneumeth.2009.11.020

Simons, J. S., & Spiers, H. J. (2003). Prefrontal and medial temporal lobe interactions in long-term memory. *Nat Rev Neurosci, 4*(8), 637-648. doi:10.1038/nrn1178

Solomon, E. A., Kragel, J. E., Sperling, M. R., Sharan, A., Worrell, G., Kucewicz, M., . . . Kahana, M. J. (2017). Widespread theta synchrony and high-frequency desynchronization underlies enhanced cognition. *Nat Commun, 8*(1), 1704. doi:10.1038/s41467-017-01763-2

Stachenfeld, K. L., Botvinick, M. M., & Gershman, S. J. (2017). The hippocampus as a predictive map. *Nat Neurosci, 20*(11), 1643-1653. doi:10.1038/nn.4650

Staresina, B. P., Fell, J., Do Lam, A. T. A., Axmacher, N., & Henson, R. N. (2012). Memory signals are temporally dissociated in and across human hippocampus and perirhinal cortex. *Nature neuroscience, 15*, 1167-1173. doi:10.1038/nn.3154

Stark, S. M., Stevenson, R., Wu, C., Rutledge, S., & Stark, C. E. (2015). Stability of age-related deficits in the mnemonic similarity task across task variations. *Behav Neurosci, 129*(3), 257-268. doi:10.1037/bne0000055

Stark, S. M., Stevenson, R., Wu, C., Rutledge, S., & Stark, C. E. L. (2015). Stability of Age-Related Deficits in the Mnemonic Similarity Task Across Task Variations. *129*, 257-268.

Stevenson, R. F., Zheng, J., Mnatsakanyan, L., Vadera, S., Knight, R. T., Lin, J. J., & Yassa, M. A. (2018). Hippocampal CA1 gamma power predicts the precision of spatial memory judgments. *Proc Natl Acad Sci U S A, 115*(40), 10148-10153. doi:10.1073/pnas.1805724115

Suchow, J. W., Brady, T. F., & Alvarez, G. A. (2013). Modeling visual working memory with the MemToolbox. *13*, 1-8. doi:10.1167/13.10.9.doi

Suchow, J. W., Brady, T. F., Fougnie, D., & Alvarez, G. A. (2013). Modeling visual working memory with the MemToolbox. *J Vis, 13*(10). doi:10.1167/13.10.9

Suthana, N., & Fried, I. (2014). Deep brain stimulation for enhancement of learning and memory. *Neuroimage, 85 Pt 3*, 996-1002. doi:10.1016/j.neuroimage.2013.07.066

Suthana, N. A., Donix, M., Wozny, D. R., Bazih, A., Jones, M., Heidemann, R. M., . . . Bookheimer, S. Y. (2015). High-resolution 7T fMRI of Human Hippocampal Subfields during Associative Learning. *J Cogn Neurosci, 27*(6), 1194-1206. doi:10.1162/jocn_a_00772

Sutterer, D. W., & Awh, E. (2016). Retrieval practice enhances the accessibility but not the quality of memory. *Psychon Bull Rev, 23*(3), 831-841. doi:10.3758/s13423-015-0937-x

Tort, A. B. L., Komorowski, R. W., Manns, J. R., Kopell, N. J., & Eichenbaum, H. (2009). Theta-gamma coupling increases during the learning of item-context associations. *Proceedings of the National Academy of Sciences of the United States of America, 106*, 20942-20947. doi:10.1073/pnas.0911331106

Tulving, E. (1984). Precis of Elements of episodic memory. *The Behavioral and Brain Sciences, 7*, 223-268.

Turrigiano, G. G., & Nelson, S. B. (2004). Homeostatic plasticity in the developing nervous system. *Nat Rev Neurosci, 5*(2), 97-107. doi:10.1038/nrn1327

Vogels, T. P., & Abbott, L. F. (2009). Gating multiple signals through detailed balance of excitation and inhibition in spiking networks. *Nat Neurosci, 12*(4), 483-491. doi:10.1038/nn.2276

Von Stein, A., & Sarnthein, J. (2000). Different frequencies for different scales of cortical integration: From local gamma to long range alpha/theta synchronization. *International Journal of Psychophysiology, 38*, 301-313. doi:10.1016/S0167-8760(00)00172-0

Voytek, B., Kramer, M. A., Case, J., Lepage, K. Q., Tempesta, Z. R., Knight, R. T., & Gazzaley, A. (2015). Age-Related Changes in 1/f Neural Electrophysiological Noise. *J Neurosci, 35*(38), 13257-13265. doi:10.1523/JNEUROSCI.2332-14.2015

Watrous, A. J., Tandon, N., Conner, C. R., Pieters, T., & Ekstrom, A. D. (2013). Frequency-specific network connectivity increases underlie accurate spatiotemporal memory retrieval. *Nat Neurosci, 16*(3), 349-356. doi:10.1038/nn.3315

Watson, B. O., Ding, M., & Buzsaki, G. (2018). Temporal coupling of field potentials and action potentials in the neocortex. *Eur J Neurosci, 48*(7), 2482-2497. doi:10.1111/ejn.13807

Winson, J. (1978). Loss of hippocampal theta rhythm results in spatial memory deficit in the rat. *Science (New York, N.Y.), 201*, 160-163.

Wirth, S., Avsar, E., Chiu, C. C., Sharma, V., Smith, A. C., Brown, E., & Suzuki, W. A. (2009). Trial outcome and associative learning signals in the monkey hippocampus. *Neuron, 61*(6), 930-940. doi:10.1016/j.neuron.2009.01.012

Yassa, M. a., Lacy, J. W., Stark, S. M., Albert, M. S., Gallagher, M., & Stark, C. E. L. (2011). Pattern separation deficits associated with increased hippocampal CA3 and dentate gyrus activity in nondemented older adults. *Hippocampus, 21*, 968-979. doi:10.1002/hipo.20808

Yassa, M. A., & Stark, C. E. (2009). A quantitative evaluation of cross-participant registration techniques for MRI studies of the medial temporal lobe. *Neuroimage, 44*(2), 319-327. doi:10.1016/j.neuroimage.2008.09.016

Yassa, M. A., & Stark, C. E. L. (2009). A quantitative evaluation of cross-participant registration techniques for MRI studies of the medial temporal lobe. *Neuroimage, 44*, 319-327. doi:10.1016/j.neuroimage.2008.09.016

Yeung, N., & Nieuwenhuis, S. (2009). Dissociating Response Conflict and Error Likelihood in Anterior Cingulate Cortex. *Journal of Neuroscience, 29*, 14506-14510. doi:10.1523/JNEUROSCI.3615-09.2009

Yonelinas, A. P., Aly, M., Wang, W. C., & Koen, J. D. (2010). Recollection and familiarity: examining controversial assumptions and new directions. *Hippocampus, 20*(11), 1178-1194. doi:10.1002/hipo.20864

Zhang, W., & Luck, S. J. (2008). Discrete fixed-resolution representations in visual working memory. *Nature, 453*(7192), 233-235. doi:10.1038/nature06860

Zheng, C., Bieri, K. W., Hwaun, E., & Colgin, L. L. (2016). Fast Gamma Rhythms in the Hippocampus Promote Encoding of Novel Object–Place Pairings. *3*, 1-16. doi:10.1523/ENEURO.0001-16.2016

Zheng, J., Anderson, K. L., Leal, S. L., Shestyuk, A., Gulsen, G., Mnatsakanyan, L., . . . Lin, J. J. (2017). Amygdala-hippocampal dynamics during salient information processing. *Nat Commun, 8*, 14413. doi:10.1038/ncomms14413

Zola-Morgan, S., Squire, L. R., Amaral, D. G., & Suzuki, W. A. (1989). Lesions of perirhinal and parahippocampal cortex that spare the amygdala and hippocampal formation produce severe memory impairment. *The Journal of neuroscience : the official journal of the Society for Neuroscience, 9*, 4355-4370.

APPENDIX: SUPPLEMENTARY MATERIAL FOR CHAPTERS 2-4

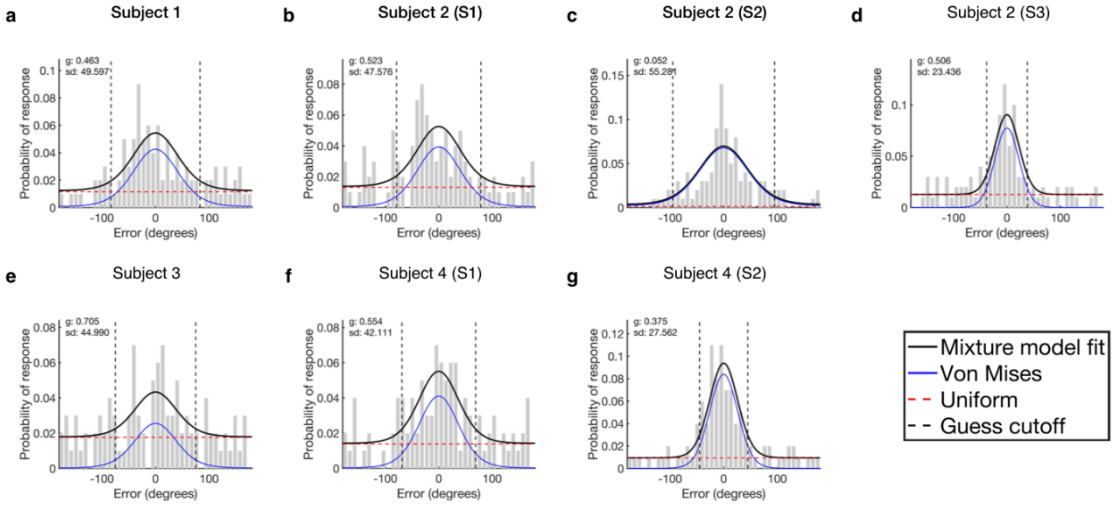

Fig. S2.1. Error histograms, mixture model fit, and cutoff values for the Guess condition for each session. a-g, The black curve indicates the mixture model fit, the blue curve indicates the pdf of the Von Mises distribution, the red dashed line indicates the pdf of the uniform distribution, and the black dashed lines indicate the cutoff values for the Guess condition. g: guess rate; sd: standard deviation of the Von Mises distribution (SDMem); pdf: probability density function; S1: Session 1; S2: Session 2; S3: Session 3.

Table S2.2 Number of MTL contacts in each subregion across subjects.								
MTL subregion	CA1	Sub	DG/CA3	HC (mixed subfields)	Sub/EC	EC	PRC	PHC
Number of contacts	10	6	0	5	2	5	2	2
Sub, subiculum; HC, hippocampus; EC, entorhinal; PRC, perirhinal cortex; PHC, parahippocampal cortex.								

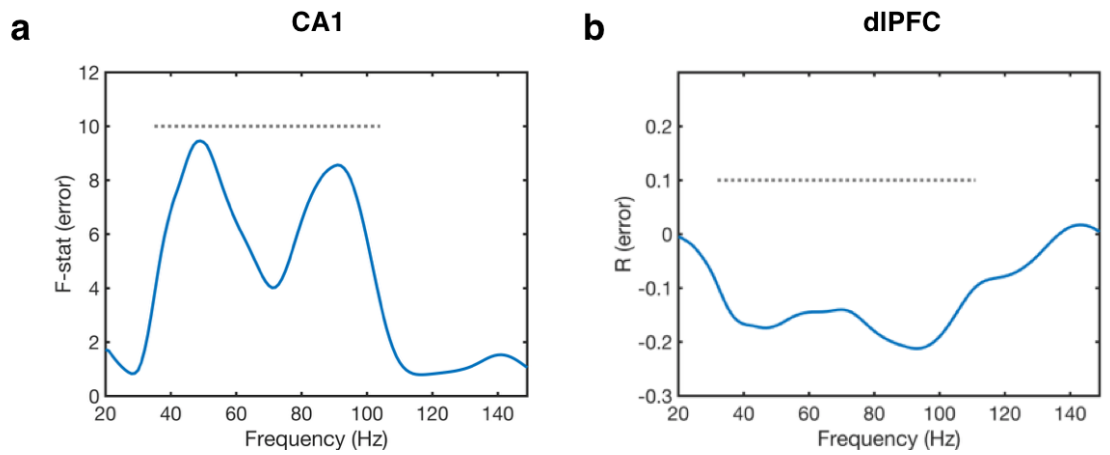

Fig. S2.3. Gamma frequency range and task performance. We calculated the mean CA1 power during the retrieval window at successive gamma frequency ranges using a sliding window moving average of 20 Hz. The center frequencies showing a significant effect of error across conditions (High precision, Low precision, and Guess) ranged from 35 to 104 Hz, consistent with our a priori selection of 40-100 Hz as our gamma frequency range of interest **(a)**. The center frequencies showing a significant correlation between gamma power and error **(b)** covered a similar range (32 to 111 Hz). Dotted gray horizontal line indicates $p < 0.05$.

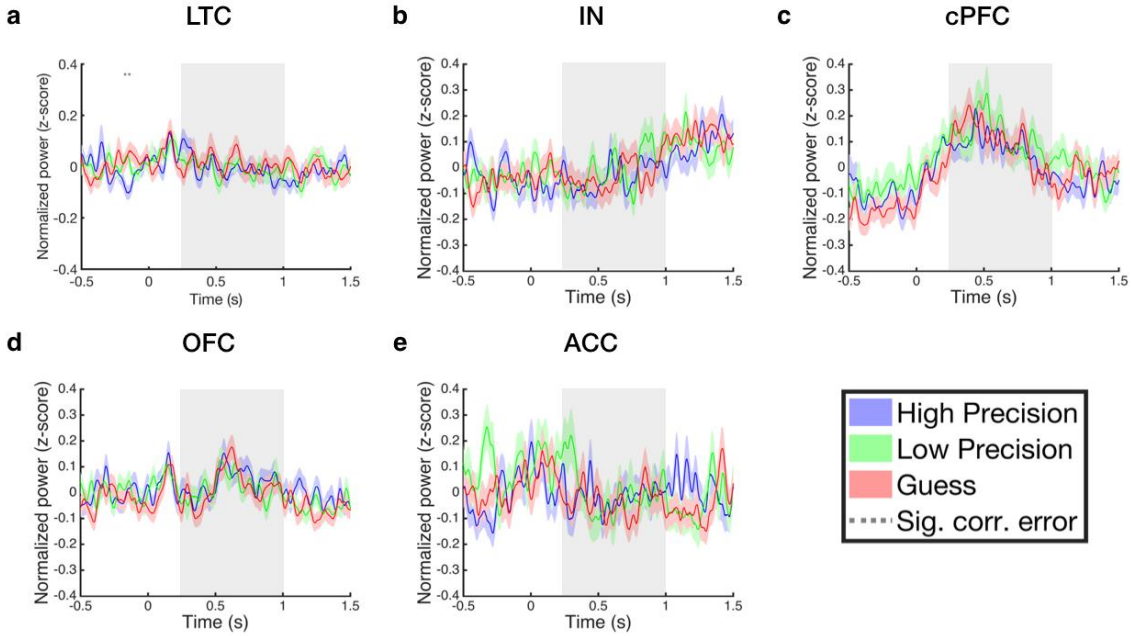

Fig. S2.4. **Gamma power and error.** Time course of gamma power in the lateral temporal cortex **(a)**, insula **(b)**, caudal prefrontal cortex (Brodmann areas 6/8) **(c)**, orbitofrontal cortex **(d)**, and anterior cingulate cortex **(e)**. Stimulus onset is at time zero and the retrieval window (0.25 to 1 second post-stimulus onset) is shaded in gray. Gray horizontal lines indicate time points where there are significant correlations between gamma power and error ($p < 0.05$). The lateral temporal cortex showed a significant effect of error pre-stimulus onset. Colored shaded regions indicate s.e.m.

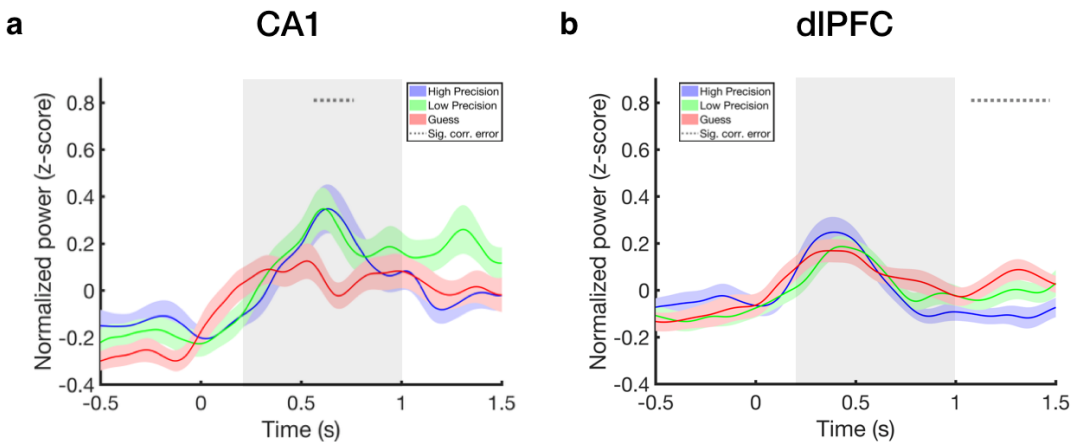

Fig. S2.5. Theta power and error. Time course of theta (3-8 Hz) power in the CA1 subfield **(a)** and dlPFC **(b)**. Stimulus onset is at time zero and the retrieval window (0.25 to 1 second post-stimulus onset) is shaded in gray. Dotted gray horizontal lines indicate time points where there are significant correlations between gamma power and error ($p < 0.05$, cluster-corrected). Colored shaded regions indicate s.e.m. We found a significant negative correlation between theta power and error during the retrieval window in CA1 and a significant positive correlation that emerged after the retrieval window in dlPFC. Neither of these regions showed a significant correlation between theta power and precision.

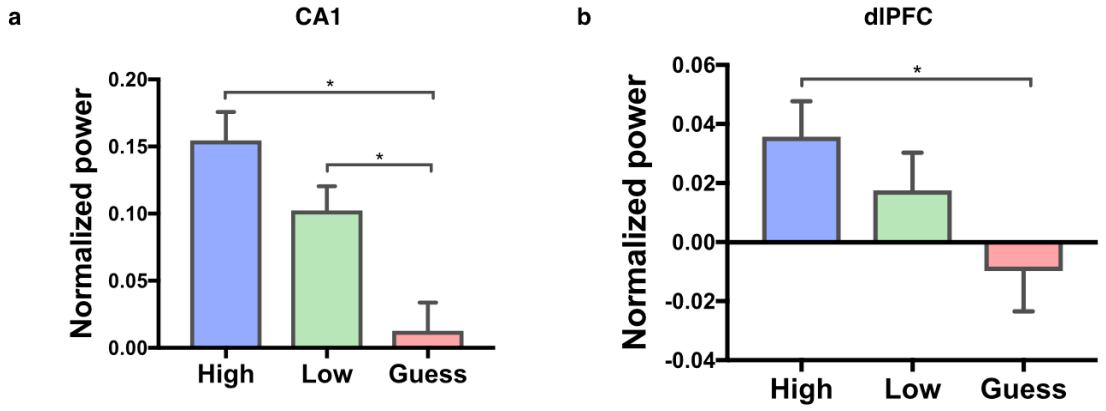

Fig. S2.6. Gamma power in the CA1 and dlPFC: number of expected guesses balanced across High and Low precision conditions. Mean gamma power over the retrieval window (.25 to 1 second post-stimulus onset) in the CA1 **(a)** and dlPFC **(b)** for High precision, Low precision and Guess conditions with the number of expected guesses balanced across High and Low precision conditions. We ran a one-way ANOVA across conditions (High, Low, and Guess) in each region. The results of these ANOVAs were similar to those obtained without balancing (CA1: $F(2, 462) = 12.5$, $p = 5 \times 10^{-6}$; High vs. Guess: $p = 3 \times 10^{-6}$; High vs. Low: $p = 0.06$; Low vs. Guess: $p = 0.004$; dlPFC: $F(2, 651) = 3.19$, $p = 0.04$; High vs. Guess: $p = 0.037$; High vs. Low: $p = 0.32$; Low vs. Guess: $p = 0.25$).

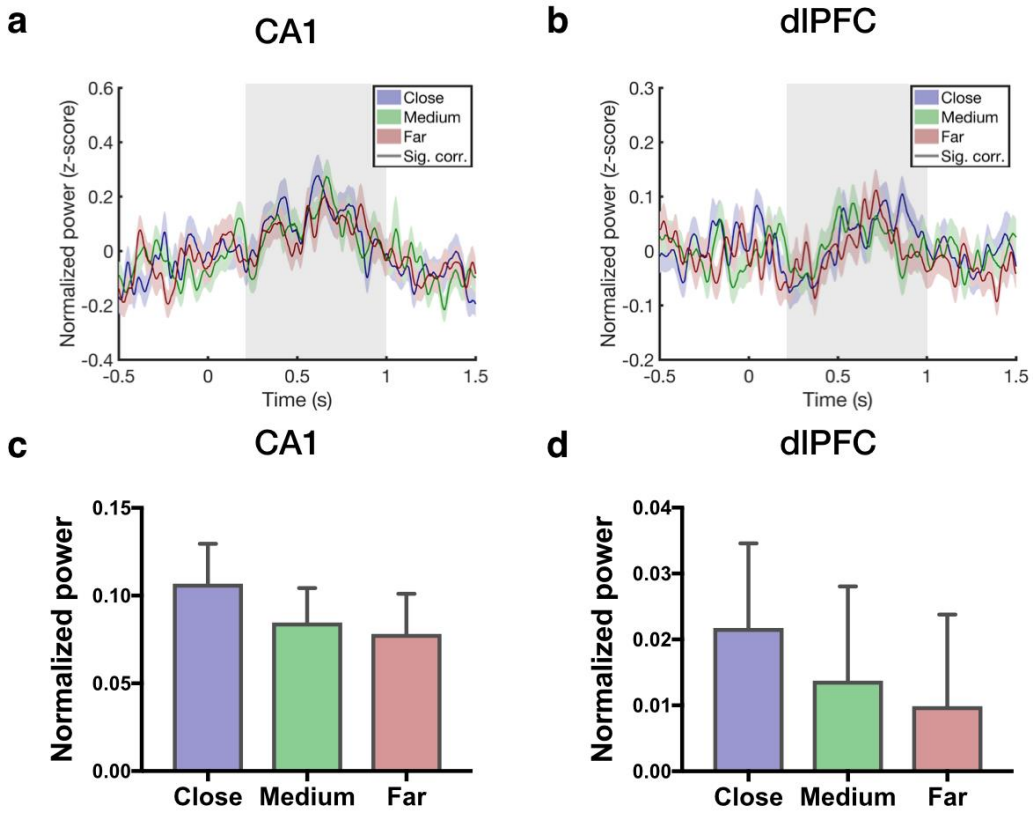

Fig. S2.7. Gamma power is unrelated to the distance object was moved. We examined the relationship between gamma power and the distance the object was moved by calculating the angular distance from the top of the screen (the starting point) to where the subjects placed each object. Trials were sorted by this distance and divided evenly into three conditions: Close, meaning objects that were placed closer to the top of the screen, Medium, meaning objects that were placed a medium distance from the starting point, and Far. The time course of gamma power is shown in the CA1 **(a)** and dlPFC **(b)** for Close, Medium, and Far Trials. No significant correlations between gamma power and distance were found at any time point ($p > 0.05$, cluster corrected). Additionally, CA1 **(c)** and dlPFC **(d)** gamma power was averaged over the retrieval window and a one-way ANOVA was performed across the three conditions. These ANOVAs did not show a significant effect of distance in either region (CA1: $F(2, 426) = 1.1$; $p = 0.32$; dlPFC: $F(2, 603) = 0.78$; $p = 0.46$). Colored shaded regions and error bars indicate s.e.m.

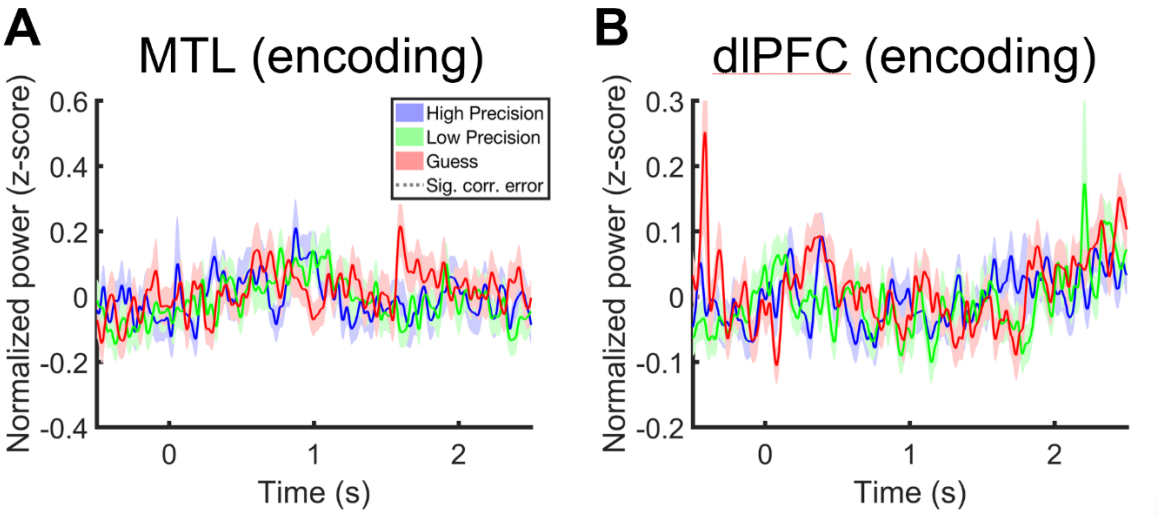

Fig. S2.8. **Gamma power at encoding and subsequent error.** Time course of gamma power at encoding in the MTL **(a)**, dlPFC **(b)** for trials that were subsequently designated high, medium and low precision at retrieval. Gray horizontal lines indicate time points where there are significant correlations between gamma power at encoding and subsequent error ($p < 0.05$). The lateral temporal cortex showed a significant effect of error pre-stimulus onset. Colored shaded regions indicate s.e.m.

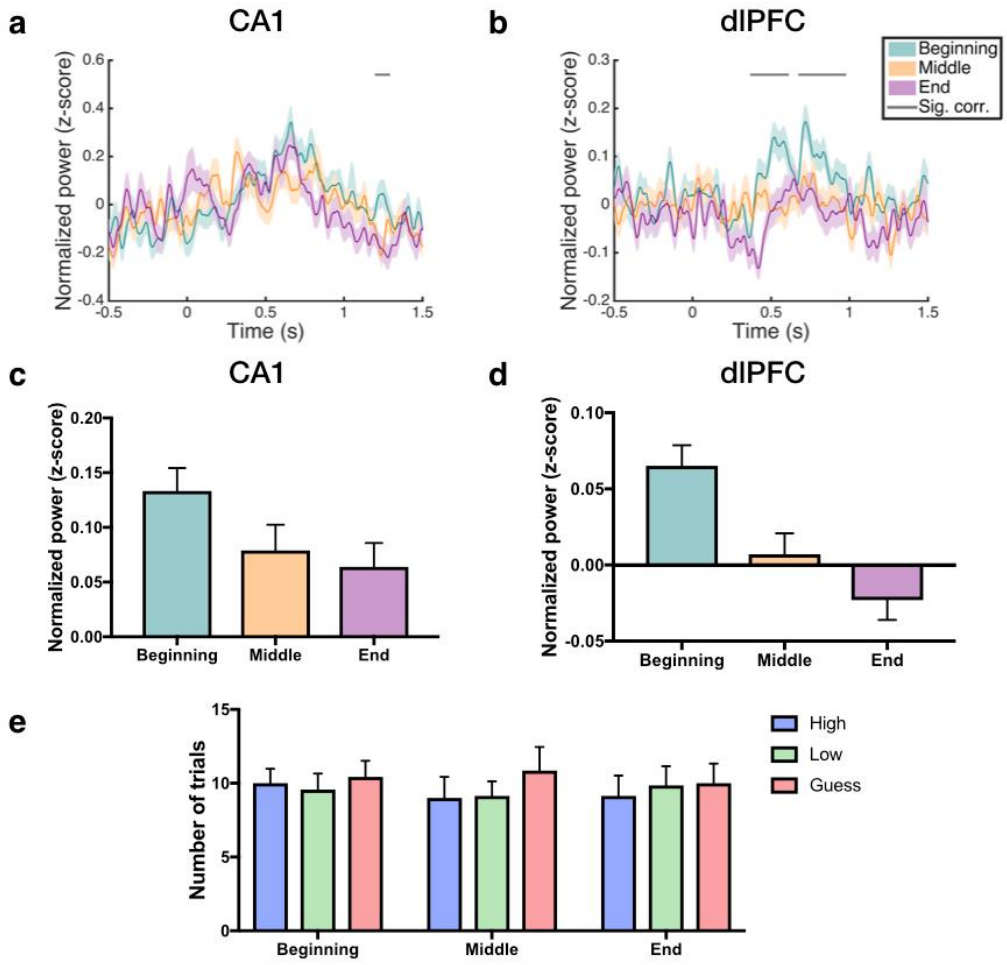

Fig. S2.9. Gamma power decreases over the course of the test session do not drive the error/precision effects. To assess the relationship between gamma power and trial order, trials were divided evenly into three conditions: Beginning, meaning trials from the first third of the test session, Middle, and End. The time course of gamma power in the CA1 (a) and dlPFC (b) is shown for trials at the Beginning, Middle, and End of the test session. Gray horizontal lines indicate time points where there are significant correlations between gamma power and trial order ($p < 0.05$, cluster corrected). Colored shaded regions indicate s.e.m. c, d, Mean gamma power over the retrieval window (.25 to 1 second post-stimulus onset) for trials at the Beginning, Middle, and End of the test session in the CA1 (c) and dlPFC (d). One-way ANOVAs with trial order (Beginning, Middle, and End) as fixed factors revealed a significant effect of order in the dlPFC ($F(2, 603) = 11.2$; $p = 0.00002$) and a marginal effect in the CA1 ($F(2, 426) = 2.7$; $p = 0.07$). Error bars indicate s.e.m. e, To assess the relationship between trial order and precision, the number of High precision, Low precision, and Guess trials was calculated for each condition (Beginning, Middle, and End), and a two-way ANOVA was performed with trial order (Beginning, Middle, and End), and precision (High, Low, and Guess) as fixed factors. This ANOVA resulted in p values > 0.05 (Trial order: $F(2, 12) = 0.5$, $p = 0.6$; Error: $F(2,12) = 0.3$, $p = 0.7$; Interaction: $F(4, 24) = 0.2$, $p = 0.9$), indicating that the number of High precision, Low precision, and Guess trials does not change over the course of the test session.

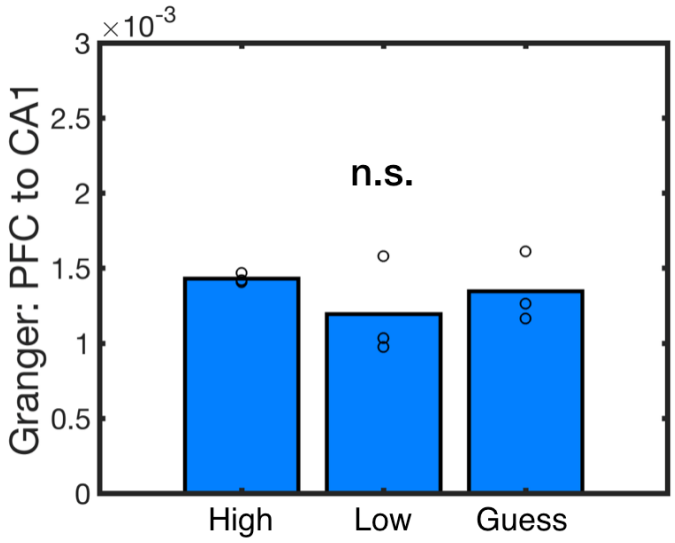

Fig. S2.10. Mean dlPFC to CA1 Granger prediction values for each condition. P > 0.05 as determined by permutation testing.

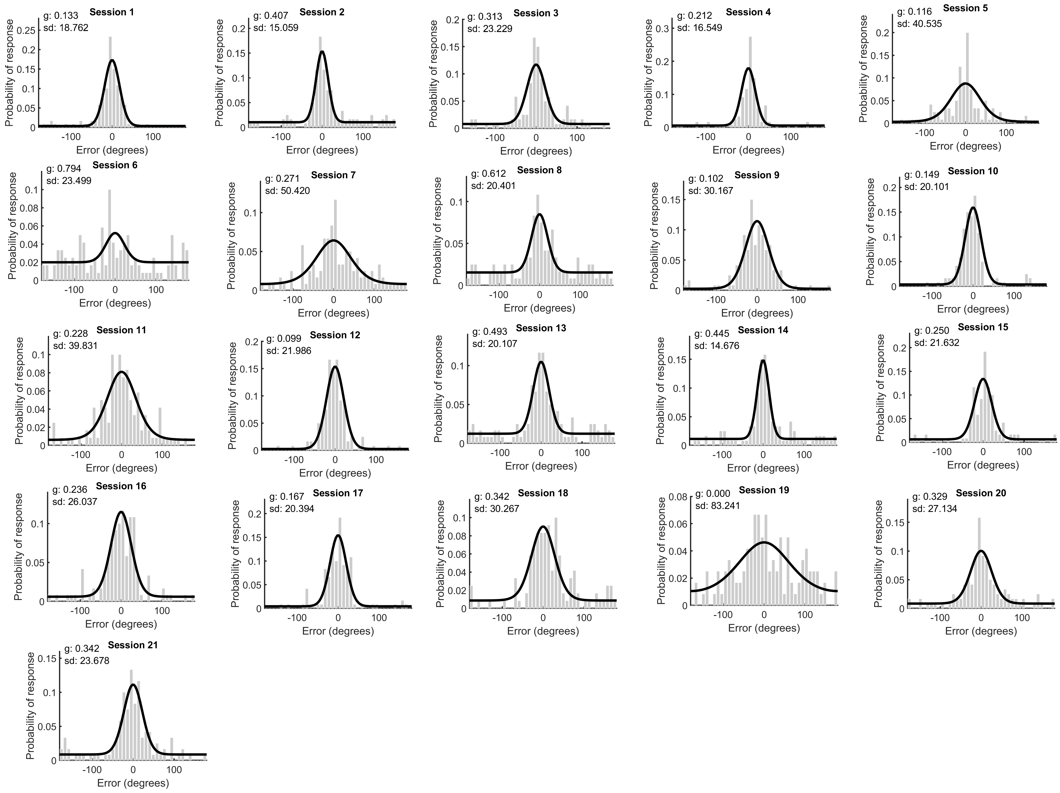

S3.1. **Mixture model fit for all sessions.** Histograms showing the distribution of error for all trials pooled across sessions and mixture model fit for each session. S: session, g: guess rate, sd: standard deviation of the von Mises distribution.

Table S3.2 Number of MTL contacts in each subregion across subjects.									
MTL subregion	CA1	Sub	DG/CA 3	HC (mixed subfields)	Sub/EC	CA1/PH C	EC	PRC	PHC
Number of contacts	5	7	3	3	2	2	4	1	5
Sub, subiculum; HC, hippocampus; EC, entorhinal; PRC, perirhinal cortex; PHC, parahippocampal cortex.									

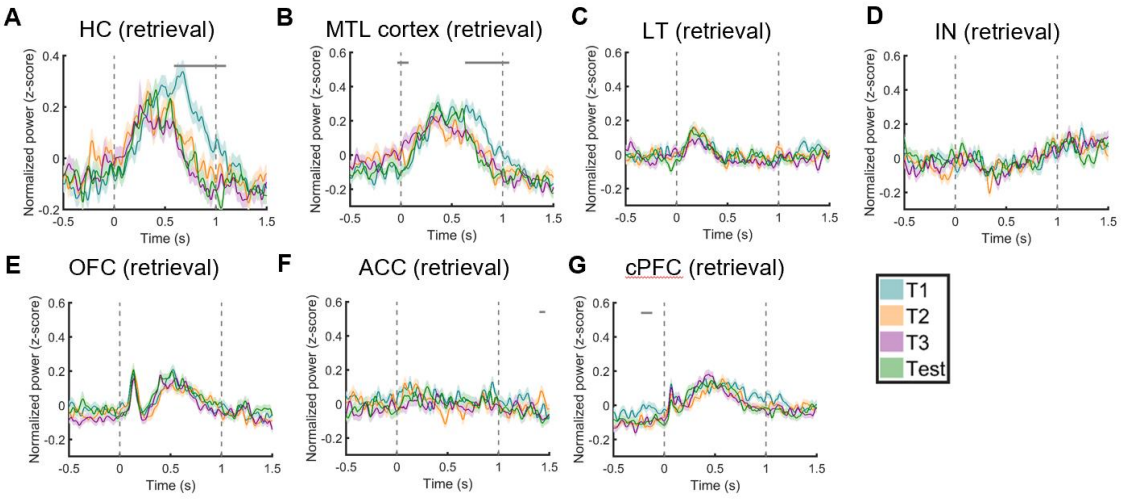

S3.3. **Gamma power across task blocks at retrieval**. Time course of gamma power across task blocks in all regions. Gray horizontal lines indicate time points where there were significant differences between conditions (ANOVA, $p < 0.05$, cluster-corrected). The start and end of the retrieval window are indicated by vertical dotted lines. Colored shaded regions indicate s.e.m.

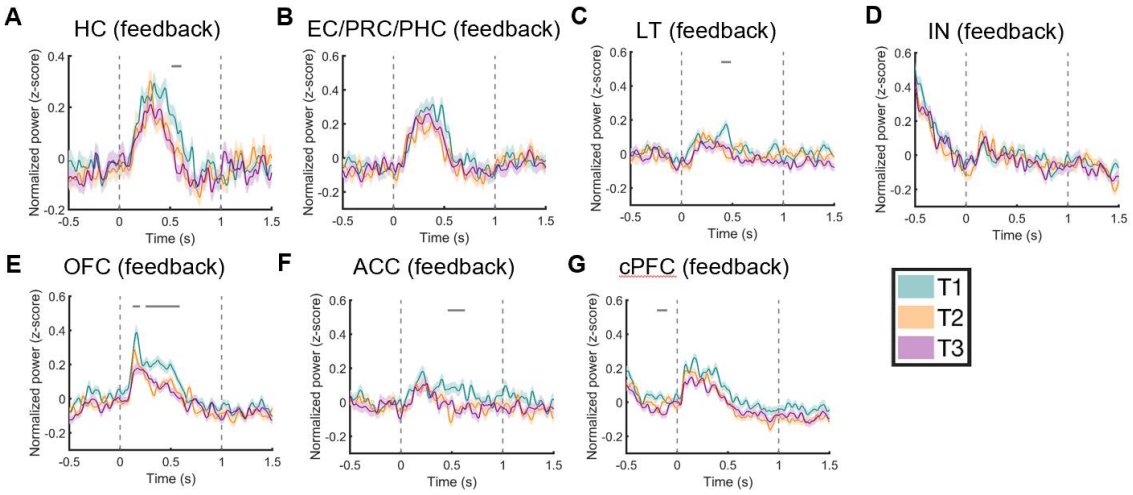

S3.4. **Gamma power across task blocks at feedback**. Time course of gamma power across task blocks in all regions. Gray horizontal lines indicate time points where there were significant differences between conditions (ANOVA, $p < 0.05$, cluster-corrected). The start and end of the feedback window are indicated by vertical dotted lines. Colored shaded regions indicate s.e.m.

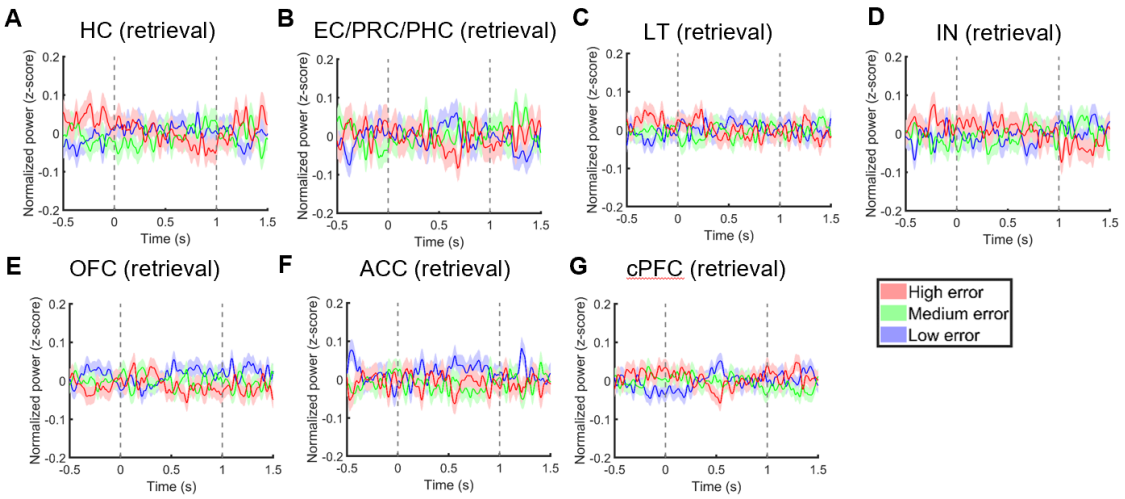

S3.5. **Gamma power and error at retrieval**. Time course of gamma power normalized within blocks for high, medium, and low error trials. Gray horizontal lines indicate time points where there were significant differences between conditions (ANOVA, $p < 0.05$, cluster-corrected). The start and end of the retrieval window are indicated by vertical dotted lines. Colored shaded regions indicate s.e.m.

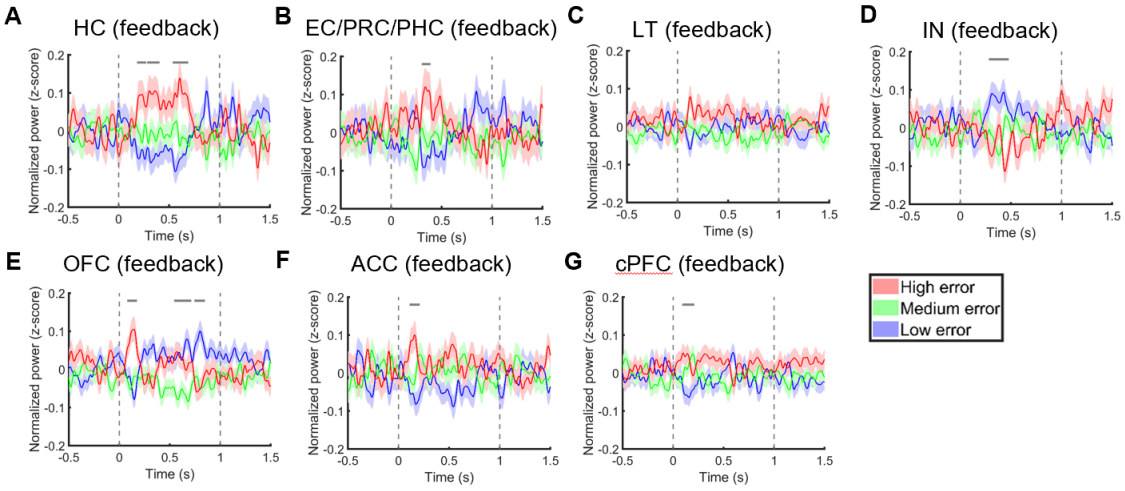

S3.6. **Gamma power and error at feedback**. Time course of gamma power normalized within blocks for high, medium, and low error trials. Gray horizontal lines indicate time points where there were significant differences between conditions (ANOVA, $p < 0.05$, cluster-corrected). The start and end of the feedback window are indicated by vertical dotted lines. Colored shaded regions indicate s.e.m.

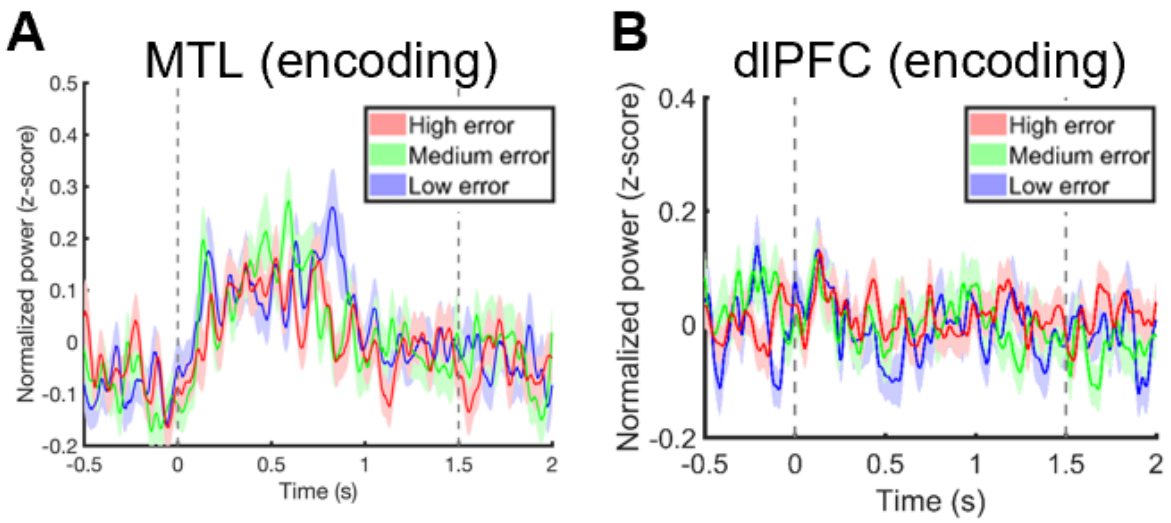

Fig. S3.7 Gamma power at encoding and subsequent error. Time course of gamma power at encoding for trials subsequently placed in the high, medium, and low error conditions. Gray horizontal lines indicate time points where there were significant differences between conditions (ANOVA, $p < 0.05$, cluster-corrected). The start and end of the encoding window (0-1.5s post-stimulus onset) are indicated by vertical dotted lines. Colored shaded regions indicate s.e.m.

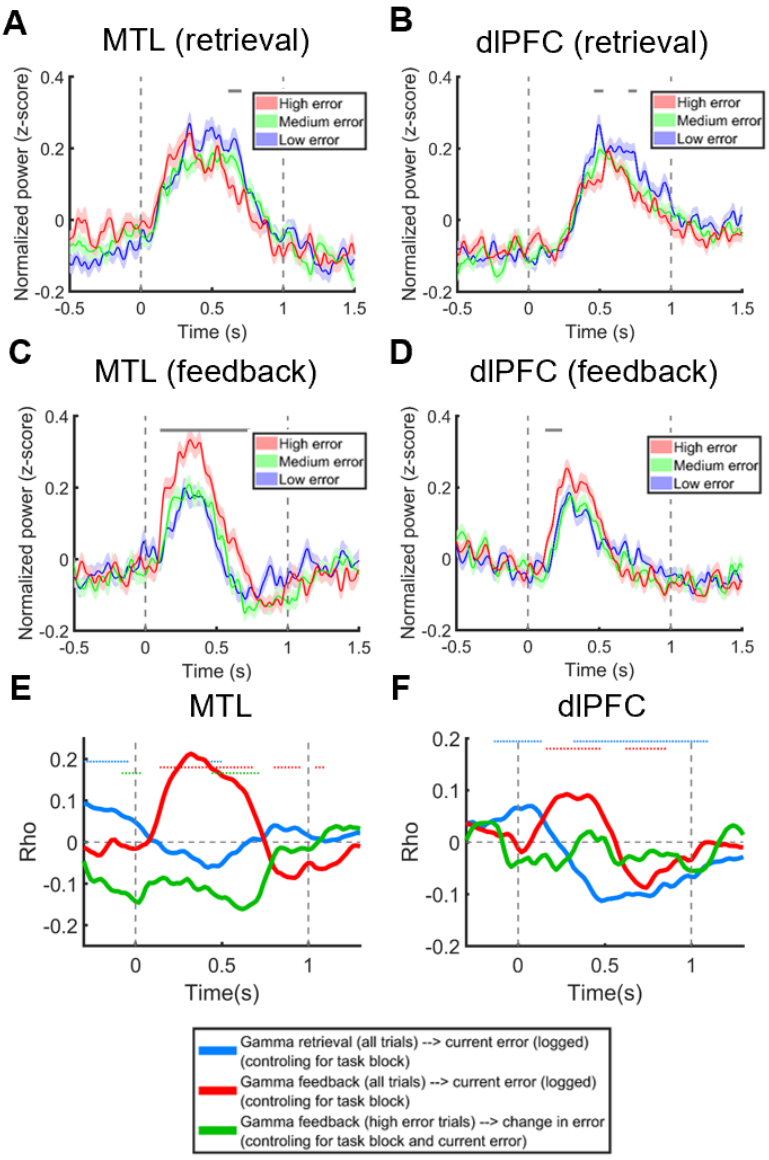

Fig S3.8. MTL gamma power predicts error within blocks and learning across blocks. A-D, Time course of MTL and dlPFC gamma power for high error trials within blocks, meaning the top 1/3 trials with the highest error within each block, medium error trials, meaning the middle 1/3 trials, and low error trials at retrieval (A-B) and feedback (C-D). Gray horizontal lines indicate time points where there are significant differences between conditions (ANOVA, $p < 0.05$, cluster-corrected). Colored shaded regions indicate s.e.m. E-F, Partial correlations between MTL (E) and dlPFC (F) gamma power and current error, controlling for task block, for all trials at retrieval (blue) and at feedback (red), as well as gamma power at feedback and the subsequent change in error for high error trials from one task block to the next (green, controlling for task block and current error).

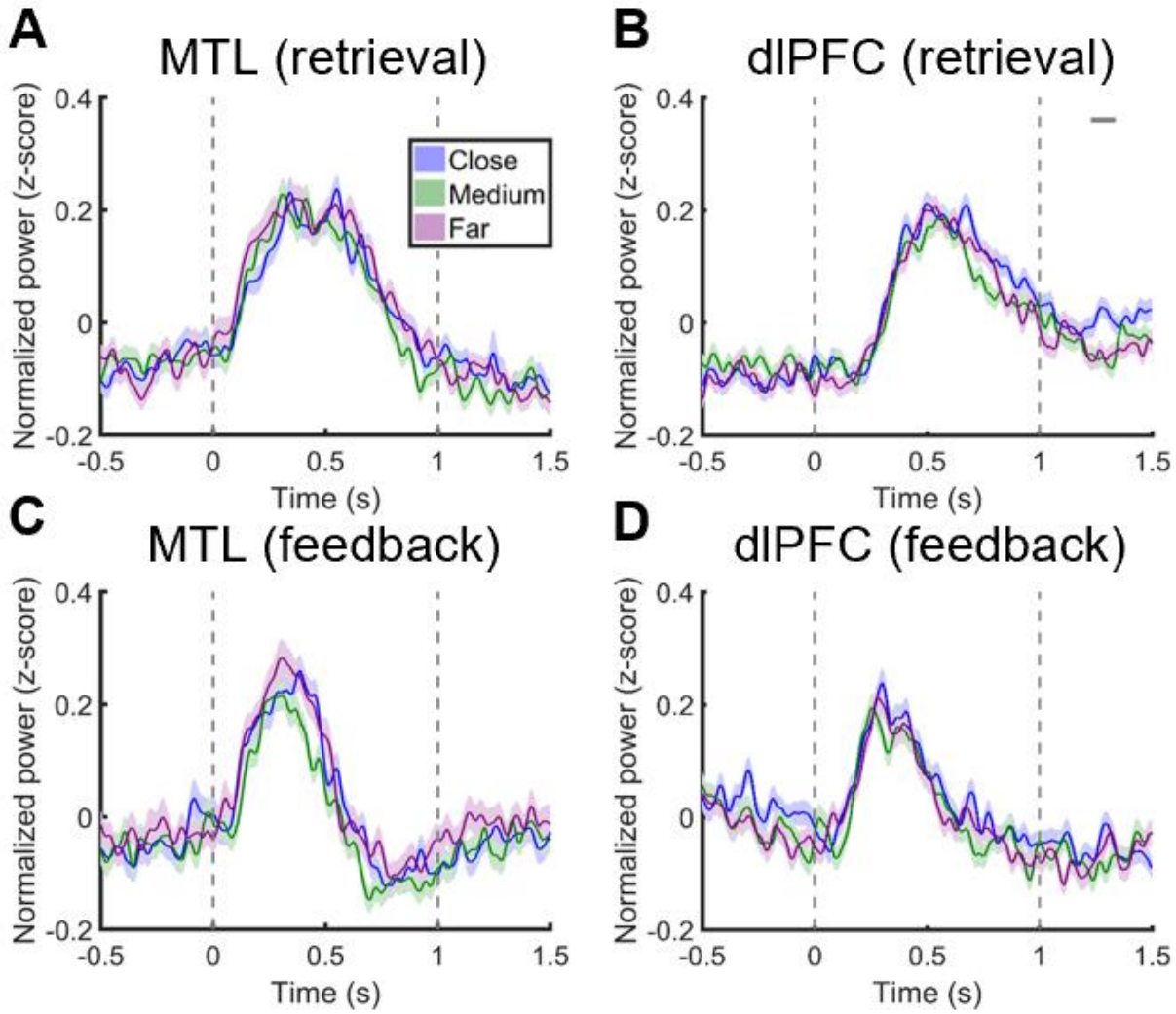

Fig. S3.9. Gamma power is unrelated to the distance object was moved. We examined the relationship between gamma power and the distance the object was moved by calculating the angular distance from the top of the screen (the starting point) to where the subjects placed each object. Trials were sorted by this distance and divided evenly into three conditions: Close, meaning objects that were placed closer to the top of the screen, Medium, meaning objects that were placed a medium distance from the starting point, and Far. The time course of gamma power is shown in the CA1 **(a)** and dlPFC **(b)** for Close, Medium, and Far Trials. No significant differences between distances were found during the retrieval or feedback windows (ANOVA, $p > 0.05$, cluster-corrected). Increased gamma power for Close trials was observed in the DLPFC following the retrieval window (ANOVA, $p < 0.05$, cluster-corrected).

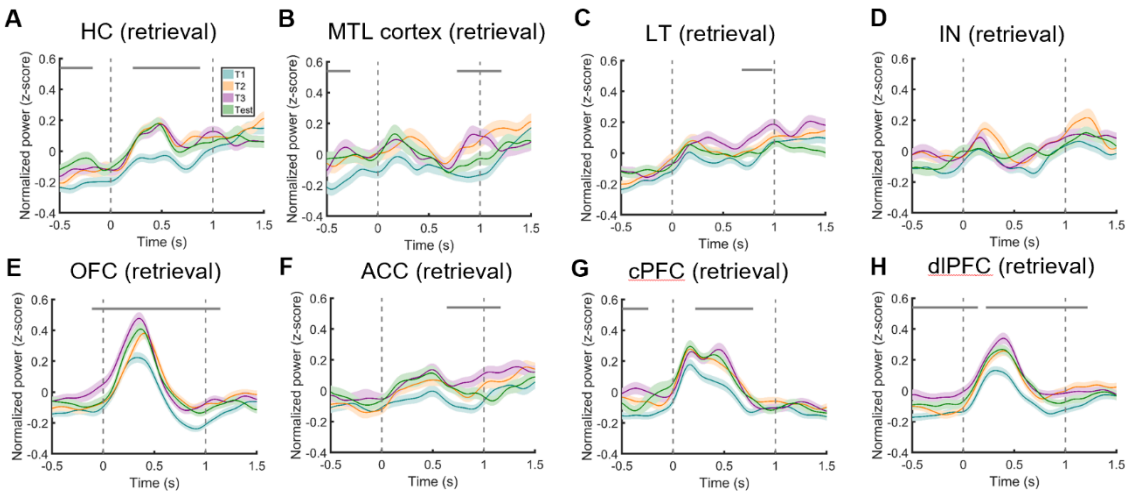

Fig. S4.1. Theta power across blocks at retrieval. Time course of theta power for all regions for all task blocks. Gray horizontal lines indicate time points where there were significant differences between conditions (ANOVA, $p < 0.05$, cluster-corrected). The start and end of the retrieval window are indicated by vertical dotted lines. Colored shaded regions indicate s.e.m.

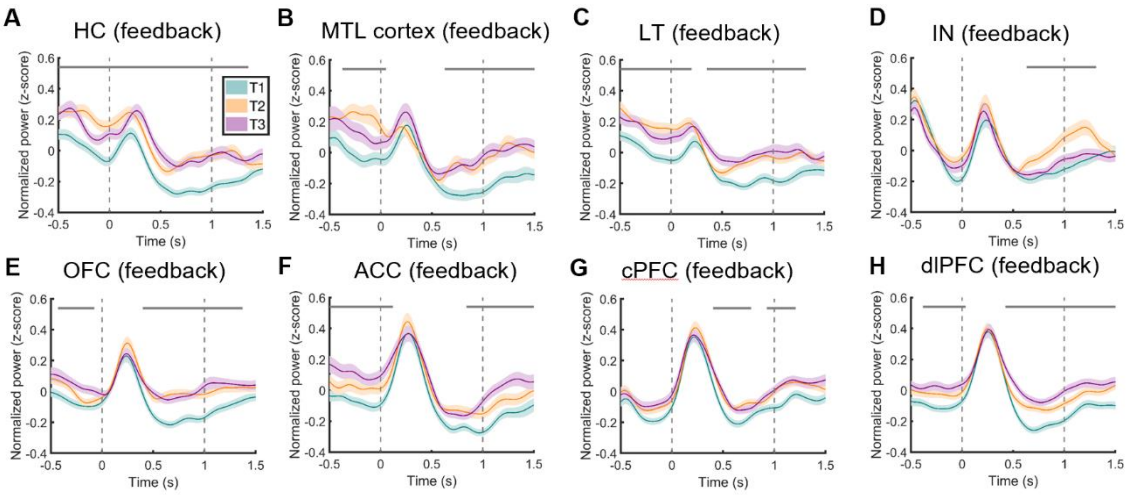

Fig. S4.2. Theta power across blocks at feedback. Time course of theta power for all regions for all training blocks. Gray horizontal lines indicate time points where there were significant differences between conditions (ANOVA, $p < 0.05$, cluster-corrected). The start and end of the feedback window are indicated by vertical dotted lines. Colored shaded regions indicate s.e.m.